

**UNIVERSITATEA DE ȘTIINȚE AGRICOLE ȘI MEDICINĂ
VETERINARĂ "ION IONESCU DE LA BRAD" IAȘI**

LUCRĂRI ȘTIINȚIFICE

**VOL. 61
MEDICINĂ VETERINARĂ**

PARTEA A 2-A

EDITURA "ION IONESCU DE LA BRAD" IAȘI 2018

Coordonatorii Revistei

Redactor responsabil: Prof. dr. Vasile VÎNTU - USAMV Iași

Redactor adjunct: Prof. dr. Liviu-Dan MIRON - USAMV Iași

Membri:

- Prof. dr. Costel SAMUIL - USAMV Iași
- Prof. dr. Lucia DRAGHIA - USAMV Iași
- Prof. dr. Gheorghe SAVUȚA - USAMV Iași
- Prof. dr. Paul-Corneliu BOIȘTEANU - USAMV Iași

Colegiul de Redacție al Seriei "Medicină Veterinară"

Redactor șef:

Prof. dr. Gheorghe SAVUȚA - USAMV Iași

Redactor adjunct:

Prof. dr. Mihai MAREȘ - USAMV Iași

Membri:

Prof. dr. Gheorghe SOLCAN - USAMV Iași
Prof. dr. Gheorghe DRUGOCIU - USAMV Iași
Conf. dr. Geta PAVEL - USAMV Iași
Conf. dr. Viorel Cezar FLORIȘTEAN - USAMV Iași
Conf. dr. Valentin NĂSTASĂ - USAMV Iași
Asist. dr. Mariana GRECU – USAMV Iași

Referenți științifici:

Prof. dr. Abdelfatah NOUR - Purdue University, SUA
Prof. dr. Gheorghe SAVUȚA - USAMV Iași
Prof. dr. Liviu MIRON - USAMV Iași
Prof. dr. Gheorghe SOLCAN - USAMV Iași
Assoc. Prof. Dorina CARTER - University of Liverpool, UK
Prof. dr. Elena VELESCU - USAMV Iași
Prof. dr. Gheorghe DRUGOCIU - USAMV Iași
Prof. dr. Vasile VULPE - USAMV Iași
Prof. dr. Cornel CĂTOI - USAMV Cluj-Napoca
Prof. dr. Gabriel PREDOI - USAMV București
Prof. dr. Viorel HERMAN - USAMVB Timișoara
Prof. dr. Mihai MAREȘ - USAMV Iași
Conf. dr. Narcisa MEDERLE - USAMVB Timișoara
Conf. dr. Valentin NĂSTASĂ - USAMV Iași
Conf. dr. Sorin-Aurelian PAȘCA - USAMV Iași

on -line ISSN 2393 – 4603

ISSN–L 1454 – 7406

CONTENTS

Computed tomography examination of periodontal disease in dog	78 - 81
Robert Cristian Purdoi, Melinda Adriana Costache, Ionel Papuc, Sabina Ghergariu, Sorin Mârza, Cristian Popovici, Adela Lazăr, Radu Lăcătuș	
Computed tomography evaluation of lung parenchyma in dogs	82 - 87
Robert Cristian Purdoi, Felix Lucaci, Ionel Papuc, Cosmin Peștean, Sorin Mârza, Cristian Popovici, Adela Lazăr, Radu Lăcătuș	
Hysterosalphyngography in female dogs	88 - 90
Radu Lăcătuș, Octavian Duță, Raul Alexandru Pop, Sorin Mârza, Laura Condor, Robert Cristian Purdoi	
Identification of dorsal cutaneous perforator vessels using angio CT technique	91 - 94
Radu Lăcătuș, Iulian Moldovan, Ileana Matei, Filip Ardelean, Cosmin Peștean, Sorin Mârza, Laura Condor, Robert Cristian Purdoi	
Incidental histological changes in the canine central nervous system	95 - 104
Mihai Negru, Marian Taulescu, Cornel Cătoi	
Histological aspects concerning the stomach of grass snake <i>Natrix Natrix</i>	105 - 109
Stefania Mariana Raita, Valerica Danacu, Petronela Rosu, Bogdan Georgescu, Florica Barbuceanu, Raluca Rizac	
Histological research of the muscular stomach in <i>Struthio camelus</i>	110 - 118
Ștefania Mariana Raita, Valerica Danacu, Petronela Rosu, Bogdan Georgescu, Florica Barbuceanu	
The prophylaxis of chalkbrood in bees by laboratory methods - microscopic testing of pollen	119 - 127
Ion Rădoi, Gheorghe Florentin Milea, Alexandros Rădulea, Vasilică Savu, Agripina Sapcaliu, Maria Măgdici, Luiza Badic	
The relevance of a digital system based on nanoparticles biosensors in assessing the antioxidant potential of some foods	128 - 134
Sebastian Ognean, Titus Crișan, Constantin Bele, Octavia Tamas-Krumpe, Andreea Buta, Helga Demeny, Laurenț Ognean	

Application of haccp (hazard analysis critical control point) to cow telemea cheese production 135 - 141

Alina Borș, Oana Raluca Rusu, Ionuț Borș, Viorel Floriștean

Left sided congestive heart failure due to severe aortic degeneration and insufficiency in a dog – a case report 142 - 148

R.A. Baisan, E. Condurachi, V. Vulpe, S.A. Pașca

Canine pyometra: microbiological diagnosis and therapy 149 - 152

George Cosmin Nadăș, Cosmin Dan Filipoi, Flore Chirilă, Cosmina Maria Bouari, Ioana Buzura-Matei, Nicodim Iosif Fiț

COMPUTED TOMOGRAPHY EXAMINATION OF PERIODONTAL DISEASE IN DOG

Robert Cristian PURDOIU^{1*}, Melinda Adriana COSTACHE¹, Ionel PAPUC¹, Sabina GHERGARIU¹,

Sorin MĂRZA¹, Cristian POPOVICI¹, Adela LAZĂR², Radu LĂCĂTUȘ¹

¹Department of Semiology, Ethopathology and Medical imaging. University of Agricultural Sciences and Veterinary Medicine, Cluj Napoca.

²Department of Oral Rehabilitation, Health and Management of Dental office, Faculty of Dental Medicine, "Iuliu Hatieganu" University, Cluj-Napoca, Romania

*Corresponding author, e-mail: robert.purdoi@usamvcluj.ro

Abstract

Periodontal disease is a very common disease in dogs, with an incidence of 85%, which affects both the health and the quality of life of the animals (Shearer, 2010, Kortegaard et al 2014). Dog periodontitis has become a priority disease for both pet owners and practitioners. Taking in consideration the high incidence of the periodontal disease in dogs and the fact that the clinical diagnostic is limited, the aim of this study was to highlight the role and importance of imaging diagnostic tools such as Computed Tomography in the diagnostic of this pathology. The study was conducted on 20 dogs (30% female and 70% male) with age from 1 year to 12 years. The patients were clinically examined and after that were sedated and a radiographic evaluation and a CT scan of the head was performed. Classification of periodontal disease take in consideration the retraction of alveolar bone and formation of periodontal pocket, retraction of alveolar bone was visible on CT examination compared to radiographic examination in which the overlapping of bony structures of the mandible and maxilla make the bone retraction less evident. Computed tomography examination is more accurate than radiography, giving the possibility to evaluate all the roots of the teeth and bone retraction, and come to complete the clinical evaluation.

Keywords: Periodontal diseases, dog, Computed Tomography, head

Introduction

Periodontal disease is one of the most prevalent disease in dogs and result in infections with inflammation of the gums and gingival pocket formation (Pavlica *et al.* 2008; Shearer, 2010; Kortegaard et al 2014). Periodontal disease diagnostic is based on clinical examination and 2D radiography, the last method present difficulty in assessing the gums and bone retraction in advance stages of periodontitis. Introduction of Computed Tomography (CT) examination for periodontal disease help evaluate the bone level changes and three-dimensional architecture of osseous defects (Mish et al 2006).

Taking in consideration the high incidence of the periodontal disease in dogs and the fact that the clinical diagnostic is limited, the aim of this study was to highlight the role and importance of imaging diagnostic tools such as Computed Tomography in the diagnostic of this pathology.

Materials and Methods

The study was conducted on 20 dogs (30% female and 70% male) with age from 1 year to 12 years. The patients were clinically examined and after that were sedated and a radiographic evaluation and a CT scan of the head was performed.

In the first stage of the clinical evaluation the gums and the presence of dental plaque was evaluated, the second stage of the clinical evaluation consist in evaluation of teeth mobility and bone retraction using a marked periodontal probe of 2 cm that was introduced in the gingival sulcus for evaluation of gingival retraction and apparition of gingival and periodontal pocket. All the data were registered in a dental examination sheet.

CT examination was performed after the patients were sedated, the CT images were obtained using a 512*512 matrix, bone tissue kernel and a pitch of 0.85. The patient was positioned

in ventral decubitus. The images were evaluated and the measurement were performed using RadiAnt DICOM viewer.

Results and discussions

The most common symptoms that indicate the occurrence of periodontitis are in descending order: dental plaque, gingivitis, bone and gum retractions, dental mobility and halitosis. Dental plaque is usually the first visible symptom that occurs being visible from clinical examination. Classification of periodontal disease take in consideration the retraction of alveolar bone and formation of periodontal pocket, (Niemiec, 2008; Glickman et al, 2011) retraction of alveolar bone was visible on CT examination compared to radiographic examination in which the overlapping of bony structures of the mandible and maxilla make the bone retraction less evident).

The capability of Computed Tomography to render a 3D image base on the DICOM scanned images help evaluate the retraction of the bone, this method is less invasive than the evaluation of the periodontal pocket with a probe.

Evaluation of the periodontal disease stages is based on the support loss of the dental structures that became more easily done on the CT.

Retraction of the gums with formation of the periodontal pocket, make in time visible the furcation of the teeth, a periodontal pocket dipper than 5 mm indicate bone loss, normal sulcal depth in dog is between 0 and 3 mm (Niemiec, 2008). CT evaluation of the teeth permit measurement of the bone loss and also evidentiatio of furcation.

The measurement are done starting from the teeth crown until at the base of the alveolar bone (Fig. 1, Fig. 2). Other convenient aspect of the CT examination is that on the 3D reconstruction the retraction of the bone is visible showing the early stages if the furcation, this is not evident all the time in clinical evaluation because the dental plaque can cover the presence of furcation (Fig. 3, Fig. 4).

Late complication of the periodontal disease, like oro-nasal fistula and decay of the bone can be seen on the CT scan. The CT scan better delineate the bone loss and the degeneration of the bone tissue than classic radiography (Fig. 5).

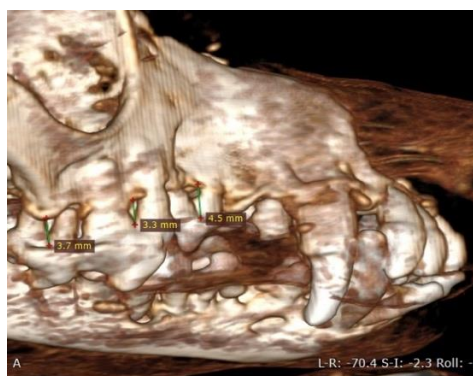


Figure 1 Evidentiatio of furcation

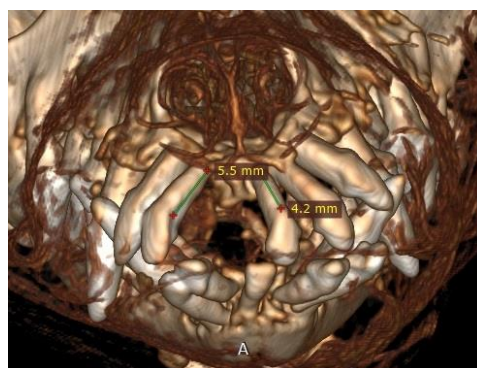


Figure 2 Massive bone loss of the incisive alveolar bone

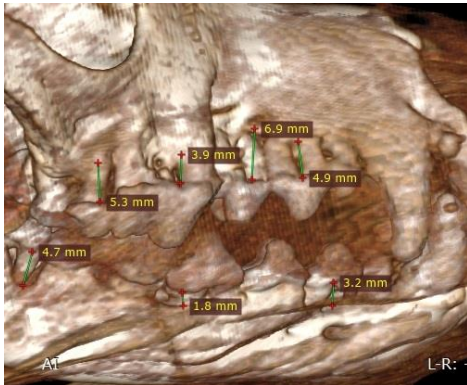


Figure 3 CT aspect with bone los and evidention of furcation



Figure 4 At inspection the furcation is not evident even so the CT scanning show furcation and bone loss (see Fig 3)

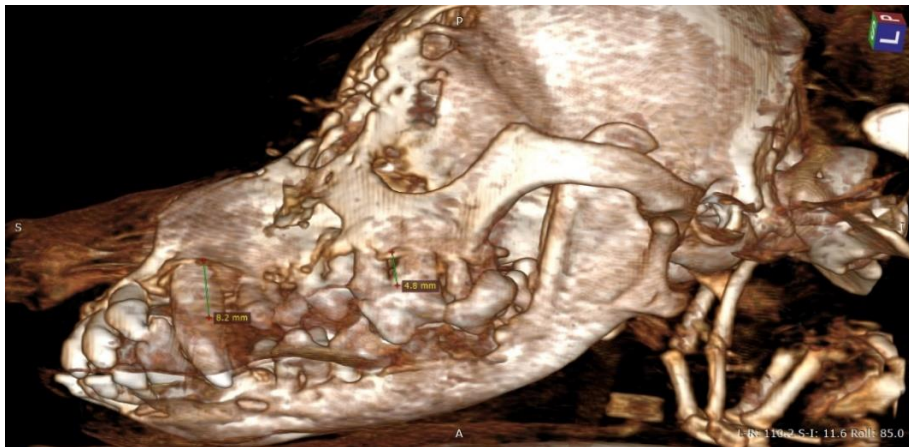


Figure 5 Bone decay and nasal fistula formation

Conclusions

Computed tomography examination is more accurate than radiography, giving the possibility to evaluate all the roots of the teeth and bone retraction, and come to complete the clinical evaluation. CT examination give additional information that help staging the periodontal disease.

Acknowledgement

This study was performed in the Radiology department of FMV Cluj Napoca being part of internal department research grant.

References

1. Craig R.G., Kamer Angela R. (2016), A clinicia`s guide to systemic effects of periodontal disease, Ed: Springer, New York,USA, 1-17.
2. Glickman L.T., Glickman N.W., Moore G.E., Lund E.M., Lantz G.C., Pressler B.M. (2011) Association between chronic azotemic kidney disease and the severity of periodontal disease in dogs, Preventive Veterinary Medicine, 99 (2-4):193-200.

-
3. Kortegaard H.E., Eriksen T, Badum V. (2014), Screening for periodontal disease in research dog- a methodology study, *Acta veterinaria scandinavica*, 57:77.
 4. Mish K.M., Yi S.E., Sarment D.P., (2006), Accuracy of Cone Beam Computed Tomography for Periodontal Defect Measurements, *Journal of Periodontology*, 77(7):1261-1266.
 5. Niemiec B.A. (2008) Periodontal disease, *Topics in Companion Animal Medicine*, 23(2):72-80.
 6. Pavlica Z., Petelin M., Juntos P., Erzen D., Crossley D.A., Skaleric U., (2008). Periodontal disease burden and pathological changes in organs of dogs. *J. Vet. Dent* 25(2): 97-105.
 7. Shearer P. (2010), Periodontal literature review, Banfield applied research and knowledge team, Portland, Oregon, 1-8.

COMPUTED TOMOGRAPHY EVALUATION OF LUNG PARENCHYMA IN DOGS

Robert Cristian PURDOIU^{1*}, Felix LUCACI¹, Ionel PAPUC¹, Cosmin PEȘTEAN¹, Sorin MĂRZA¹,

Cristian POPOVICI¹, Adela LAZĂR², Radu LĂCĂTUȘ¹

¹Department of Semiology, Ethopathology and Medical imaging. University of Agricultural Sciences and Veterinary Medicine, Cluj Napoca.

²Department of Oral Rehabilitation, Health and Management of Dental office, Faculty of Dental Medicine, "Iuliu Hatieganu" University, Cluj-Napoca, Romania

*Corresponding author, e-mail: robert.purdoiu@usamvcluj.ro

Abstract

The imaging examination of the respiratory apparatus is a difficult exam, assuming detailed knowledge of the anatomy of the chest cavity. The respiratory system is in constant contact with the environment, being responsible for the facility of gas exchange between the body and the environment, which also implies an increased interaction between the lung and the pathogens in the environment. The radiological examination is the main exam in assessing the pathology of the thoracic cavity and pulmonary parenchyma. With the evolution of technology, the CT test has begun to be used more and more frequently in veterinary medicine. The limitation of the radiological examination in the pulmonary cavity examination is the biplanar image and overlapping of the lung structures. In human medicine CT examination of the lung cavity is the gold standard in the diagnosis of pathology located at this level.

Keywords: lungs pattern, dog, Computed Tomography

Introduction

Computed tomography is considered to be the best imaging modality for pulmonary parenchyma assessment. High resolution computed tomography (HRCT) is capable of providing morphological details of normal and abnormal pulmonary parenchyma and has been widely accepted in human medicine as an imaging gold standard in lung parenchyma assessment. Many reports have confirmed the high diagnostic value of this technique, particularly in the study of diffuse or generalized pulmonary disease where the HRCT protocol allows imaging at intervals of 10 or 20 mm. Spiral CT, and in particular CT spiral multi-detector rows, has made enormous changes in imaging and also has significant potential for the study of lung parenchyma.

This procedure is indeed capable of generating volumetric high resolution images that provide a continuous and detailed view of lung parenchyma. This view is no longer limited to the axial plane, as multi-plane reconstructions and three-dimensional volumetric reconstructions can easily be accomplished. In addition, very detailed imaging of pulmonary parenchyma is no longer reserved for diffuse and interstitial lung diseases being available for the study of all lung pathology.

Materials and Methods

The CT examination was performed on 30 dogs aged between 1 and 11 years, with different breeds, age and sex. The cases were selected from patients examined in the radiology laboratory of the Faculty of Veterinary Medicine during 2016-2018.

Before the CT examination the patients were clinically examined, the weight was measured, and an individual anesthetic protocol was determined for each patient.

The CT examination was performed using a 16-slices Siemens Somatom Scope. To obtain images, a matrix of 512X512, 130 Kv, 110-120 mAs, total collimation of 9.6, a pitch of 0.5-0.8 was used.

Chest scanning was performed with the patient in the dorsal decubitus, this position helps to reduce breathing artifacts.

For scanning, the default chest and abdomen protocol were used, giving a cross-scan at a thickness of 3-5 mm. Scanning at this slice thickness allows to reduce the amount of time needed to get images and reduce breathing artifacts. After the scan, the images were processed to achieve transversal, dorsal and sagittal multi-planar reconstruction (MPR) at 1 or 2 mm, using soft tissue and pulmonary reconstruction windows.

Images obtained through MPR reconstruction were post-processed using DICOM viewer software (HOROS Dicom), this program allows the contrast to be changed, making it possible to highlight the aspects of lung parenchyma.

Results and discussions

The principle of interpreting a CT scan of the chest cavity is based on three principles: 1) Proper identification of lung patterns; 2) Modality of distribution of changes in pulmonary parenchyma; 3) Correlation of information obtained from CT imaging and patient history.

Depending on the appearance of the lesions, the changes in the pulmonary parenchyma can be categorized into four categories (Verschakelen and Wever, 2007):

- Changes associated with increased pulmonary opacity (increased pulmonary attenuation).
- Changes associated with decreasing pulmonary opacity (low pulmonary attenuation).
- Changes that cause nodular opacities.
- Changes that cause linear opacity.

The increase in attenuation of pulmonary parenchyma is determined by the increase in density. The density of pulmonary parenchyma on the CT image is slightly higher than that of air, being determined by three components: pulmonary tissue, blood from capillaries and tissue and air.

Pulmonary opacity is determined by:

- The thickness of the parenchyma,
- Increased pulmonary blood volume or pulmonary vessel distention,
- When the relative amount of air from the lungs decreases, which may be the result of loss of lung volume or of the replacement of air in the alveoli with fluid and / or cells.

Increasing pulmonary attenuation is often the result of two or more of these processes. Depending on the degree of involvement of lung parenchyma, two types of increased opacity can be described:

- Appearance of ground glass or ground glass attenuation when lung parenchyma is mildly affected (fig. 1),
- Consolidation when parenchymal damage is more advanced (fig. 2).

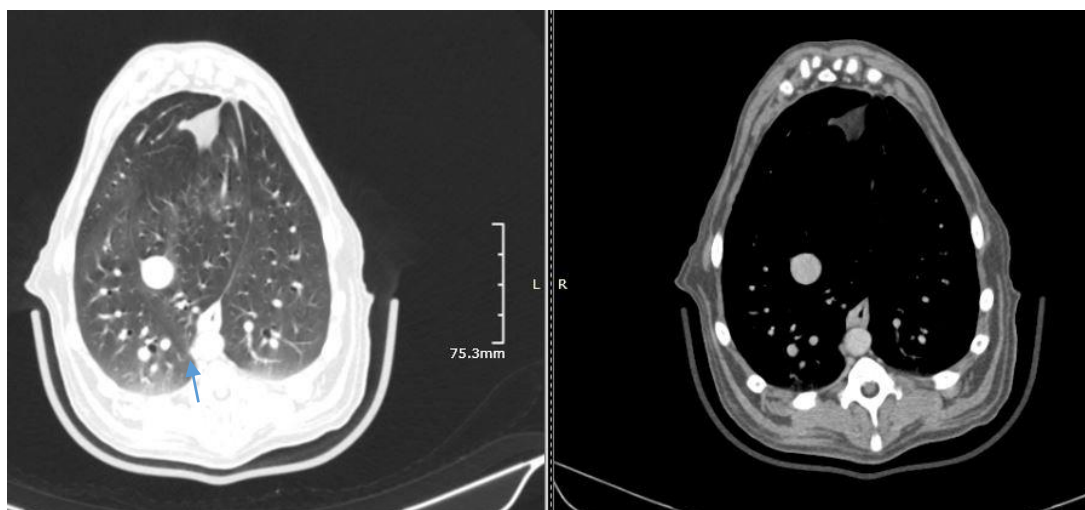


Figure 1 Ground Glass attenuation (arrow), lung window and soft tissue window

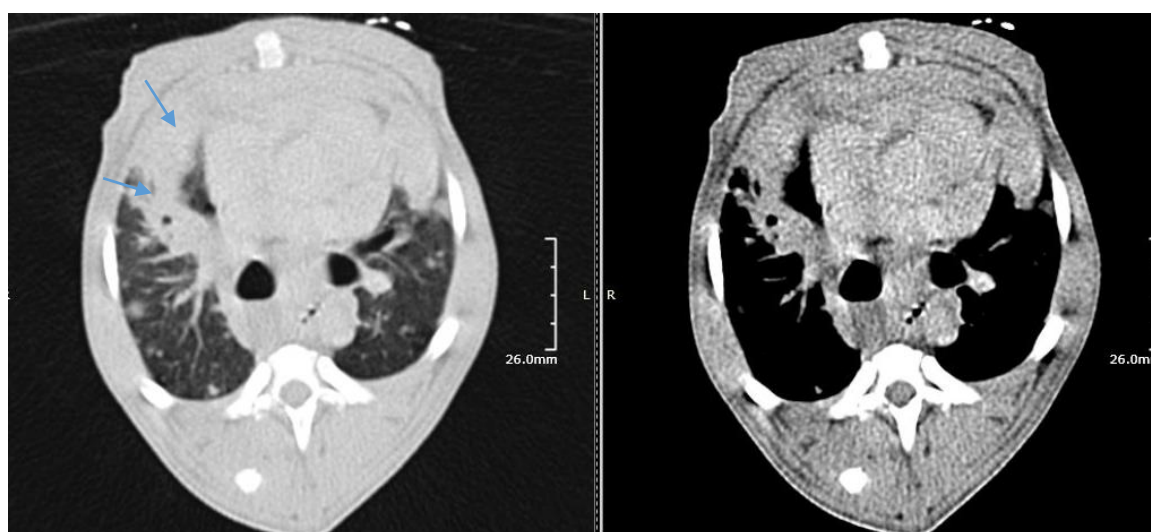


Figure 2 Consolidation of the lung parenchyma

The term ground-glass attenuation is used to describe a diffuse modification of the opacity of the pulmonary parenchyma while preserving the bronchial-vascular demarcation (Austin et al., 1996, Verschakelen and Wever, 2007).

Pulmonary consolidation, on the other hand, always has a pathological implication and this term is used to describe an increase in attenuation of lung parenchyma that masks delineation of vessels and airways (Austin et al., 1996, Tuddenham 1984, Webb et al. 1993).

Compared to increased pulmonary attenuation, decreasing pulmonary attenuation is partly caused by opposite phenomena. An abnormal increase in air volume, an abnormal decrease in intravascular blood volume and, as a result, an abnormal size of vessels that are beyond CT

resolution, but also tissue destruction and loss of density are responsible for a decrease in pulmonary attenuation (fig. 3).

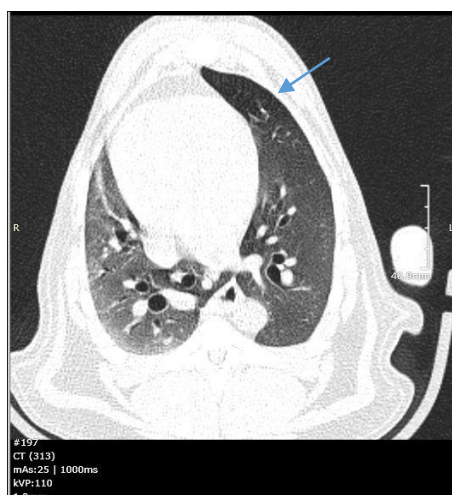


Figure 3 Decrease opacity on left cardiac lung lobe (arrow)

The nodular model (fig. 4) is characterized by the presence of multiple nodular opacities with a maximum diameter of 3 cm. A nodule with a diameter of less than 1 cm can be defined as a small nodule, while a nodule greater than 1 cm is often called a large node (Grenier et al., 1991). The term "micronodule" usually refers to nodules no larger than 7 mm in diameter (Austin et al., 1996). CT evaluation of the nodular model is based on:

- Their dimensions (small or large)
- Their appearance (well defined or undefined)
- Their attenuation (soft tissue density or matte glass)
- Distribution of these (lymphatic (peri) lymphatic, centrilobular, at random).

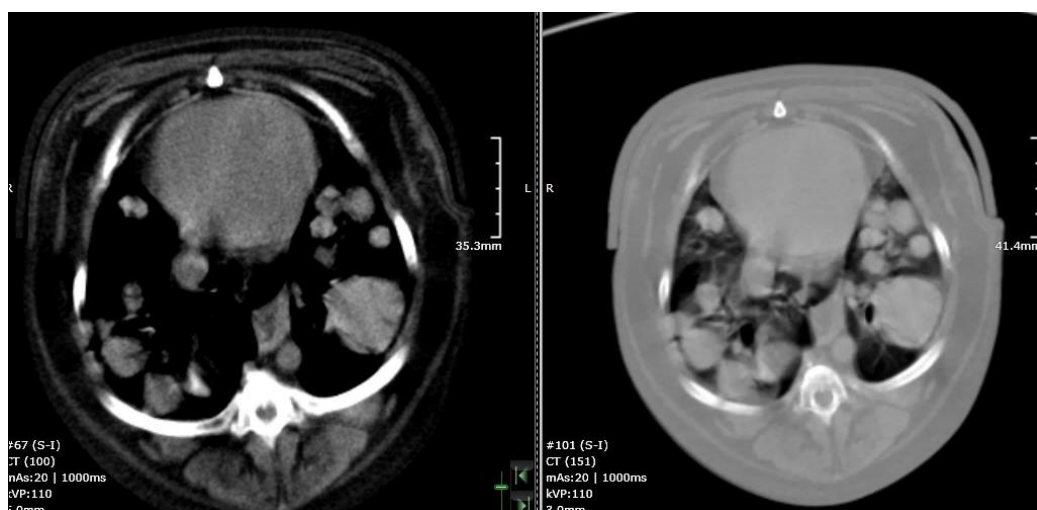


Figure 4 Nodular lung pattern (soft tissue window and bone window)

The evaluation of the nodule characteristics is based predominantly on the study of the edges (clear or unclear) and density (solid or matte glass). Using these features, pulmonary nodules can often be divided into interstitial nodules and alveolar nodules. Other characteristics such as the size, cavity and presence of calcium may be considered (Muller et al., 2003a-d; Tsuchiya 2005).

The linear model is characterized by the presence of several lines. Because these lines often intersect with each other, the term "reticular pattern" is also used. However, the appearance of a network aspect does not have to be present, while the number of lines can also be limited. In this situation, the term "linear opacity" is preferred (fig. 5). The differential diagnosis of pulmonary linear opacity is mainly based on the identification of their location and appearance (smooth, irregular) (Verschakelen and Wever, 2007).



Figure 5 Linear opacity of the lungs

Sometime a mixt pulmonary pattern is present, which often complicates the interpretation of anomalies. A combination of patterns may be caused by a new disease overlapped with an already existing lung disease (fig. 6).

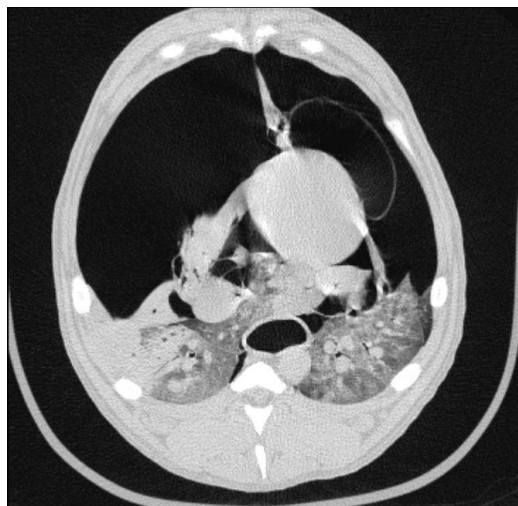


Figure 6 Mixt pulmonary pattern – lung emphysema

Conclusions

The correct diagnosis of lung disease involves the correlation of CT data with anamnesis, inspection, palpation, percussion, auscultation and laboratory examinations. The CT examination in lung disease in the dog has a major diagnostic relevance on the basis of which the lung model can be established in relation to the type of condition.

In the pulmonary CT examination, the interpretation of lung patterns is the key to establishing a correct diagnosis in lung disease. Depending on the affected lung area, several pulmonary models may be found: nodular pulmonary model, linear pulmonary model or mixed pulmonary model.

Acknowledgement

This study was performed in the Radiology department of FMV Cluj Napoca being part of internal department research grant.

References

8. Austin JH, Müller NL, Friedman PJ et al (1996) Glossary of terms for CT of the lungs: recommendations of the Nomenclature Committee of the Fleischner Society. *Radiology* 200:327–331
9. Muller N, Fraser R, Lee K et al (2003d) Miscellaneous pulmonary diseases. In: Muller N, Fraser R, Lee K (eds) *Diseases of the lung. Radiologic and pathologic correlations*, 1st edn. Lippincott, Philadelphia, pp 352– 376
10. Grenier P, Valeyre D, Cluzel P et al (1991) Chronic diffuse interstitial lung disease: diagnostic value of chest radiography and high-resolution CT. *Radiology* 179:123– 132
11. Tsuchiya R (2005) Implication of the CT characteristics of subcentimeter pulmonary nodules. *Semin Thorac Cardiovasc Surg* 17:107–109
12. Tuddenham WJ (1984) Glossary of terms for thoracic radiology: recommendations of the Nomenclature Committee of the Fleischner Society. *AJR Am J Roentgenol* 143:509–517
13. Verschakelen J.A., W. De Wever , 2007 , *Computed Tomography of the Lung A Pattern Approach* , Ed. Springer

HYSTEROSALPHYNGOGRAPHY IN FEMALE DOGS

Radu LĂCĂTUȘ¹, Octavian DUȚĂ¹, Raul Alexandru POP¹, Sorin MÂRZA¹, Laura CONDOR¹
Robert Cristian PURDOIU¹

¹University of Agricultural Sciences and Veterinary Medicine Cluj Napoca, Romania, Calea
Manastur 3-5

Corresponding author: robert.purdoi@usamvcluj.ro

Abstract

Hysterosalpingography (HSG, uterine and fallopian tube radiography) is a medical procedure performed to visualize radiological examination of the female genitalia and to test the permeability of the fallopian tubes. The main problems of the genital apparatus in the bitch are: Ovarian cysts so that the female may no longer be in the estrus or may show signs of continuous estrus, obstructions of the fallopian tubes, uterine and vaginal tumors, metritis, pyrometer.

Key words: bitch, genital apparatus, Visipaque, radiography.

Introduction

Hysterosalpingography (HSG, uterine and fallopian tube radiography) is a medical procedure performed to visualize radiological examination of the female genitalia and to test the permeability of the fallopian tubes.

The purpose of this study was to highlight the permeability of female genital tract using a non-ionic contrast agent, technically known as hysterosalpingography.

The objectives of the study are:

Identification of a method of approaching the female genital apparatus by means of special instruments for the purpose of hysterosalpingography. Determining the amount of non-ionic contrast agent required for hysterosalpingography. Identifying the best approach and radiological exposure of the posterior train to achieve hysterosalpingography in the bitch.

Material and methods

The biological material was represented by a 7 females' dog of different breed, age and sex. The patients were sedated using an association of ketamine and xylazine 2%. A catheter was inserted into the vagina and cervix (fig 1) using radiological guidance (fig 2). The contrast media used was represented by Visipaque 320, the doses were between 4 and 6.5 ml of contrast. After the contrast was injected, for each patient 2 exposure were obtained, one in latero-lateral view and the second one in dorso-ventral view.



Figure 1. Catheterisation of the cervix

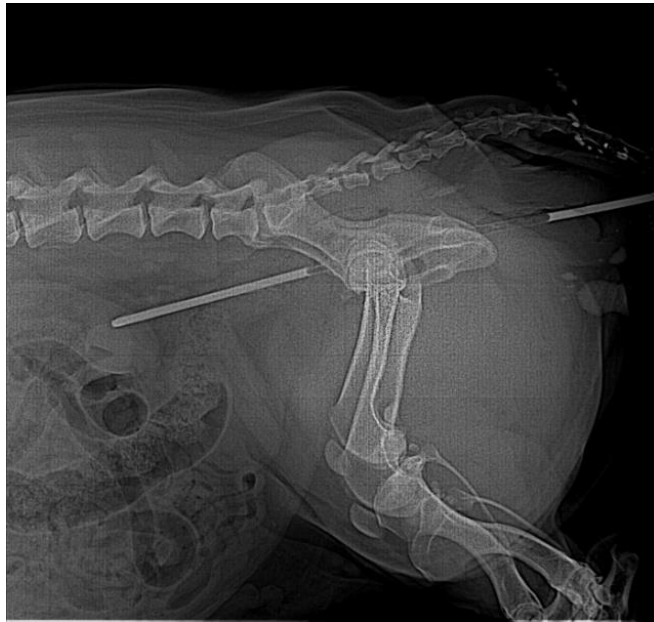


Figure 2 Radiographic evaluation of cervix catheterisation

Results and discussion

Administration of contrast media highlight the cervix and the uterine horn depending of the dog position and the position of the horns. If the patient is put in latero-lateral recumbency, the lower horn will be filled first with contrast (fig 3). Other aspect that influence the contrast diffusion is given by the permeability of the uterine horn due to oestrus period (River and Johnston, 1991). The best diffusion of the contrast into the uterine horn is in estrus (Filedman and Nelson, 2004). Dorso-ventral exposure evidentiates both uterine horns (fig. 4).



Figure 3 Latero-lateral exposure of the uterine horn



Figure 4 Dorso-Ventral exposure of the uterus

The presence of air will affect the contrast distribution in the uterine horn giving the impression of uterine obstruction (fig 5). In case of uterine obstruction, the flow of contrast will be interrupted or there will be no contrast present in the uterine horns (fig. 6)



Figure 5 Presence of air in the right uterine horn

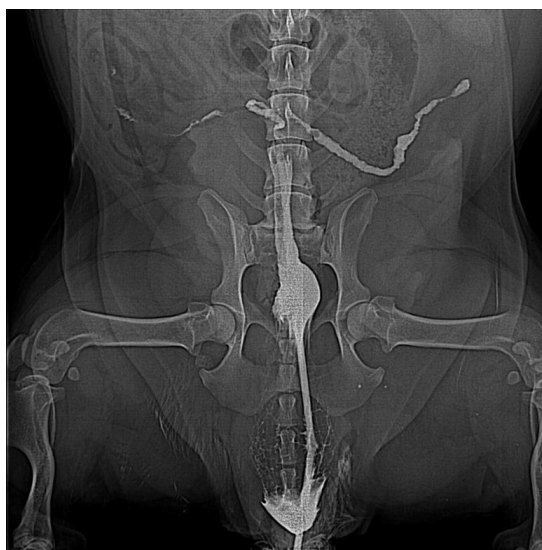


Figure 6 Abnormal flow of contrast in the left uterine horn

Discussion

One of the reasons that the HSG is not used widely in the veterinary field is because the difficult technique for cervix catheterization. The contrast distribution is influenced not only by the body position but also by the position of the uterine horns that could produce uneven contrast intake. Other possible situation that have to be taken in consideration is the rupture of the uterine horns due to increased pressure (Ackerman, 1981).

Acknowledgement: the studies was conducted in the laboratory of Medical Imaging – Radiology and are part of the internal grand research conducted by the Radiology laboratory.

References

1. Ackerman N, (1981) Radiographic evaluation of the uterus: A review. *Vet Radiol* 22:252
2. Feldman E.C and Nelson R., (2004) *Canine and Feline Endocrinology and Reproduction*, Saunders, USA
3. Rivers B and Johnston GR, (1991), *Diagnostic Imaging of the Reproductive Organs of the Bitch: Methods and Limitations*, 21(3):437-466

IDENTIFICATION OF DORSAL CUTANEOUS PERFORATOR VESSELS USING ANGIO CT TECHNIQUE

Radu LĂCĂTUȘ¹, Iulian MOLDOVAN¹, Ileana MATEI², Filip ARDELEAN², Cosmin PEȘTEAN¹, Sorin MĂRZA¹, Laura CONDOR¹, Robert Cristian PURDOIU^{1*}

¹University of Agricultural Sciences and Veterinary Medicine Cluj Napoca, Romania, Calea Manastur 3-5

²Rehabilitation Hospital Cluj Napoca, Str. Viilor, 46-50, Cluj Napoca, Romania,
Corresponding author: robert.purdoiu@usamvcluj.ro

Abstract

The pig is used very often as an experimental model in plastic surgery. Identification of the correct skin flap require also identification of the cutaneous perforate vessel that irrigate the flap. The contrast medium used in radiology and CT have the capability to highlight the small vessel of the skin.

Key words: pig, CT angiography, dorsal cutaneous perforator.

Introduction

In order to ensure a reconstructive similitude as large as possible, but also to reduce the morbidity of the donor and recipient areas, as well as the surgical time for free flaps, surgeon preoccupation has been to develop and increase the applicability of local or regional flaps, based on cutaneous perforators.

Through this study, we aimed to improve the technique of detecting the main cutaneous perforator vascular branches in the dorsal region of the pig, via angio-CT.

Material and methods

The biological material used in the research was represented by a group consisting of 5 PIC F II pigs (3 females and 2 males) with body mass ranging from 25 kg to 40 kg.

Choice of pig type: Given the morphological characteristics of pig breeds to achieve the proposed objectives, namely the detection of the main perforated vascular branches at the whole-body surface area of the pig, we chose the PIC-F 11-337 meat hybrid. We have chosen this type of hybrid because:

- the fat layer is small;
- has a good ability to adapt to the new environmental conditions encountered in the research environment;
- has increased resistance to diseases and pests.

For preoperative angiographic exploration, the pigs were sedated by intramuscular or intravenous (neurolept-analgesia) anesthesia with 0.1-0.2 ml/kg Narcoxyl 2 (20 mg / ml hydrochloric xylazine), 0.05 ml/kg Stresnil (azaperone 40 mg / ml) and 0.1 ml/kg Ketaminol 10 (100 mg / ml hydrochloric ketamine).

For angiography the contrast delivery was done using an automated CT 9000 ADV Contrast Delivery System, manufactured by Mallinckrodt. The device is designed to inject radio-opaque material into the vascular bed, making it easier for the doctor to diagnose a diagnosis. The contrast media was represented by Omnipaque 350 in dose of 2.5 ml/kg.



Figure 1 Ct scanning

Results and discussion

The scanning was performed using bolus tracking technique. On the images obtained on the premonitoring scan a marker was set on the aorta. The automatic scan was started when the HU values registered on the aorta was greater than 100.

The first scan highlights the heart and main arteries (fig. 2, fig 3) and the deep muscular artery without putting in evidence de vascularity of the skin.

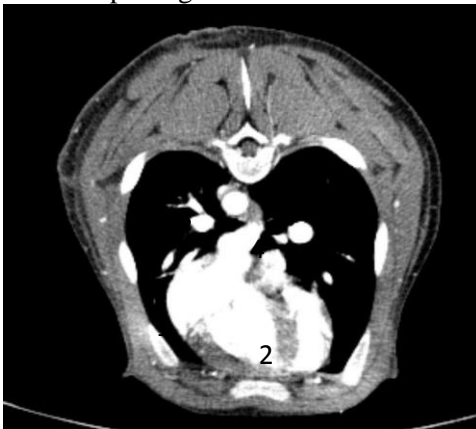


Figure 2 Axial scan in the arterial time. 1 – Left ventricle; 2 – Right ventricle; 3 – Aorta; 4 – Vena Cava

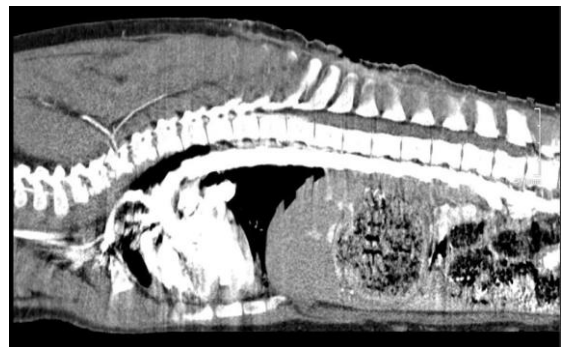


Figure 3 Sagittal scan in the arterial time

After 30 seconds from the first scan another scan was done in the venous time (fig. 4). The cutaneous perforants begins to be visible after 3 minutes after the bolus injection (fig. 5). The dorsal cutaneous perforants are more visible in dorsal MPR on the lateral side of the abdominal and thoracic area (fig 6).

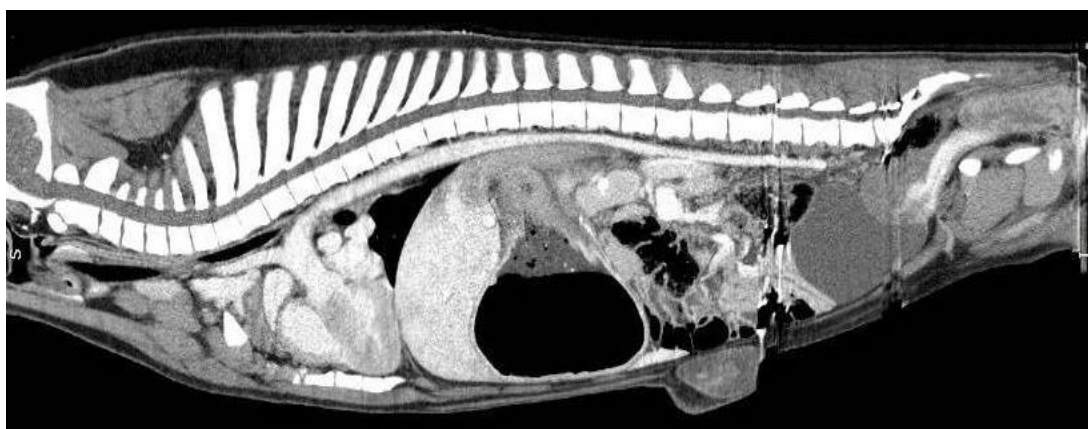


Figure 4. Sagittal scan in the venous time.

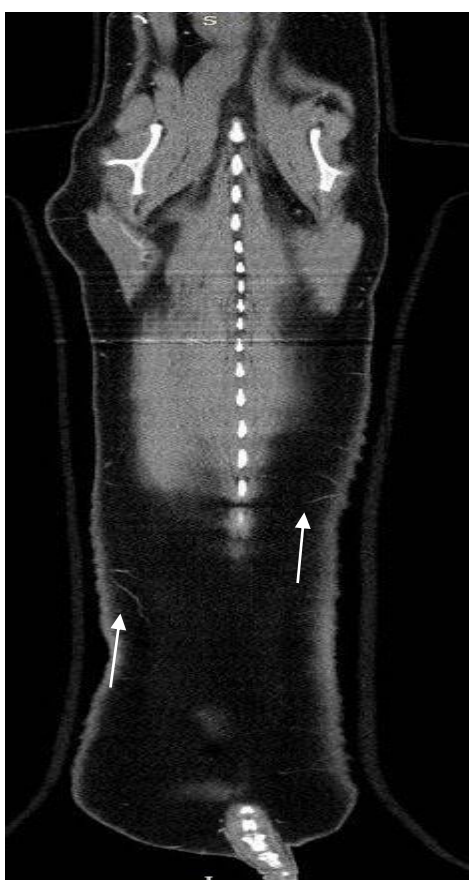


Figure 5 Presence of dorsal cutaneous perforants (white arrow)

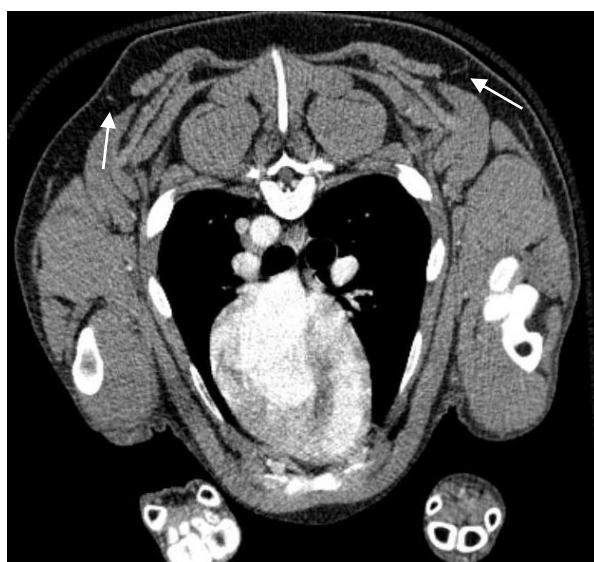


Figure 6 Thoracic cutaneous perforants (white arrow)

Discussion

Properly identifying the supply vessel of the cutaneous flap help reduce the morbidity of the donor site (Kirki and Narayan, 2012; Lăcătuș et al, 2016). Using Angio-CT technique the

surgeon is able to visualize the in real time the peripheral vascularization of the skin identifying the best area from where a skin flap can be prelevated. The most visible flap vascularization was evident in the dorsal-lateral abdominal area.

Acknowledgement: the studies was conducted in the laboratory of Medical Imaging – Radiology and are part of the internal grand research conducted by the Radiology laboratory.

References

1. Lăcătuș R., Ignat V, Scurtu I., Peștean C., Matei I., Ardelean F., Papuc I., Purdoi R.C., (2016) Identification of abdominal cutaneous perforator artery in pig using Angio-CT technique, *Lucrări științifice Medicina veterinară, Iași*, 59(4):373-375
2. Karki D and Narayan RP, 2012. Clinical Study. The versatility of Perforator-Based Propeller Flap for reconstruction of distal leg and ankle defects. *Hindawi Publishing Corporation Plastic Surgery International Volume 2012, Article ID 303247*

INCIDENTAL HISTOLOGICAL CHANGES IN THE CANINE CENTRAL NERVOUS SYSTEM

Mihai NEGRU, Marian TAULESCU, Cornel CĂTOI

Pathology Department, University of Agricultural Sciences and Veterinary Medicine,
3-5 Mănăştur Street, Cluj-Napoca, Romania
Email: mihaingr@yahoo.com

Abstract

The canine central nervous system pathology includes a series of histopathological changes, which are often underdiagnosed or misdiagnosed due to insufficient research in this field. The aim of the present paper is to emphasize the main cerebral changes identified incidentally in the canine species, involving 38 dogs from the Department of Pathological Anatomy (FVM Cluj-Napoca), diagnosed with various pathologies that did not develop nervous symptoms. Gross and histological exams of the encephalus from all dogs were carried out. The main important incidental findings of canine nervous system were represented by lipofuscinosis (68,4%), cerebral congestion and edema (47,3%) hemosiderosis (28,9%), neuromelanosis (21%), neuronal necrosis associated with satellitosis and neuronophagia (13,1%), vascular mineralization and diffuse meningeal fibrosis (13,1%). Perivascular cuffing and gliosis (13,1%), corpora amilacea bodies (5,2%), spheroid bodies (5,2%), have also been identified with a lower incidence. There have also been single-case findings during this study, represented by Alzheimer type II astrocytes, a psammomatous-type meningioma and parasitic Neospora spp. cysts. Thus, the results obtained and presented in this paper contribute to the enhancement of knowledge regarding the main lesions of the central nervous system in dogs, most of which were, at times, asymptomatic.

Key words: brain, canine, histopathology, incidental findings, lesions, nervous system, senescence.

Introduction

In the canine central nervous system (CNS), a large number of specialized normal structures, various unusual cell types, artifacts, findings of unknown significance and various postmortem changes are usually identified. Because of this plethora of neuropathological processes and postmortem or artifactual changes, a correct diagnosis may be difficult to establish for an inexperienced pathologist (Wohlsein et al., 2013). The CNS cell population consists of neurons, astrocytes, oligodendroglia, microglia, choroid plexus epithelial cells, vascular endothelial cells and ependymal cells. Anatomically, the CNS is arranged in two parts: 1) the gray matter, which is typified by neuronal cell bodies, axons, dendrites, neuropil, and 2) the white matter, which consists of axons, oligodendroglia, astrocytes and microglial cells (Zachary et al., 2012).

Due to the high sensitivity of the nervous tissue to over-manipulation and also the fast onset of postmortem autolytic changes and invasion of micro-organisms, it is mandatory for the pathologist to differentiate artifacts from authentic lesions. Various types of vacuolization, the presence of so-called “dark neurons”, cerebellar conglutination, Buscaino bodies, and shrinkage artifacts must all be taken in perspective as non-lesion changes of the nervous tissue (Wohlsein et al., 2013).

A large variety of histological alterations are common in the CNS of older individuals. These include: diffuse meningeal fibrosis, vascular mineralization, increased numbers of corpora amylacea within astrocytic processes near blood-brain or cerebrospinal fluid-brain interfaces, accumulation of lipofuscin and also neuromelanin in neurons from all of the brain regions (Mrak et al., 1997).

The aim of our study consists of identification of the main incidental lesions in the canine central nervous system in order to increase the degree of understanding of these various changes and help pathologists in elaborating a correct diagnosis.

Materials and methods

In this study, the central nervous system was evaluated in a total of 38 randomly selected dogs of different breeds (predominated by mixed breeds), aged between 1.5 and 18 years, registered in the Department of Pathology, Faculty of Veterinary Medicine Cluj-Napoca. The standard necropsy examination was performed in all the dogs included in the study, after which the encephalus was prelevated in 10% formalin for further histopathological examination. Four cross sections were processed through paraffin embedding techniques and hematoxylin-eosin staining for each brain. The first section was performed in the septal region of the telencephalon, anterior to the optic chiasm, crossing the cerebral cortex, the cingulate gyrus, the 1st lateral ventricle and the basal nuclei (putamen, claustrum, caudate and globus pallidus). The second section was performed in the diencephalon, caudally to the mammillary body, passing through the cerebral cortex, cerebral white matter, lateral ventricle, ventricle III, claustrum nucleus, part of the hippocampus, pyriform lobe, thalamus and thalamic nuclei. The third section passed through the rostral colliculus of the mesencephalon, the lateral ventricle, substantia nigra, pyriform lobe, crus cerebri and hippocampus whilst the fourth and final section passed through the myelencephalon following the cerebellar vermis, crossing the cortex, white matter, pyramidal tract and fourth ventricle. The photomicrographs were taken using an Olympus SP 350 digital camera and Cell[^]B basic imaging software (Olympus Corporation, Tokyo, Japan).

Results and discussion

Lipofuscin

In the current study, we identified the presence of lipofuscin pigment within cytoplasm of neurons (Fig. 1 A-D) in 26 cases, from the age of 3 to 18 years. There was a significant increase in lipofuscinosis relative to age. Unlike case 8 (aged 3 years) where lipofuscin was present in a small number of neurons, lipofuscinosis was marked in cases 30-38 (ages 14-18), the pigment being present in large quantities in most neurons.

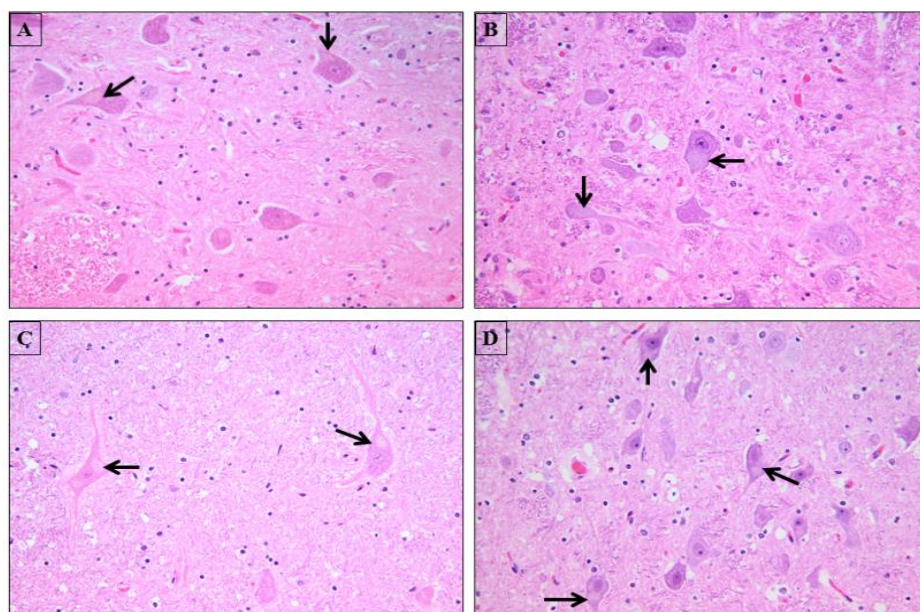


Figure 1. A-D. Neuronal lipofuscinosis, dog. The microphotographs showing intracytoplasmic yellow-brown granular pigment consistent with lipofuscin (arrows) HE stain, 20x.

Lipofuscin is a yellow-brown granular pigment resulted from oxidative metabolism of lipids, accumulating intracytoplasmatically in neurons, in variable amounts. The presence of moderate quantities of lipofuscine has a poorly understood pathological significance, especially in elderly dogs (Borràs et al., 1999). However, intracytoplasmic accumulation of lipofuscin predisposes neurons to oxidative stress. An advanced degree of lipofuscinosis can be associated with neurodegenerative diseases, leading to clinical manifestations (Marani et al., 2009).

The appearance of lipofuscin is similar in the case of H&E staining with the appearance of ceroids. Ceroids are also pigments of lipid origin, very similar to lipofuscin, but whose intra-neuronal accumulation is always considered to be pathological. Their presence can be correlated with either genetic diseases or enzymatic defects of metabolism. As oposed to lipofuscin which accumulates strictly in the neurons, ceroids can also appear extracellularly (Riga et al., 1995).

Neuronal ceroid lipofuscinosis is a neurodegenerative disease with autosomal recessive transmission, which usually starts in youth, the Bull Terrier, Staffordshire Terrier and the Irish Setter being the most prone breeds (Vandeveldt et al., 2012).

Neuromelanin

We found the presence of neuromelanin, especially in the 3rd section, in cases no. 16, 19, 22, 27, 31, 32, 33 and 37 (Fig. 2 A-D). We observed an increase of the neuromelanin pigment particularly in aged dogs. This demonstrates the accumulation of neuromelanin pigment with age due to prolonged action of oxidative stress and various toxic substances at this level throughout life (Zecca et al., 2008).

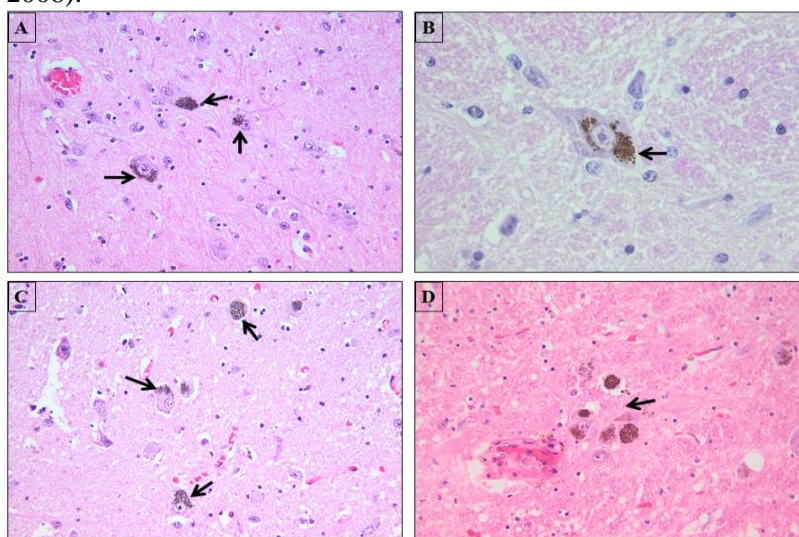


Figure 2. A, C, D - Photomicrographs showing the presence of a dark-brown intracytoplasmic pigment consistent with neuromelanin (arrows) HE stain, 20x;
B – Neuromelanin, HE stain, 100x.

Neuromelanin is a dark-brown intracytoplasmic pigment, very similar structurally to melanin. It is found in the hypothalamic neurons and in the neurons of the substantia nigra, gradually accumulating with age. Numerous studies have shown that neuromelanin has a role in chelating metal ions, protecting neurons from oxidative stress. Neuromelanin also protects against several classes of organic and inorganic toxins. In humans, the loss of dopamine neurons in the

substantia nigra pars compacta is correlated with the occurrence of Parkinson's disease (Zecca et al., 2001).

Spongiosis

In 7 cases (no. 32-38) we noted the presence of extensive spongiosis in both white and gray matter. This is correlated with the kidney and liver dysfunctions reported in the anamnesis and the lesions identified during the necropsy exam. Renal lesions were present in the following cases: no.33 - renal cortical necrosis, 35 – chronic interstitial nephritis, 34 and 36 with other causes of chronic renal failure (renal fibrosis and atrophy), 38 - acute renal failure (ethylene glycol poisoning). Hepatic lesions consisted of liver cirrhosis identified in case 32 and hepatic lipidosis in case 37, where we also found kidney damage (chronic kidney infarcts).

Spongiosis is a degeneration of the brain tissue, characterized by the presence of clear vacuoles of different sizes in the white and gray matter. This degeneration occurs due to the action of several pathogens, as well as in various intoxications and metabolic encephalopathies. Spongiosis occurs in the gray matter following vacuolization of neuronal processes, astrocyte edema, or degeneration of the myelin sheaths in the white matter. Also, diffuse spongiosis may be found in very old patients, being associated with gradual cerebral cortex atrophy (Bolon and Butt, 2011).

Actual spongiosis needs to be differentiated from artifactual vacuolization, the latter being encountered in samples that are not processed or fixed appropriately. Artifactual vacuoles have irregular shapes, are not clearly delimited and predominate in the white matter, whilst in the gray matter they appear as clear perineuronal, perivascular and periglial spaces (Vandeveld, 2012).

Hemosiderosis

During the histological examination we identified the presence of hemosiderosis in 11 cases. Hemosiderosis was associated with multiple haemorrhages in case no. 8 (Fig. 5-D) and the presence of congestion in cases no. 33, 29, 25, 23, 22 and 12.

Hemosiderosis represents the presence of intracellular hemosiderin, a ferric pigment resulting from the degradation of hemoglobin. These deposits occur either as a result of haemorrhages or chronic congestion (Stankiewicz et al., 2007).

Cerebral congestion

Cerebral congestion is associated with any kind of acute inflammation at this level, with cardiac pathologies or any mechanism that prevents blood drainage from the brain (Zachary and McGavin, 2007). In our study, different degrees of cerebral congestion were identified in 18 cases. The congestion present in cases no. 33, 25, 22 and 7 was most likely induced by chronic heart failure, confirmed by the presence of right dilative cardiomyopathy, respectively left cardiac hypertrophy identified during the necropsy exam.

Cerebral edema

In most cases where we identified congestion during the histological examination, there was also edema of the nervous tissue, located predominantly in the periventricular, submeningeal and perivascular regions (Fig. 3-B). Edema occurs in both white and gray matter as a non-specific lesion found in various pathologies of toxic, degenerative, inflammatory, neoplastic, vascular or traumatic nature. Edema of the central nervous system may be cytotoxic, caused by direct lesions to the glial cells (cellular edema) or vasogenic, due to alteration of the blood-brain barrier.

Vasogenic edema is predominantly found in the white matter and the cytotoxic type in the gray matter (Bolon and Butt, 2011).

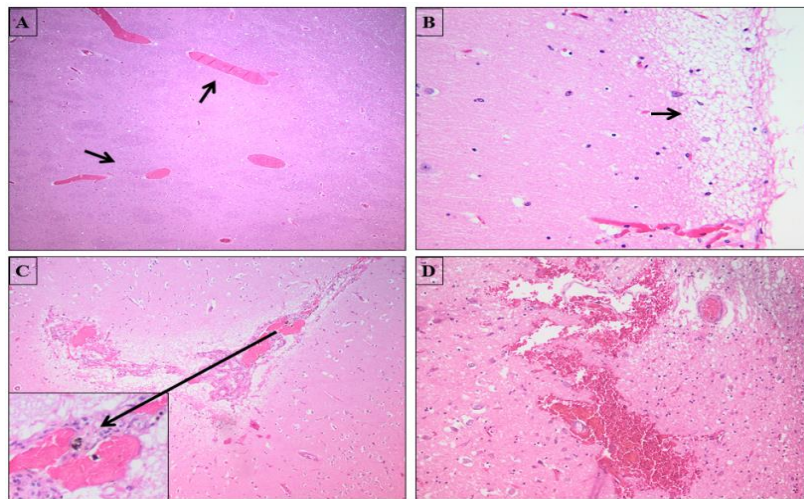


Figure 3. A - Blood vessel ectasia (congestion) (arrows), H&E stain, 4x;
B - Subpial edema of gray matter, H&E stain, 20x;
C - Presence of hemosiderin laden macrophages due to chronic congestion (arrows), H&E stain, 4x;
D - Severe cerebral hemorrhages, H&E stain, 20x.

Neuronal necrosis

The most extensive phenomenon of neuronal necrosis and neuronophagy was identified in cases no. 13, 14, 20, 21 and 24 (Fig. 4 B-D). In cases no. 13, 14 and 21, neuronophagia and marked satellitosis were associated with respiratory insufficiency. Neurons are very sensitive to decreased oxygen intake which directly causes necrosis. In cases no. 20 and 24, malignancies of the splenic hemangiosarcoma and mammary gland adenocarcinoma were identified; both lesions were associated with multiple hepatic metastases, being directly correlated with hepatic failure and neuronal injury.

Neuronal necrosis is always a pathological issue, being caused by extracellular pathogens such as ischemia, hypoglycemia, viral infections and trauma. Necrotic neurons are diminished in size, have a typical acidophilic and shrunken cytoplasm, and pyknotic nuclei. Neuronal necrosis should be differentiated from so-called “dark neurons” (Jortner, 2006).

Dark neurons (Fig. 4-A) are frequent artifacts in histological slides of nervous tissue which is over-manipulated before the fixation step. These neurons have a monomorphic appearance, the cytoplasm and nucleus are stained with the same intensity and perineuronal glial reaction is absent (Jortner, 2006). Necrotic neurons have a heteromorphic appearance with vacuolized and highly acidophilic cytoplasm, and are usually accompanied by inflammation (Garman, 2011).

Satellitosis and neuronophagia were identified in 5 of cases taken into this study, representing microglial responses to various neuronal injuries. Neuronophagia is the phenomenon by which activated microglia phagocyte cellular debris resulted from neuronal necrosis (Cantile et al., 2016).

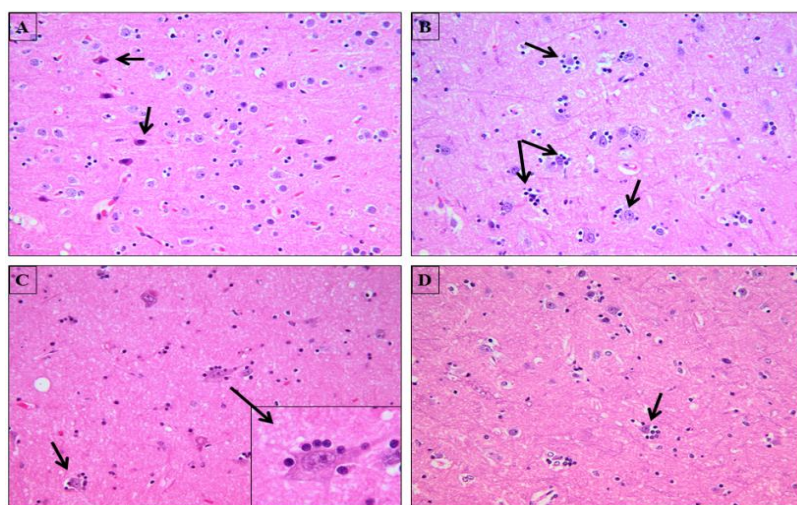


Figure 4. A - Microphotographs showing multiple artifactual “dark neurons” (arrows), H&E stain, 10x; B, C, D - Various stages of neuronal necrosis, satellitosis and phagocytosis (arrows), H&E stain, 20x.

Perivascular cuffing and gliosis are lesions associated with inflammatory (viral, bacterial, parasitic) or immune pathologies. We observed the presence of perivascular cuffing in 5 of the examined cases (Fig. 5 A-B).

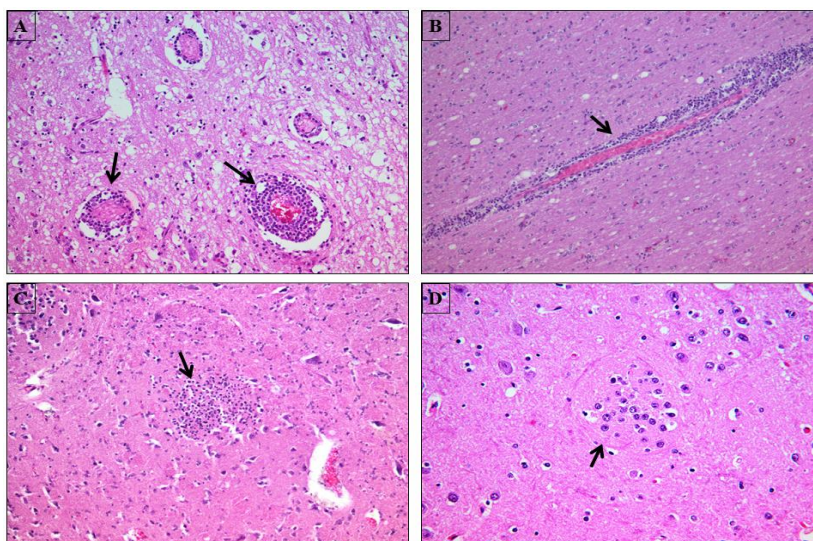


Figure 5. A, B - Severe perivascular cuffing of mononuclear cells within canine cerebral cortex, HE stain, 20x; C, D - Foci of microglial cells, HE stain, 10x, 20x.

Corpora amilacea bodies have been identified in cases 20 and 38, with no pathological significance (Fig. 6 - A, B, C). Morphologically, these are round structures with a concentric blade-like appearance, measuring between 10 and 50 μm . Development of these bodies occurs in the cytoplasm of astrocytes, being made up of glucose and protein polymers, and in their center are calcium salts. They are localized predominantly in the subpial and perivascular areas, being found

in small numbers in old dogs. Large agglomerations of such structures are found only in neurodegenerative diseases (Pisa et al., 2016).

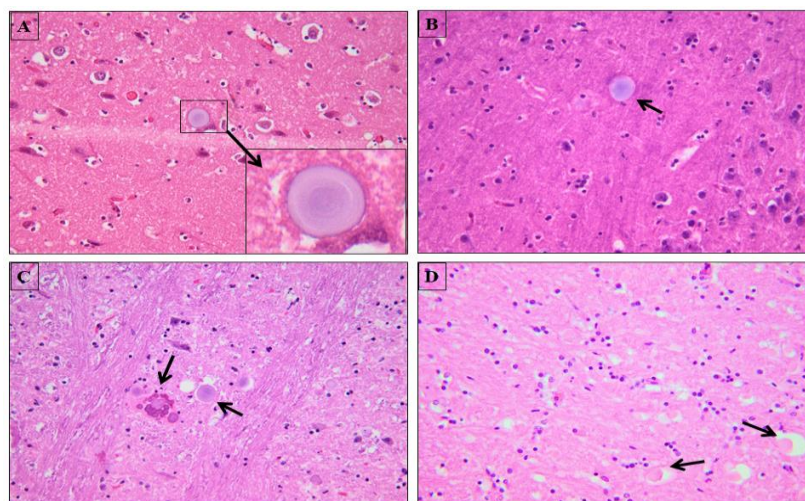


Figure 6. A, B, C – Microphotographs of brain tissue showing numerous round structures with a concentric blade-like appearance consistent with corpora amilacea bodies (arrows), H&E stain, 40x;
D – Multifocal axonal degeneration - Spheroid bodies (arrows), H&E stain, 40x.

Spheroid bodies

In this study, we identified the presence of spheroid bodies in cases no. 31 and 30 (Fig. 6 - D), in both situations in the 3rd section. Histologically, these are ovoid, homogeneous, eosinophilic formations found in the nervous substance. These structures are in fact a focal axonal degeneration, secondary to a degeneration of the myelin sheath. If these spheroid bodies are present in large numbers, the evolution of diseases manifested by axonal dystrophies must be taken into account (Wohlsein et al., 2012).

Other ***non-specific, senescence associated lesions*** found in 5 dogs aged between 12 to 17 years, consisted of vascular mineralization and meningeal fibrosis (Fig. 7).

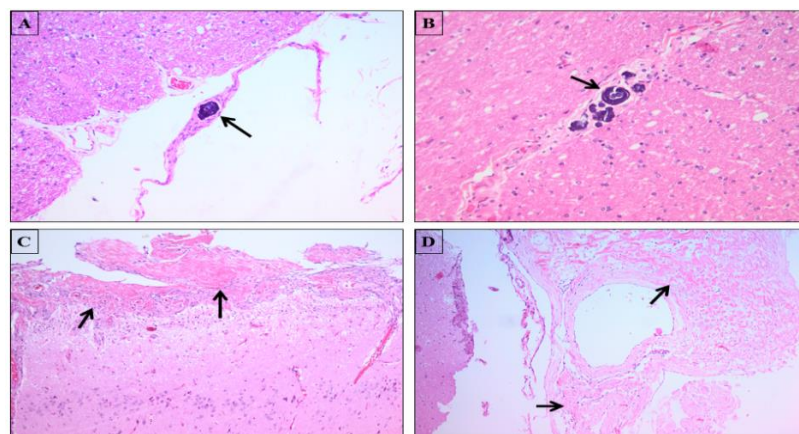


Figure 7. A, B - Microphotographs showing vascular mineralization in the canine CNS (arrows), H&E stain, 10x, 20x;
C, D – Age-related lesions - diffuse meningeal fibrosis (arrows), H&E stain, 10x.

Alzheimer type II astrocytes

In our study, the presence of Alzheimer type II astrocytes was associated with cerebral edema, congestion, perivascular glial reaction and extensive spongiosis in case no.28 (Fig. 8), a 14-year-old mixed breed dog. Mammary tumors, pulmonary metastases and liver cirrhosis were identified at the necropsy exam. In this regard and also considering the clinical manifestations of convulsions, it can be argued that these cerebral lesions are the expression of hepatic encephalopathy.

Type II Alzheimer astrocytes have large, vesicular nuclei which are arranged peripherally. These astrocytes are usually found in groups of two associated with hepatic encephalopathy due to excessive increase of neurotoxic ammonia in the blood (Norenberg et al., 2007). This histological change of astrocytes is more common in the cerebral cortex and basal nuclei (Mullen and Prakash, 2010).

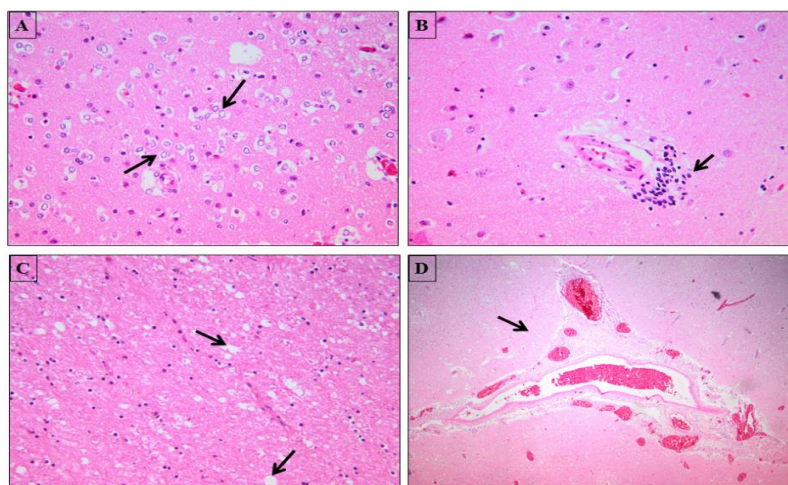


Figure 8. A - Microphotographs showing groups of Alzheimer type II astrocytes (arrows), H&E stain, 40x;
B - Moderate perivascular cuffing of mononuclear cells, H&E stain, 40x;
C - Presence of clear vacuoles of different sizes in the white matter - Diffuse spongiosis (arrows),
H&E stain, 20x;
D - Severe cerebral congestion and edema (arrow), H&E stain, 4x.

In case no. 26, a 14-year-old Pekingese with a clinical history of mammary tumors, we found a 2-cm-diameter, white-grayish mass in the frontal lobe of the cerebrum. It was well delimited by the nervous tissue, firm and had a slightly granular aspect. Compression atrophy of the frontal lobe was evident. During the histopathological exam, a *psammomatous-type meningioma* diagnosis was established (Fig. 9). Psammoma bodies are spherical structures having a concentric lamellar aspect, initially being clusters of neoplastic cells and collagen fibers that become calcified. They are commonly found in psammomatous meningiomas; the benign tumors account for about 40% of all primary cerebral tumors in the dog (Vandevelde, 2012).

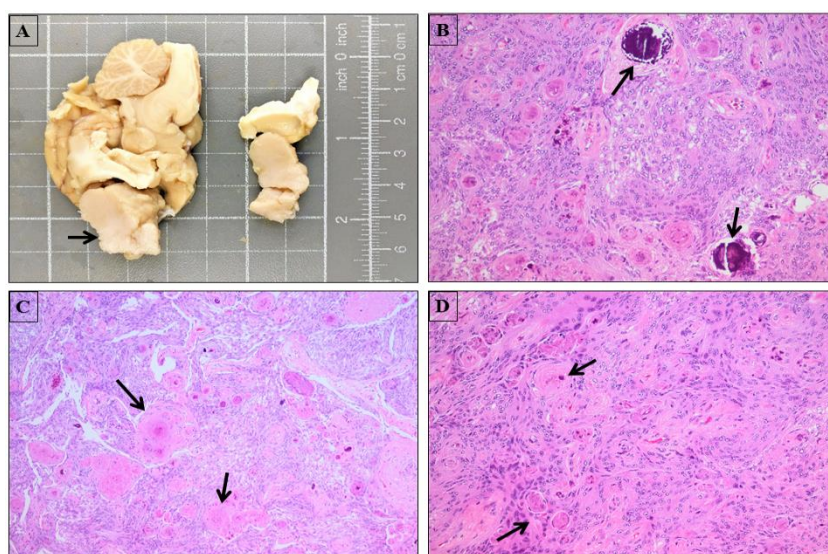


Figure 9. A - Presence of a white-grayish mass (meningioma) in the frontal lobe area of a 14-year-old dog (arrow);
B, C, D – Histological features of cerebral meningioma containing large numbers of psammoma bodies (arrows),
H&E stain, 20x.

Another aspect identified during this study was the presence of *parasitic Neospora spp. cysts* in the cerebellum of a 16-year-old standard Poodle dog (case 33).

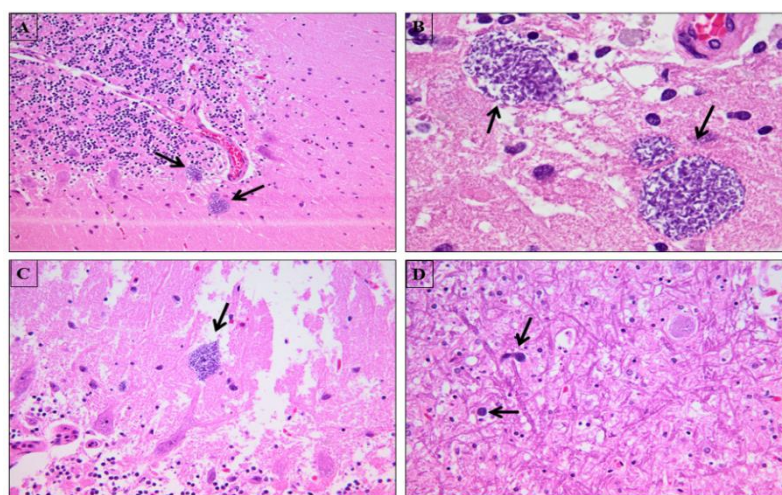


Figure 10. Microphotographs showing the presence of *Neospora spp.* cysts in the cerebellum of a 16-year-old standard Poodle dog (arrows). A, B, C, D, H&E stain, 10x, 100x, 20x, 4x.

Conclusions

This research provides additional information on the main incidental lesions that can be identified in the canine central nervous system, most of the subjects taken in this study being diagnosed with different morbid entities that did not involve the nervous tissue. Some cerebral

“lesions” are processing artifacts, such as dark neurons or pericellular vacuolization of the nervous tissue, that may pose diagnostic problems for pathologists.

The histological changes identified and presented in this study are relevant only in the context of their interpretation and correlation with the clinical symptoms and necropsy diagnosis, many of these not having an obvious clinical manifestation.

References

1. Bolon B., M.T. Butt, *Fundamental Neuropathology for Pathologists and Toxicologists*, Publisher Wiley, Nex Jersey, 2011, pg. 3-63, 125-139, 463-475.
2. Borrás D., I. Ferrer, and M. Pumarola, Age-related Changes in the Brain of the Dog, *Veterinary Pathology*, 1999, 36:202–211.
3. Cantile Carlo, Sameh Youssef, Chapter 4 – Nervous System. In: Jubb, Kennedy, and Palmer's *Pathology of Domestic Animals Volume 1*, Sixth Edition, Elsevier, 2015, pages 250-407.
4. Garman R.H., *Histology of the Central Nervous System, Toxicologic Pathology*, 2011, 39: 22-35.
5. Jortner Bernard, The return of the dark neuron. A histological artifact complicating contemporary neurotoxicologic evaluation, *NeuroToxicology Volume 27*, Issue 4, July 2006, Pages 628-634.
6. Marani E., K.G. Usunoff, H.K. Feirabend, Lipofuscin and Lipofuscinosis, *Encyclopedia of Neuroscience*, 2009, 481-486.
7. Mrak Robert E., W. Sue T. Griffin, David I. Graham, Aging-associated Changes in Human Brain, *Journal of Neuropathology & Experimental Neurology*, Volume 56, Issue 12, 1 December 1997, Pages 1269–1275
8. Mullen K.D, R.K. Prakash, *Hepatic Encephalopathy*, Publisher Humana Press, New York, 2010, pg. 7-35.
9. Norenberg M. D., A.R. Jayakumar, K.V. Rama Rao, K.S. Panickar, New concepts in the mechanism of ammonia-induced astrocyte swelling, *Metab Brain Dis*, 2007, 22, 219–34.
10. Pisa Diana, R. Alonso, A. Rabano, L. Carrasco, Corpora Amylacea of Brain Tissue from Neurodegenerative Diseases Are Stained with Specific Antifungal Antibodies, *Journal Frontiers in Neuroscience*, 2016,10:86.
11. Riga D., S. Riga, Lipofuscin and ceroid pigments in aging and brain pathology. A review. 1. Biochemical and morphological properties, *Rom. J. Neurol. Psychiat.*, 1995, 33,2. p. 121-136.
12. Stankiewicz J., S.S. Panter, M. Neema, A. Arora, C. Batt, R. Bakshi, Iron in Chronic Brain Disorders: Imaging and Neurotherapeutic Implications, *Neurotherapeutics*, 2007, 4(3):371-386.
13. Vandevelde M., R.J. Higgins, Anna Oevermann, *Veterinary Neuropathology Essentials of Theory and Practice*, Publisher Wiley Blackwell, 2012, pg. 7-80, 92-122, 129-191.
14. Wohlsein P., Deschl U., Baumgärtner W., Nonlesions, unusual cell types, and postmortem artifacts in the central nervous system of domestic animals, *Veterinary Pathology*, 2013 Jan;50(1):122-43.
15. Zachary J.F., M.D. McGavin, *Pathologic Basis of Veterinary Disease 5th Edition*, Publisher Elsevier Mosby, Missouri, 2012, pg. 771-839, 854-859.
16. Zecca L., D. Tampellini, M. Gerlach, P. Riederer, R. G. Fariello, D. Sulzer, Substantia nigra neuromelanin: structure, synthesis and molecular behaviour, 2001, *J Clin Pathol: Mol Pathol* 54:414-418.
17. Zecca Luigi , C. Bellei, P. Costi et al., New melanic pigments in the human brain that accumulate in aging and block environmental toxic metals, *PNAS* November 11, 2008 105 (45) 17567-17572.

HISTOLOGICAL ASPECTS CONCERNING THE STOMACH OF GRASS SNAKE *Natrix natrix*

Stefania Mariana RAITA, Valerica DANACU, Petronela ROSU, Bogdan GEORGESCU,
Florica BARBUCEANU, Raluca RIZAC

University of Agronomic Sciences and Veterinary Medicine of Bucharest, Faculty of Veterinary
Medicine

Bucharest, district 5, Splaiul Independenței no. 105

e-mail: stefania.raita@yahoo.ro

Abstract

Recent studies have described the importance of snakes, in relation to their utility in several medicinal fields. However, gaps are common in the field of snake histology, which is part of the basic knowledge on these animals. Similarly, not enough information has been published on the digestive system of the grass snake (*Natrix natrix*). *Natrix natrix* was first described in 1758, by Linnaeus. It is sometimes called the ringed snake or water snake, and it belongs to Reptilia Class, Squamata Order, Serpentes Suborder, Colubridae Family, *Natrix* Genus. The grass snake is widely distributed in mainland Europe, northern Africa and the Middle East. It is considered one of the most common snakes in Romania. The gastric wall reveals four layers: mucosa, submucosa, muscular layer and serosa. The mucosa has projections to the lumen, similar to those of the mammals and is composed of a lining epithelium with non-ciliated simple columnar cells (cambered), lamina propria and gastric glands. Lamina propria is composed of richly vascularized connective tissue. Two categories of glands were observed: mucosal glands, located on top, made of mucosal cells, with flattened nuclei at basal pole and vacuolar cytoplasm; serous glands, located at the bottom, made of serous cells, with central spherical nuclei and intensely colored cytoplasm. The submucosa is well represented and richly vascularized. The muscle layer of the wall was composed of an inner circular, and an outer longitudinal layer. the maximum thickness is associated with the posterior area. The serosa is composed of richly vascularized and innervated connective tissue.

Keywords: snake, gastric tissue, gastric tunics, glands

Introduction

An increased interest in the macro- and microscopical structures of the entire alimentary canal has been noticed in reptiles (Abo-Taira AM et al., 1988; Zaher MM at al., 1991; Abdeen AM et al., 1994) and has been highlighted by recent research (Gogone ICV et al., 2017). Modern snakes (*Serpentes* suborder snakes) belong to the *Ophidia* suborder. Most of the histological research on the members of *Squamata* Order has been directed to the members of *Lacertilia* suborder (Dehlawi G.Y et al., 1989), while not enough attention has been paid to *Ophidia* and subsequently *Serpentes* suborders. The gastrointestinal tract of the snake reveals several distinctions from mammals, birds and other reptiles. A review of the literature indicates that the stomach has a small non-glandular region, presenting low folds. After this small non-glandular section, glands begin to appear and gradually increase in number. The largest amount of glands appear in the middle area, with more branching folds resulting in a decrease in the lumen diameter (Khamas W. et al., 2011). This study aims at further in depth information acquisition on the gastric histological structure of *Natrix natrix* snake (of *Reptilia* Class, *Squamata* Order, *Serpentes* Suborder, *Colubridae* Family, *Natrix* Genus), which is one of the most common snakes found in Romania.

Materials and methods

Romanian *Natrix natrix* snake was used in the present investigation. A healthy specimen was caught nearby Bistra Forest, 35 km from Bucharest. The snake was dissected carefully by making a longitudinal incision at the mid ventral surface, the stomach was fixed in 10% formaldehyde solution and then stained with hematoxylin-eosin. Ten permanent slides were prepared. The examination and photography of the prepared slides was performed using a Motic Panthera microscope, with 4, 10 and 40x objectives.

Results and discussions

The gastric wall revealed four tunics: gastric mucosa, made of epithelium, glandular chorion and muscular mucosa. Submucosa is composed of abundant connective tissue, richly vascularized. The muscle layer of the wall was composed of two layers: one inner circular, and another outer longitudinal. The outermost layer of the stomach is the serosa, consisted of intensely vascularized connective tissue (fig. 1) .

The mucosa reveals numerous folds, oriented longitudinally, better represented and more obvious when the stomach is empty. Using a magnifying glass, gastric crypts (gastric infundibula) resulted from epithelial invagination, may be examined. At the bottom of these pits, gastric glands opening may be noticed. The gastric glands are located within the chorion (fig. 3). The surface epithelium of the gastric mucosa is made of simple columnar epithelium, also covering the crypts, consisting of two types of cells: tall columnar cells, at the surface of the mucosa and basal cells, with a wide basal pole and a narrow apical pole, this shape allowing for grouping at the bottom of the gastric pits. The columnar cells of the epithelium own oval nuclei, located within the inferior third of the cell height, as well as glycoproteic secretion specific organelles. The mucous-secreting columnar epithelium allows for mucus build-up at the apical pole. The basal epithelial cells account for surface epithelium cell supply, which they can replace in case of wearing or destruction. These cells have a lower secretory capacity, but keep mitotic ability (fig. 4). Simple columnar cells were also found in the gastric mucosal epithelium of other reptilians such as *Chamaeleon africanus*, in the geckos *Pristurus rupestris* or *Stenodactylus slevini* (Hamida H et al., 2014), in *Bothrops jararaca* and *Crotalus durissus* (Gogone ICV et al, 2017).

The chorion of the gastric mucosa is hosting the gastric glandular apparatus. The mucosal glands are located in contact with the basal membrane of the surface epithelium. They consist of mucosal cells with flattened nucleus, located at the basal pole and vacuolar cytoplasm. Deep within the mucosa, serous glands could be noticed (these cells are responsible for hydrochloric acid and pepsinogen production) (fig. 2-3). The serous cells are columnar, with spherical nucleus located within the basal third of the cell and intensively colored cytoplasm. These cells resemble the pancreatic or salivary glands serous cells. The muscular mucosa reveals two layers of smooth muscle cells: one inner circular and another outer longitudinal. These cells account for the mucosal movement, are responsible for lowering the venous pressure of the submucosa and promote secretion expelling from the gastric glands (fig. 5).

Submucoasa is made of richly vascularized connective tissue (fig. 7). The muscular layer is made of two smooth muscle layers: an inner circular and an outer longitudinal layer (fig. 6). These are responsible for peristaltic contractions which allow gastric chyme propulsion. These observations are in agreement with that of Zaher MM et al. (1991) and is supported also by the more recent research of Hamida H. et al. (2014). Serosa is constituted of mesothelial fasciculated tissue.

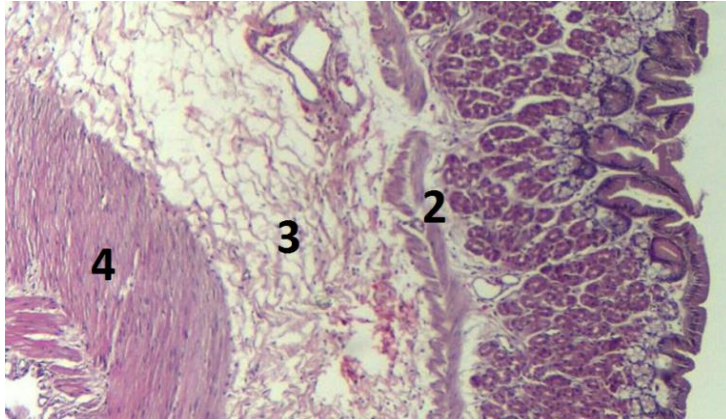


Figure 1 Snake stomach - overall view Ob. 4X (original) HE dye
1-gastric mucosa, 2 –muscular mucosa, 3 – submucosa, 4 – muscular layer

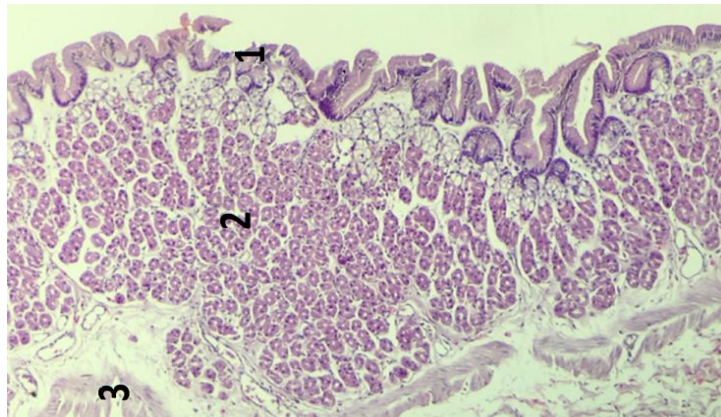


Figure 2 Snake stomach - overall view Ob. 4X (original) HE dye
1- Surface epithelium, 2 – mucosal gastric glands, 3 – muscular mucosa

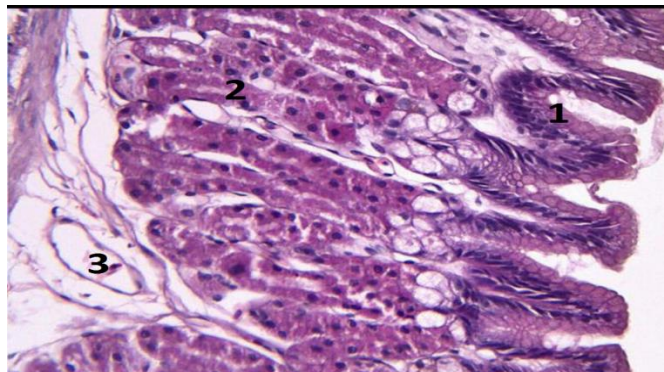


Figure 3 Snake stomach - overall view Ob. 10X (original) HE dye
1 – Simple columnar epithelium, 2 – gastric glands-longitudinal section, 3 – blood vessel

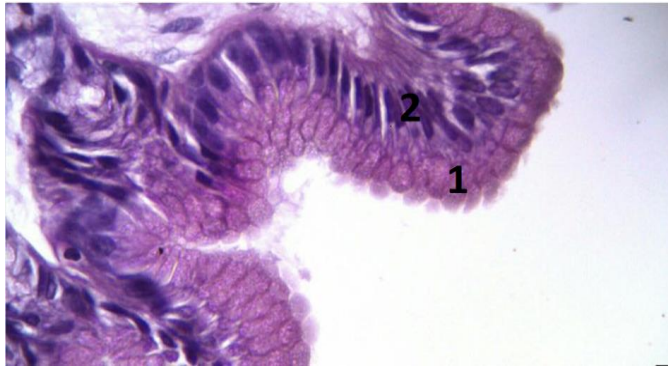


Figure 4 Snake stomach - overall view Ob. 40X (original) HE dye
1 – vacuolar cytoplasm at apical pole, 2 – columnar cell nuclei at basal pole

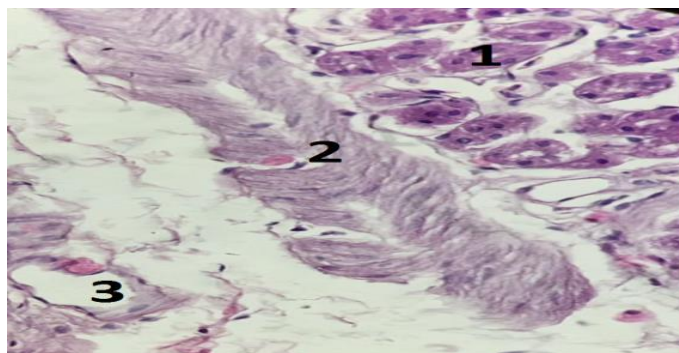


Figure 5 Snake stomach - overall view Ob. 10X (original) HE dye
1 – inferior gastric glands - cross section, 2- smooth muscular cell - diagonal section (muscular mucosa),
3 – blood vessel

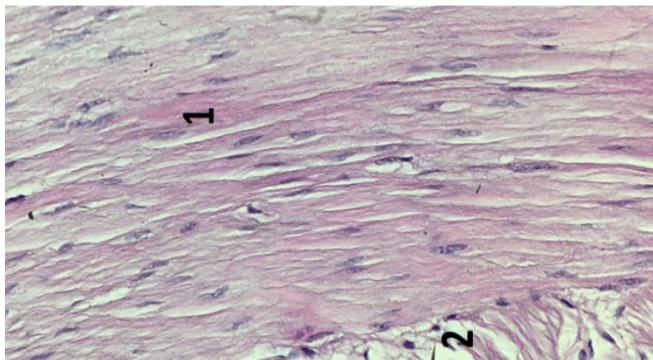


Figure 6 Snake stomach - overall view Ob. 40X (original) HE dye
1-inner circular layer of muscular gastric layer, 2 – outer longitudinal layer

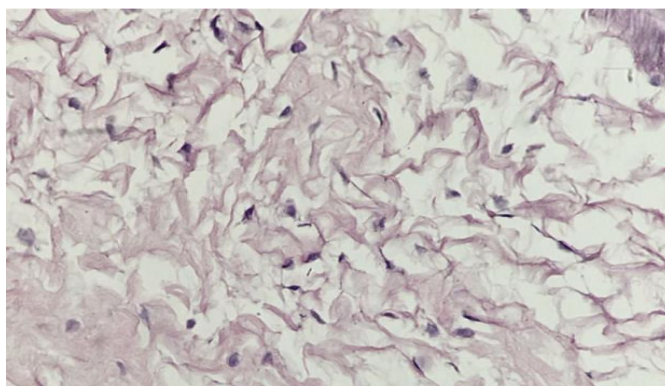


Figure 7 Snake stomach - overall view Ob. 40X (original) HE dye
Submucosal view – connective tissue present

Conclusions

The gastric wall revealed four tunics: mucosa, submucosa, muscular layer and serosa. The gastric mucosa revealed simple columnar epithelium and crypts which resemble those of the mammals. However, unlike for mammals, which have several categories of glands, the *Natrix natrix* gastric crypts shelter only two categories of glands. The submucosa is richly vascularized. The muscular layer is made of two smooth muscle cell layers, unlike the mammals, which have three layers. The serosa is made of mesothelial fasciculated tissue. Our results support those of other studies, concerning the structure of the gastric wall in snakes.

References

1. Abdeen A.M., Zaher MM, Abdel Kader IY, Abdel-Rahman AA. Anatomical, histological and morphometrical characterization of the gut mucosa of the colubrid snakes, *Malpolon monspessulanus*, *Coluber florulentus* and *Tarbophis obtusus*. J. Union Arab Biologists, 1994. 2(A): 283-337.
2. Abo-Taira AM, Zaher MM, Dehlawi GY, Mansour AB. Anatomical, histological and morphometrical studies on the alimentary tract of the snake *Natrix tessellata* (Family Colubridae). Egypt. J. Histol., 1988. vol. 11(2): 221-232.
3. Dehlawi GY, Zaher MM. Histological Studies on the Alimentary Tract of the Colubrid Snake *Coluber florulentus* (Family Colubridae). J.K.A. U.: Sci., vol. 1, 1989, p. 95-112.
4. Gogone ICV, Carvalho MP, Grego KF, SANT'ANNA SS, HERNANDEZ-BLAZQUEZ FV, Catao-Dias JL. Histology of the gastrointestinal tract from *Bothrops jararaca* and *Crotalus durissus*. Braz. J. Vet. Res. Anim. Sci., São Paulo, v. 54, n. 3, p. 253-263, 2017; DOI: 10.11606/issn.1678-4456.bjvras.2017.133256.
5. Hamida H, Abdel-Wahab El-Ghareeb, Zaher M, Essa A, Lahsik S. Anatomical, Histological and Histochemical Adaptations of the Reptilian Alimentary Canal to Their Food Habits: *Chamaeleon africanus*. World Applied Sciences Journal 30 (10): 1306-1316, 2014. DOI: 10.5829/idosi.wasj.2014.30.10.82395.
6. Khamas W, Reeves R. Morphological study of the oesophagus and stomach of the Gopher snake *Pituophis catenifer*. Anat Histol Embryol. 2011 Aug;40(4):307-13. doi: 10.1111/j.1439-0264.2011.01072.x.
7. Junqueira LC, Carneiro J. Histology - handbook & atlas, Editura Medicala Callistro edition 11, 2008 (in Romanian).
8. Zaher MM, Abo-Taira AM, Abdeen AM, Badr El-Din NK, Afifi AFM. Gastrointestinal tract of snakes: Contributions to gross anatomy, morphometry and microscopic structure of the alimentary tract in *Echis carinatus* (Viperidae). J. Egypt. Ger. Soc. Zool., 1991; 5: 469-488.
9. *** <http://herpetolife.ro/sarpele-de-casa-natrix-natrix/>
10. *** <http://www.zooland.ro/anatomia-si-fiziologia-serpilor-4175>
11. *** <http://www.jouefct.com/snake-anatomy-reproductive-diagram-images-download/>

HISTOLOGICAL RESEARCH OF THE MUSCULAR STOMACH IN STRUTHIO CAMELUS

**Ștefania Mariana RAITA, Valerica DANACU, Petronela ROSU, Bogdan GEORGESCU,
Florica BARBUCEANU**

University Of Agronomic Sciences And Veterinary Medicine Of Bucharest,
Faculty of Veterinary Medicine,
Bucharest, district 5, Splaiul Independenței no. 105
E-mail: stefania.raita@yahoo.ro

Abstract

For the histological study were used muscle stomach samples from 5 ostriches, age between 6 months and 3 years. Samples were prefixed in special containers in neutral formalin sol. 10%, after that were adjusted and refitted in the same type of fixator for 24 to 48 hours. The samples were included in paraffin cubes with Kunz instruments machine, then were cut to 3-5 μ m at the microtome. The histological sections were displayed on skimmed slides and kept properly until various staining methods were applied. Ostrich muscular stomach is relatively small, compared to waist, oval, pressed from sides, the most developed component being the muscular tunic. After the exterior appearance, it resembles with hen muscular stomach. (Figure 1). The cuticle that tapes the ostrich muscular stomach mucous is thicker and denser than in notglandular area of the glandular stomach. The cuticle is gathered in large loops and in its structure it is noted inclusion of the protean matrix and the presence of desquamated cells from the surface epithelium as cellular debris and nucleus fragments. The stomach mucosa is taped with a simple columnar epithelium, in lamina propria structure, observing the simple, parallel, tubular, ventricular glands of different sizes, depending on the area examined. On top of it, the glands are slightly lengthened and begin to lose their rectilinear appearance. Muscularis mucosae, unlike hen, for example, is present, but on certain portions it can no longer be observed, being united with the muscles layers. The lymphoid tissue from mucosa is also absent. The muscular layer is best represented, composed of smooth muscle fibers with the three layers: longitudinal outer, circular middle, with the largest consistency of the inner skew layer. Connective fibers are also found at this level. In most regions, there is no exact delimitation of the muscle layers. The aponevrotic layer includes parallel collagen fibers arranged in bundles, including elongated and flattened fibroblasts. The serosa belongs to the visceral peritoneum and is composed of typical connective tissue and mesothelium.

Keywords: epithelium, gland, muscular stomach.

Introduction

In Romania there are ostrich farms, proving that it is possible to grow it here as well. Investments are not high, and lower-end agricultural land can be used.

However, it is necessary to mention that, despite the growing interest in the issue of ostrich growth, many questions regarding the ostrich morphology and physiology are not fully elucidated in the scientific literature. The ostrich meat is very fine, with a pleasant, specific taste, characterized by a low cholesterol content of at most 32 mg per 100 grams of fat (1.2%), has a high protein content of about 22% and a rich range of microelements. An adult ostrich female, with a yield of 50 eggs a year, allows to be obtained 4 tons of meat per season.

There are very few published materials about the anatomy and histology of this bird. They usually contain information about the structure of the skeleton and breeding organs.

Particularly, the morphology data of this bird's digestive system are insufficient and quite succinct, being fragmentary and with general character.

In fact, knowing the structure of ostrich digestive system has not only a general biological importance but also a practical one.

Materials and methods

For the histological study were used muscle stomach samples from 5 ostriches, age between 6 months and 3 years.

Samples were prefixed in special containers in neutral formalin sol. 10%, after that were adjusted and refitted in the same type of fixator for 24 to 48 hours. The samples were included in paraffin cubes, then were cut to 3-5 μm at the microtome. The histological sections were displayed on skimmed slides and kept properly until various staining methods were applied. 50 histological preparations were obtained which were examined using the 4, 10, 25, 50 and 100 lenses.

Results and discussions

The ostrich muscular stomach wall from the inside to the outside shows: cuticle, mucous, muscular, aponevrotic layer and serous.

The cuticle that tapes the ostrich muscular stomach mucous is thick and dense. It is gathered in large loops and in its structure, at a closer examination, it is noted inclusion of the protean matrix and the presence of desquamated cells from the surface epithelium as cellular debris and nucleus fragments (Figure 2; Figure 3).

The stomach mucosa is taped with a simple columnar epithelium, in lamina propria structure, observing the simple, parallel, tubular, ventricular glands of different sizes, depending on the area examined. On top of it, the glands are slightly lengthened and begin to lose their recurrence. Muscularis mucosae, unlike hen, for example, is present, but on certain portions it can no longer be observed, being united with the muscles layers. The lymphoid tissue from mucosa is also absent.

In the optical microscope, the cuticle is formed from the lamellae: some arranged parallel to the mucosa surface and others arranged perpendicular to the mucosa surface (Figure 4).

The stomach mucosa is taped with a simple columnar epithelium, in lamina propria structure observing the simple parallel tubular ventricles of different sizes, depending on the area examined (Figure 5). To the base, the glands are slightly lengthened and begin to lose their rectilinear appearance (Figure 6). Epithelial cells have a spherical appearance, are basophilic, and their secretion is well highlighted from their upper third (Figure 3). In some segments, the ventricular mucosa is covered by a thick cuticle, continuously secreted by the cells of the ventricular glands (Figure 7), evidence of their secretion activity, evidenced by a positive histochemical reaction (Figure 8, Figure 9). These cells have a globular appearance at the base of the gland structure, gaining a cubic appearance. Thus, the hypothesis that the activity of these cells determines holocrine secretions, which underlie the production of compounds in the formation of cuticle layers, is highlighted (Figure 10, Figure 11).

The mucosal muscle, unlike the hen, for example, here is present, but on certain portions it can no longer be observed, being united with the muscles layers. The lymphoid tissue from mucosa is also absent.

The muscular layer is best represented, consisting of smooth muscle fibers with the three layers: longitudinal outer, medial circular, with the largest consistency of the inner skew layer (Figure 12). Conjunctive fibers are also found at this level (Figure 13). In most regions, there is no exact delimitation of the specified muscle layers.

The aponevrotic layer comprises parallel collagen fibers arranged in bundles, including elongated and flattened fibroblasts.

The serosa belongs to the visceral peritoneum and is composed of typical connective tissue and mesothelium (Figure 14).

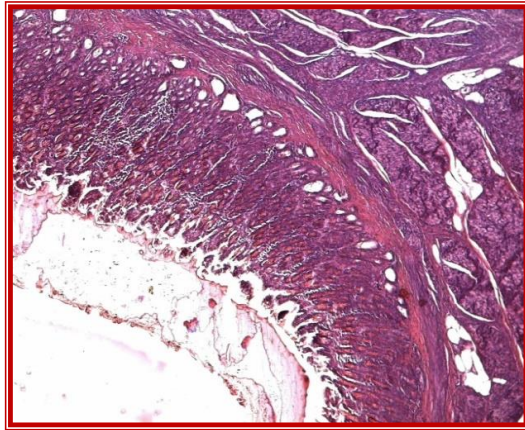


Figure 1. Muscular stomach. Hen. General view of the histostructure on muscular stomach. Col. HE x 25 (original)

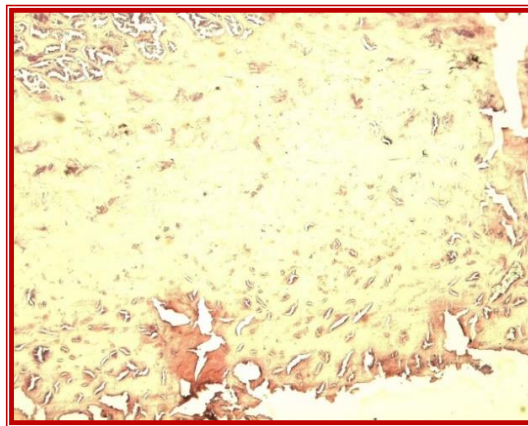


Figure 2. Ostrich. Detailed view of the ventricular cuticle. Presence of nuclear residues, of heterochromatic nucleus and of cauliflower-shaped surface formations. Col. HE x 50 (original)

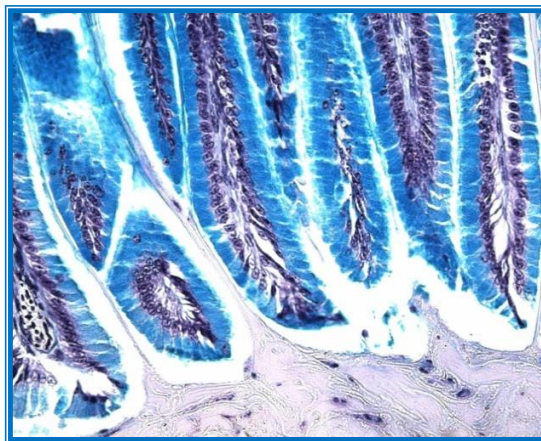


Figure 3. Muscular stomach. Ostrich. The presence in cuticle composition of protean matrix and exfoliated cells from the surface epithelium. Col. AA x 400 (original)

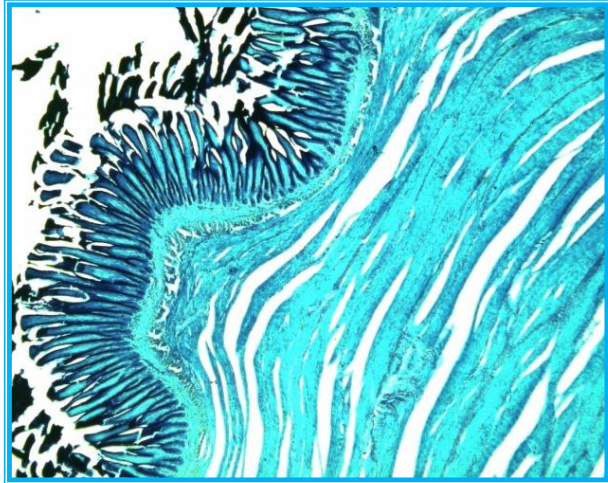


Figure 4. Ostrich. Muscular stomach. Image referring to the distribution of cuticular blades and muscle layer, which encompass muscularis mucosae
Col. HEV x 50 (original)

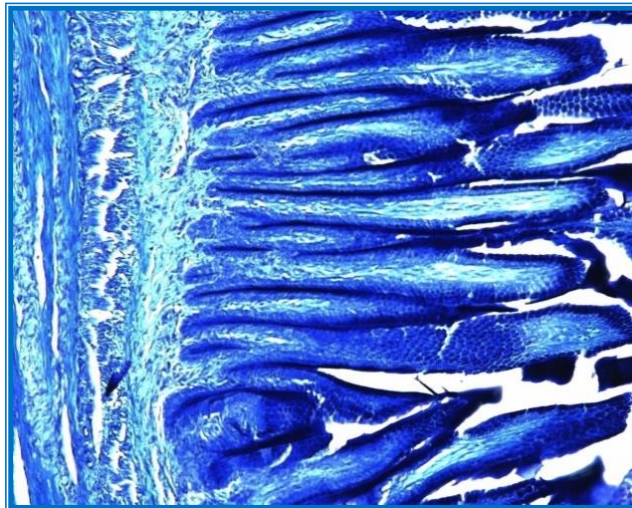


Figure 5. Ostrich. Muscular stomach. Lamina propria structure, with the distribution of simple tubular ventricular glands, in parallel position Col. AT x 200 (original)

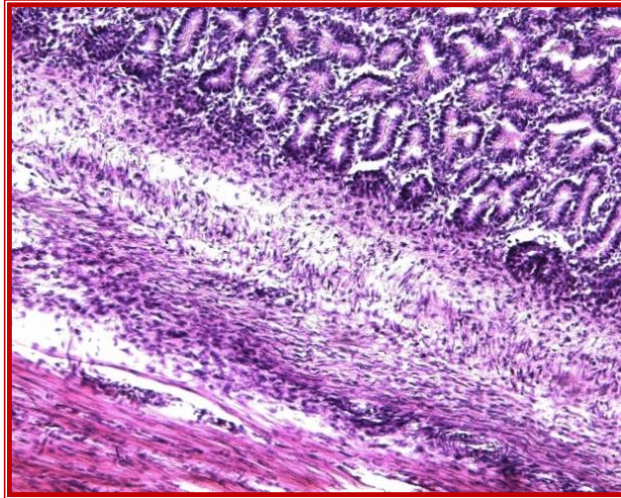


Figure 6. Ostrich. Muscular stomach. View of the widening of the glands from the ventricular mucosa toward its basis
Col. HE x 200 (original)

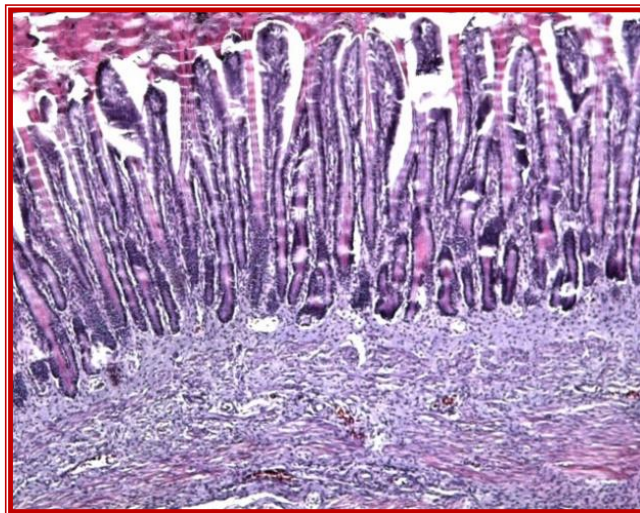


Figure 7. Ostrich. Muscular stomach. The formation of the cuticle
Col. HE x 100 (original)

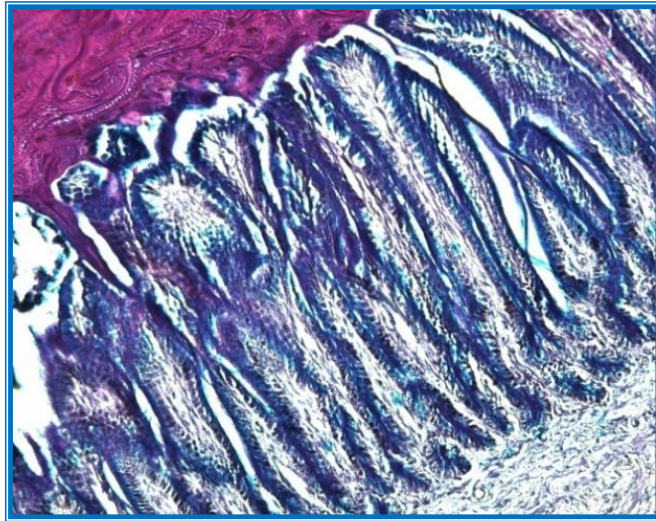


Figure. 8. Muscular stomach. Ostrich. Histochemical AA and positive PAS reaction
Col. AA-PAS x 200 (original)

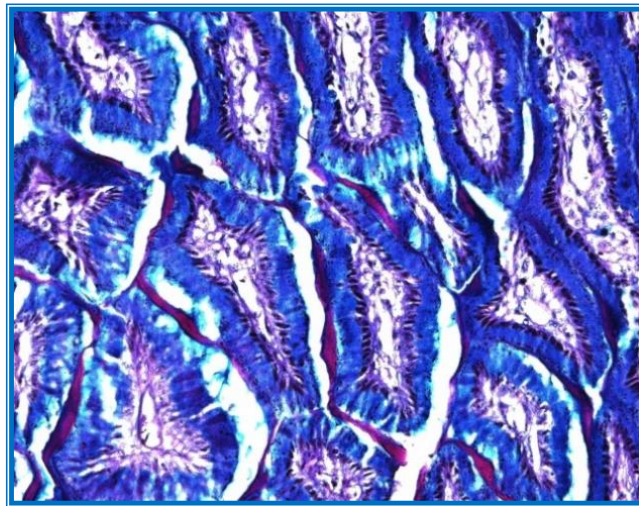


Figure 9. Muscular stomach. Ostrich. Detailed view of secretion products
of the ventricular glands
Col. AA-PAS x 400 (original)

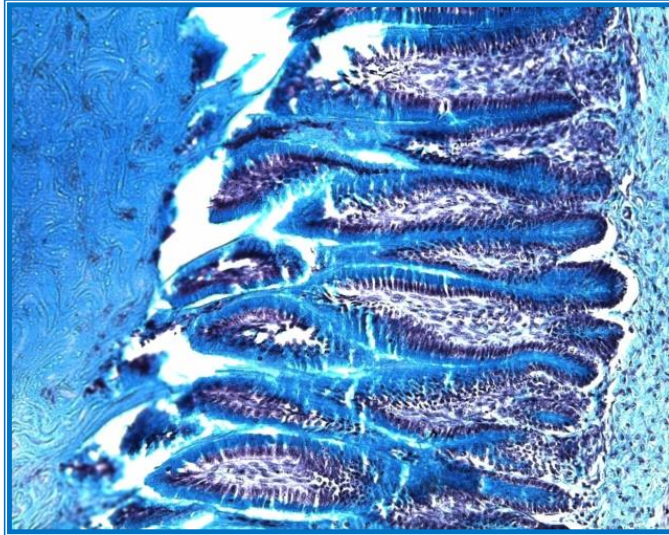


Figure 10. Muscular stomach. Ostrich. View of the continuous secretion activity of the glandular cells
Col. AA x 200 (original)

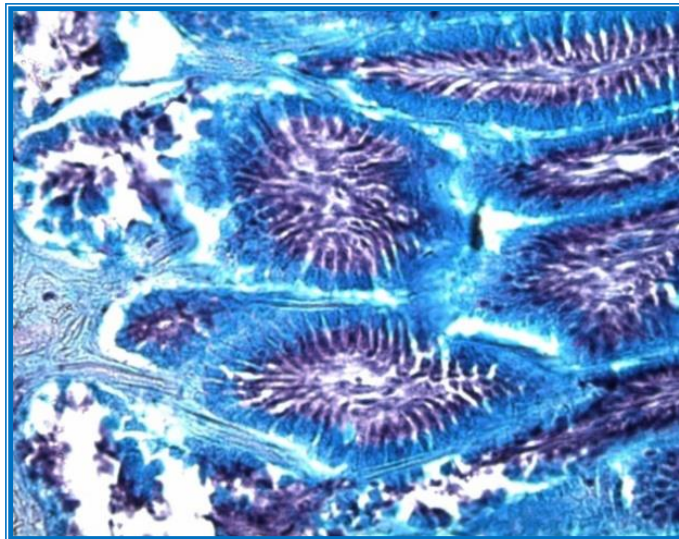


Figure 11. Muscular stomach. Ostrich. Detailed view of the glandular epithelium cells which produce MPG acids, highlighted through histochemical reaction with Alcian Blue
Col. AA x 400 (original)

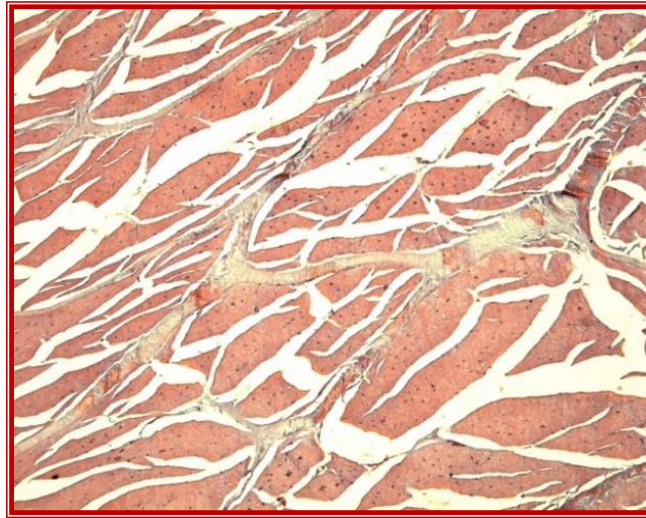


Figure 12. Ostrich. Muscular stomach. View of the external muscle layer, showing smooth muscle fibers and conjunctive fibers, blood vessels, nerves
Col. HE x 50 (original)

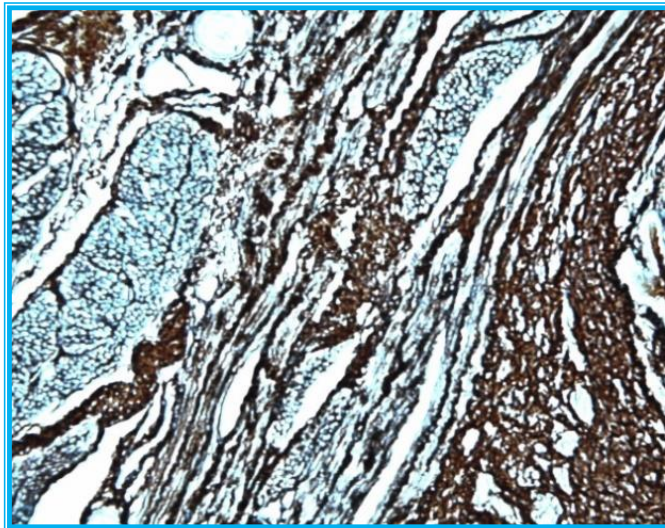


Figure 13. Muscular stomach. Ostrich. Reticulin fibers distribution in the ventricular wall structure after silver staining process
Col. Gomori x 200 (original)

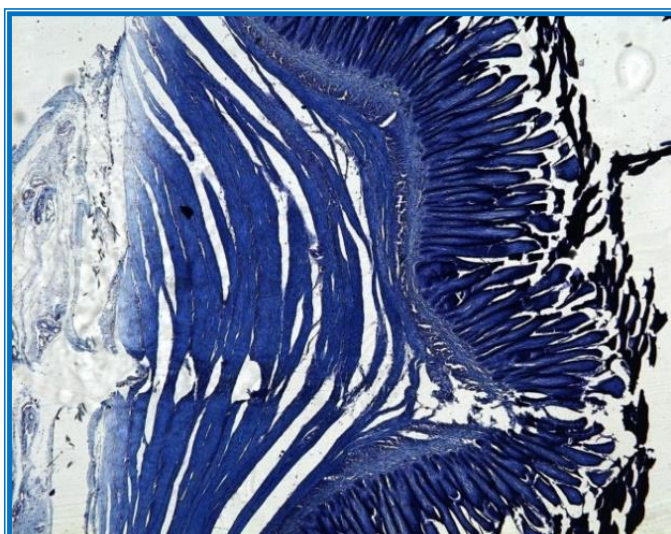


Figure 14. Ostrich. Muscular stomach. View of the serous at the ventricle level
Col. AT x 50 (original)

Conclusions

The ventricular mucosa is covered by the thick cuticle, continuously secreted by ventricular glands cells.

Muscle of the mucosa is present, but on certain portions it can no longer be observed, being united with the layers of the musculature.

The muscular layer is best represented, composed of smooth muscle fibers with the three layers: longitudinal outer, circular middle, with the largest consistency of the inner skew layer.

Bibliography

1. Agab, H. - Practical Aspects and Constraints in the Commercial Production of Ostriches (*Struthio camelus*) and Emus (*Dromaius novaehollandiae*) in Saudi Arabia, PhD.Thesis. Sudan University of Science and Technology, (2005).
2. Association Avestruces breeders craft of Chile. Anatomy of the ostrich. <http://www.acac.cl/fia/fiamain.htm>. April 2005
3. Cooper, R & Mahroze, K: Anatomy and physiology of the gastro-intestinal tract and growth curves of the ostrich (*Struthio camelus*). *Animal Science j.*, 75:491- 8, 2004.
4. Luiz Carlos Junqueira, Josen Carneiro „Histologie” - tratat & atlas, Editura Medicala Callistro editia 11, 2008.
5. Cornila N., Stefania Mariana Raita– Biologie celulara, histologie si embriologie, Vol. II, Ed. Ceres, Bucuresti, 2013.

THE PROPHYLAXIS OF CHALKBROOD IN BEES BY LABORATORY METHODS - MICROSCOPIC TESTING OF POLLEN

Ion RĂDOI¹, Gheorghe Florentin MILEA^{1*}, Alexandros RĂDULEA¹, Vasilică SAVU²,
Agripina SAPCALIU², Maria MĂGDICI², Luiza BADIC³

¹University of Agronomical Sciences and Veterinary Medicine Bucharest, Romania

²Beekeeping Research and Development Institute Bucharest, Romania, Bucharest, Romania

³Spiru Haret University Bucharest, Romania

E-mail address: florin.milea@gmail.com

Abstract

*The purpose of this study was to monitor the load of *Ascosphaera apis* spores in honey and pollen samples and to evaluate the pertinence of the method in the prophylaxis of *Ascosphaera apis* infestation by eliminating contaminated sources used in bee feed. We investigated 8 apiaries for a period of 2 years at the end of the active bee season, the collected samples consisting in pollen (39 samples) and pollen supplementary foods (7 samples). The samples were processed and tested for spores of *Ascosphaera apis* through the method OIE/2008, adapted for samples of pollen and pollen supplementary foods. The samples originated from apiaries suspected of nosema disease. Within the lot with pollen samples (46 samples), a number of 39 pollen samples belonging to the 4 dominant floral categories in Romania (polifloral, rape, sun-flower, linden) were chosen in order to determine the infestation level with *Ascosphaera apis* spores. Most of the *Ascosphaera apis* spores positive samples were represented by the rape and sunflower pollen samples. Tests evidenced the presence of *Ascosphaera apis* spores in 22 samples of pollen and pollen supplementary foods of the total of 45 examined samples during the monitoring process. The tests made on bee samples collected at the end of the beekeeping season, by comparison to the ones collected in the beginning of the following season, demonstrated a significant reduction in the infestation degree (30.43%) in bees by eliminating from consumption the sources of infestation (pollen supplementary foods and pollen) in the winter season. Testing before the inactive season for *Ascosphaera apis* spores in the reserve honey and pollen represents an important prophylactic method against *Ascosphaera apis* infestation in bees.*

Keywords: *Ascosphaera apis*, chalkbrood, microscopic testing, pollen, prophylaxis

Introduction

Chalkbrood disease is an invasive disease producing important losses by a high mortality rate of bee larvae [1, 3, 20]. Caused by the fungus *Ascosphaera apis*, who's able to infect brood of any caste (workers, drones and queens) [7, 21]. *Ascosphaera apis* spores ingested by young bee larvae (4 days for age) with their food and germinate in the gut and after mycelium penetrates the gut wall [1, 9, 15]. The formation of spore cysts is on the outside of the dead larvae and most of these spore cysts are ejected from the colony by house-cleaning bees, but many will find the healthy larvae, in brood comb where they remain infective for many years [3, 15, 20]. *Ascosphaera apis* rarely destroys the whole colony but it can cause substantial production loss [3, 22, 23]. Chalkbrood disease is common in most beekeeping countries in the temperate regions in Europe, in New Zealand, USA and Canada [18, 20, 23]. Any larvae killed by the fungus can then carry between 10^4 - 10^7 spores on their bodies [7, 9, 12]. The laboratory diagnosis is based on the demonstration of the causative agent (*Ascosphaera apis*) in diseased material, the presence of spore cysts is usually sufficient to make a diagnosis [8, 20, 23]. These spore cysts which are about 60 µm in diameter, contain smaller round bodies known as spore balls (average 12 µm in diameter) and it is in these spores (average 2.9 x 1.4 µm in diameter) that the most infective stage of the fungus is found [3, 20, 22].

Material and method

During a 2 year period a number of 8 apiaries were investigated at the end of the active beekeeping season [3, 6, 12]. 46 samples representing bee pollen (39 samples) and pollen

supplimentary foods (7 samples) were collected (Table 1) originating from apiaries suspected of *chalkbrood* disease. At the beginning and the end of the active season the infestation level with *Ascosphaera apis* spores was investigated. The evolution of the disease within the monitored and studied honeybee colonies was also investigated [4, 6, 21].

Table 1.

Total number of investigated apiaries and samples

Number of examined apiaries	Number of bee pollen samples	Number of pollen supplementary foods
8	39	7

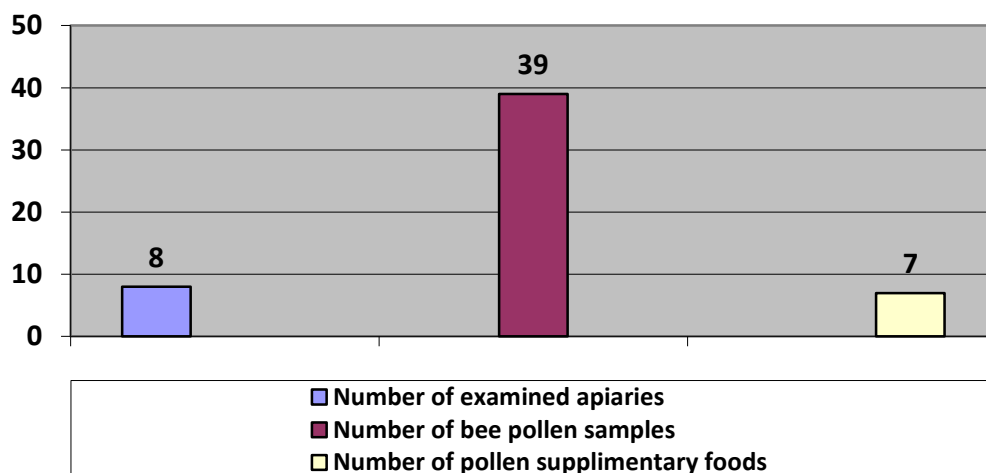


Figure 1 Repartization graphic of total number of investigated apiaries and samples

The collected samples were processed and analyzed to check the occurrence (presence) of the *Ascosphaera* apisspores using the OIE/2008 [18, 22, 23] method that was adapted for the bee pollen and *pollen supplementary foods* samples. At the beginning and the end of each active season the level of infestation with *Ascosphaera apis* spores and the evolution of the disease within the monitored honeybee's colonies [3, 6, 13].

Within the lot with pollen samples (46 samples), a number of 39 pollen samples belonging to the 4 dominant floral categories in Romania (*polifloral pollen*, rape, sun-flower, linden) were chosen in order to determine the infestation level with *Ascosphaera apis* spores. The potential variation of the infestation level correlated with the melliferous floral source was also studied (Table 2)

Table 2.

Pollen samples from various floral melliferous species in Romania examined

No. of samples <i>polifloral pollen</i>	No. of rape pollen samples	No. of sunflower pollen samples	No. of linden (<i>Tillia</i> spp.) pollen samples
17	8	8	6

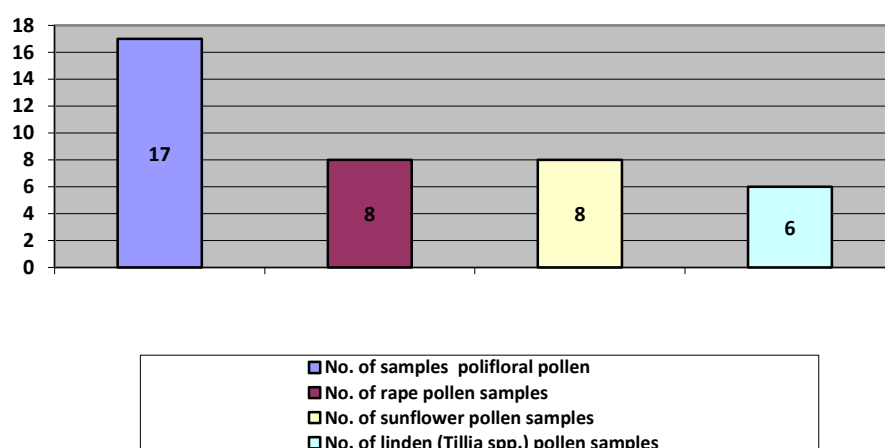


Figure 2 Representation Graphic of pollen samples from various floral melliferous species in Romania examined

Results and discussion

The direct microscopic examination [18, 21, 23] revealed the presence of the *Ascosphaera apis*, spores in 20 samples of bee pollen and *pollen supplementary foods* of the total number of 46 analyzed samples (table 3 and figure 1).

Table 3.

The samples analyzed for the presence of *Ascosphaera apis* spores

Sample type	Number of examined samples	Total number of positive samples	Total number of negative samples
Bee pollen	39	15 (38.46%)	24 (61.54%)
<i>Pollen supplimentary foods</i>	7	5 (71.42%)	2 (28.58%)
Total number of examined samples	46 (100%)	20 (43.50%)	26 (56.50%)

The number of *Ascosphaera apis* spores positive samples is shown in Figure 3.

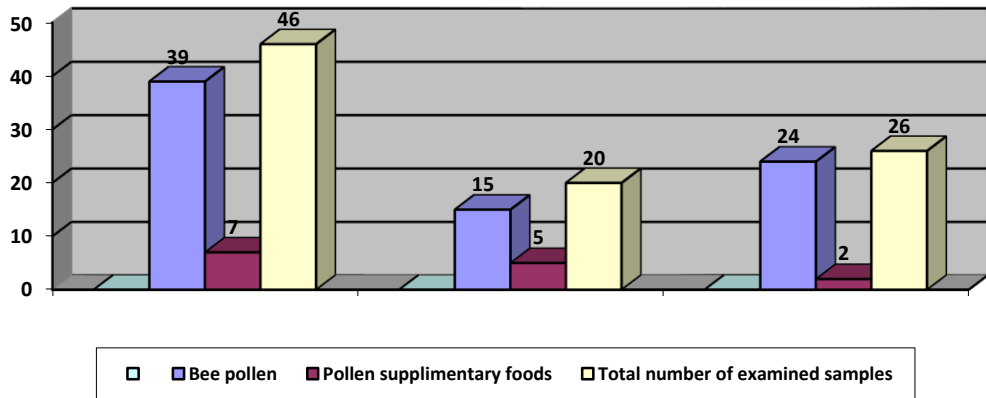


Figure 3. Graphic representation of the *Ascosphaera apis* spores positive samples

Looking at the table above, we reach the conclusion that out of 39 pollen samples, 15 were positive (38.46%) for the presence of *Ascosphaera apis* while out of the total number of 7 *pollen supplementary foods*, 5 were positive for *Ascosphaera apis*, spores (71.42%).

Analyzing the results of the study, it can be said that within the studied lots a high level of contamination was noted for 3 categories of hive products which are used as food by the honeybees (pollen, *pollen supplementary foods*).

The results made it possible to classify the level of *Ascosphaera apis* spores load in 3 categories: weak infestation (1-2 spores/microscopic field), medium (average) infestation (3-5 spores/microscopic field) and massive infestation (> 5 spores/field). (Table 4 and Fig.2,3,4).

Table 4.

The infestation level of the bee pollen and reserve honey combs

Sample type	No. of positive samples (%)	Infestation level			No. of negative sample (%)
		Weak (low) infestation (1-2 spores of <i>Ascosphaera apis</i> ./field) (%)	Medium infestation (3-5 spores of <i>Ascosphaera apis</i> ./field) (%)	Massive (high) infestation (> 5 spores of <i>Ascosphaera apis</i> ./field) (%)	
Bee pollen	15	9 (60%)	3 (20%)	3 (20%)	24
Pollen supplementary foods	5	2 (40%)	2 (40%)	1 (20%)	2

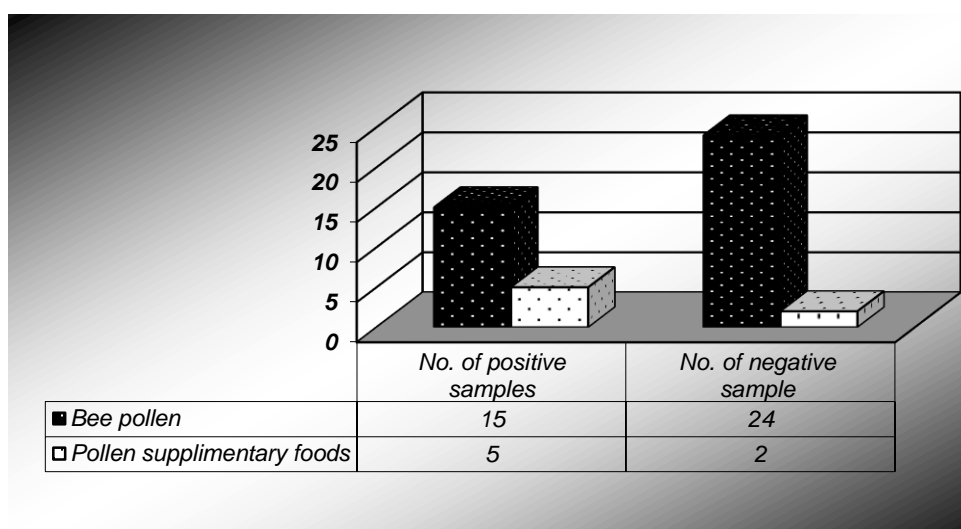


Figure 4. The number of *Ascosphaera apis* spores positive samples from 8 apiary

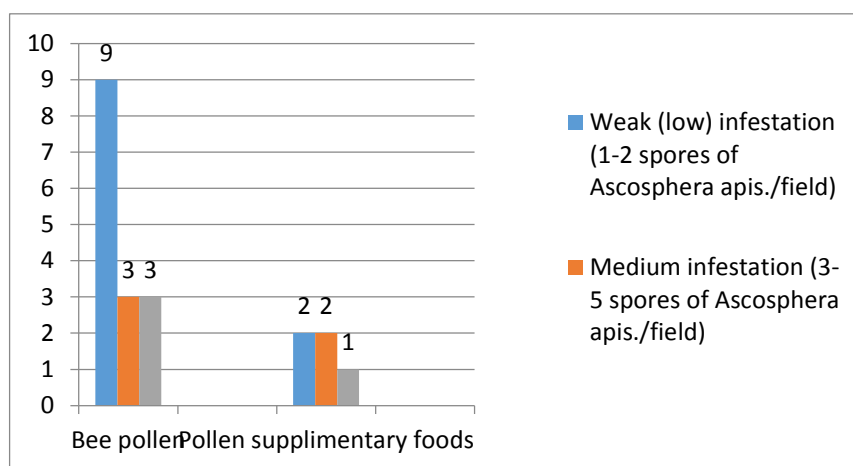


Figure 5. The infestation level of *Ascosphaera apis* spores all samples (pollen and *pollen supplementary foods*)

Following the direct microscopic examination of the pollen samples, the results made it possible to classify the 3 categories for the *Ascosphaera apis* spores load: weak infestation (1-2 spores/microscopic field, medium (average) infestation (3-5 spores/field) and massive (high) infestation >5 spores/field) (Table 5).

Table 5.

Ascosphera apis spores infestation level for the 39 pollen samples in correlation with the melliferous source

	Polifloral pollen				Rape pollen				Sunflower pollen				Linden pollen			
No. of examined samples	17				8				8				6			
No. of <i>Ascosphera apis</i> spores/field	1-2	3-5	> 5	Neg.	1-2	3-5	>5	Neg.	1-2	3-5	>5	Neg.	1-2	3-5	> 5	Neg.
No./percent of infested samples	4 (10 %)	4 (10 %)	0	9 (60 %)	1 (12.5 %)	1 (12.5 %)	1 (12.5 %)	5 (62.5 %)	- %	- %	2 (25 %)	6 (75 %)	1 (16.66 %)	1 (16.66 %)	-	4 (66.67 %)

According to the data shown in Table 5, from the total number of 17 pollen samples from polifloral pollen 8 samples (20%) were positive for *Ascosphera apis* spores. In the rest of the lot the positive values were as follows: 3 samples (37.5%) for the rape pollen, 2 samples (25%) for the sunflower pollen, 2 samples (33.66%) for linden pollen (Fig.5). Most of the *Ascosphera apis* spores positive samples were represented by the polifloral and rape pollen samples and according the data shown in fig. 5, a number of 5 samples were positive (71.43%).

The microscopic examinations of 46 samples of honeybees collected from 8 apiaries were analyzed during a 2 year interval (Fig. 7 and Fig. 8). The samples that were collected at the end of the beekeeping season (autumn), as compared to samples that were collected at the beginning of the next season (early spring), proved a significant decrease of the *Ascosphera apis* infestation level in the examined bees (the percentage was 28.50%) as a result of removing from consumption the main infestation sources during the inactive season, the infested honey and bee pollen that were given as wintering food. The level of infestation with *Ascosphera apis* spores at the end of the active beekeeping season (autumn) and at the beginning of the next active season (early spring) as well as the decrease of the infestation level is shown in table 6 and figure 6.

Table 6.

The *Ascosphera apis* infestation level at the end and the beginning of the beekeeping season

No. of pollen samples (8 examined colonies /2 years)	Level of infestation with <i>Ascosphera apis</i> spores at the end of the active beekeeping season	Level of infestation with <i>Ascosphera apis</i> at the beginning of the next active season	Decrease of infestation level with <i>Ascosphera apis</i> spores (%)
46	20 (43.5%)	3 (15%)	28.5%

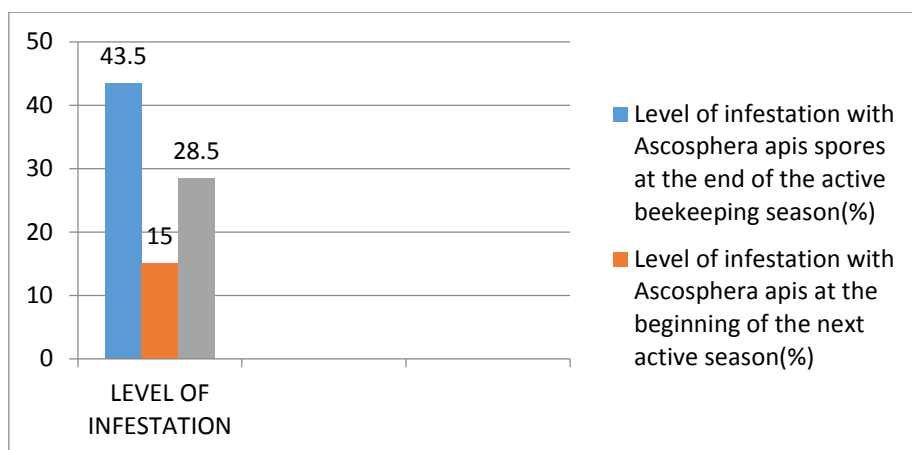


Figure 6. The *Ascospheara apis* infestation level at the end and the beginning of the beekeeping season

Removing the main contamination sources with *Ascospheara apis*, spores from the food of the honeybees during the inactive period (the wintering period) – contaminated pollen and pollen supplementary foods is an undeniable proof of the significant decrease of the infestation level of the bees during the wintering season, an element that should be highly considered if the survival of the honeybees passing wintering period is wanted.

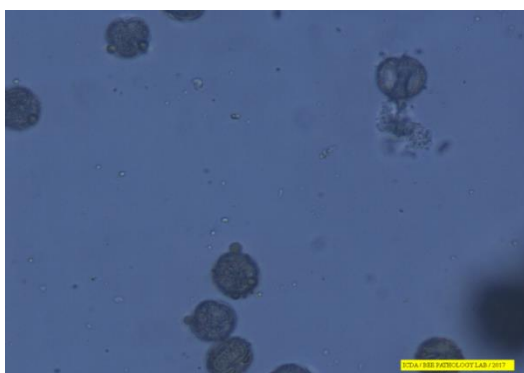
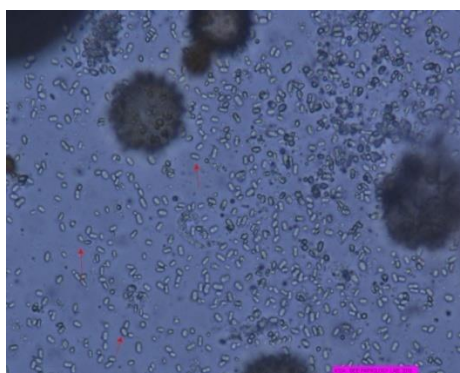


Figure 7 a) Negative sample of pollen sample (0 spores of *Ascospheara apis*./field)



b) Massive (high) infestation (> 5 spores of *Ascospheara apis*./field)

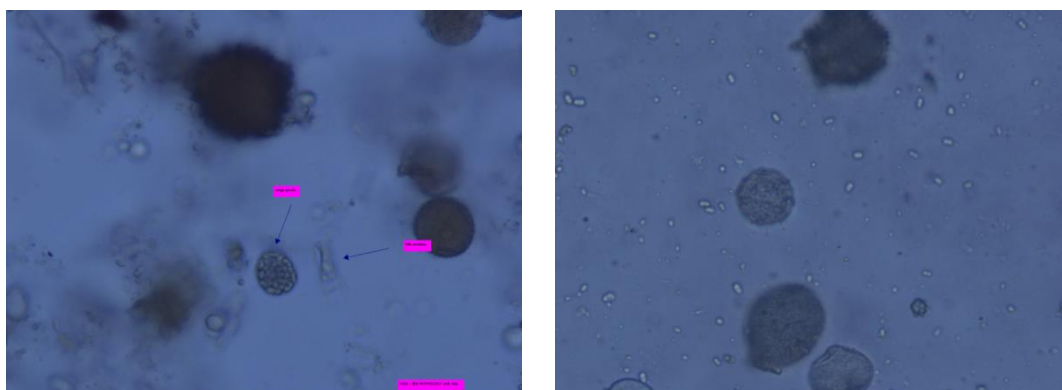


Figure 8. Figure showing: a) *A. apis* spore cyst (asoma)
b) mature ascospores (*Ascospheera apis*)

Conclusions

Out of a total number of 46 examined samples of pollen and *pollen supplementary foods*, a number of 20 samples (43.5%) were positive for the presence of *Ascospheera apis* spores.

The infestation level with *Ascospheera apis* spores of the examined samples ranged from 1-2 spores/microscopic field to more than 5 spores/microscopic field.

Most of the *Ascospheera apis* spores positive samples were represented by the rape pollen and polyfloral pollen and pollen supplementary foods samples.

The microscopic tests carried out on honeybees at the end of the beekeeping season (autumn) as compared to the honeybees that were checked at the beginning of the next beekeeping season (early spring), proved a significant decrease for the infestation level, 28.5% respectively, following the removal of the contaminated food.

The microscopic examination of pollen and pollen supplementary foods for the presence of the *Ascospheera apis* spores is an important prophylactic step against the infestation of the honeybees during the wintering period.

The examination of the presence of *Ascospheera apis* spores in the food reserves before wintering makes it possible to remove from consumption the reinfestation sources, a fact which significantly decreases the morbidity and the mortality rate among honeybees.

Acknowledgements

„Preliminary results of PhD thesis”.

References

1. ACA România, 2013. *Ghid de bune practici în Apicultură* Editura LVS Crepuscul, Ploiești, Prahova. ISBN 978-973-7680-99-0.
2. Albo GN, Córdoba SB, Reynaldi FJ, 2017. *Chalkbrood: pathogenesis and the interaction with honeybee defenses*, International Journal of Environmental & Agriculture Research (IJOEAR) ISSN:[2454-1850] [Vol-3, Issue-1]
3. Stelian A. Asiminei, autor coordonator, 2016 – *Patologia albinei melifere*. Editura Ion Ionescu de la Brad, Iasi 119-120
4. Annette Bruun Jensen¹, Kathrine Aronstein, José Manuel Flores, Svjetlana Vojvodic, María Alejandra Palacio and Marla Spivak, 2013. *Standard methods for fungal brood disease research*, Journal of Apicultural Research 52(1): DOI 10.3896/IBRA.1.52.1.13

5. Aronstein and Murray, 2010. *Chalkbrood disease in honey bees*, J. Invertebr. Pathol., *Journal of Invertebrate Pathology*, 103 S20-S29, www.elsevier.com
6. B. Jensen, K. Aronstein, J. M. Flores, S. Vojvodic, M. A. Palacio and M. Spivak, 2013. "Standard methods for fungal brood disease research", *J. Apicul. Res.*, vol. 52, pp. 1-20
7. Chorbiński P., 2004. *The Development of The Infection of Apis mellifera Larvae By Ascosphaera Apis*, Ejpau, 2004, Volume 7, Issue 2, Veterinary Medicine
8. Encarna Garrido-Bailón, et.al, 2013. *The prevalence of the honeybee brood pathogens Ascosphaeraapis, Paenibacillus larvae and Melissococcus plutonius in Spanish apiaries determined with a new multiplex PCRassay*, *MicrobBiotechnol.* 2013 Nov; 6(6): 731–739. Published online 2013 Aug 6. doi: 10.1111/1751-7915.12070
9. Flores J.M., Ruiz J.A., Ruz J.M., Puerta F., Bustos M., Padilla F., Campano F.1996. *Effect of temperature and humidity of sealed brood on chalkbrood development under controlled conditions*. *Apidologie*, 27, 185-192.
10. Human H, Brodschneider R, Dietemann V, Dively G, Ellis J, Forsgren E, et al.2013. *Miscellaneous standard methods for Apis mellifera research*. In: Dietemann V, Ellis JD, Neumann P, editors. *The COLOSS BEEBOOK, Volume I: standard methods for Apismellifera research*. *Journal of Apicultural Research*, 52.
11. J. A. Yoder, A. J. Jajack, A. E. Rosselot, T. J. Smith, M. C. Yerge and D. Sammartaro, 2013. "Fungicide contamination reduces beneficial fungi in bee bread based on an area-wide field study in honey bee, *Apis mellifera*, colonies", *J. Toxicol. Environ. Health A*, vol. 76(10), pp. 587-600,
12. J. Danihlík, K. Aronstein and M. Petřivalský, 2015. "Antimicrobial peptides: a key component of honey bee innate immunity", *J. Apicul. Res.*, vol. 54, pp. 123-136
13. Jensen AB, Aronstein K, Flores JM, Vojvodic S, Palacio MA, Spivak M.2013. *Standard methods for fungal brood disease research*. *J. Apic. Res.*52 (1):39
14. Kirsten Foley, 2013. *The ecology and evolution of Aspergillus spp. Fungal parasites in honey bees*, The University of Leeds, School of biology
15. MileaFlorentin Gheorghe, Ion RADOI, Agripina ȘAPCALIU,Vasilică SAVU, Ovidiu POPA – "Ascospherosis incidence in bees investigated for major bacteriosis in the beekeeping year 2016", *Scientific Works, Series C*, vol. LIX (4), 2017, ISSN 2065-1295, ISSN Online 2067-3663, ISSN I. 2065-1295, *Veterinary Medicine Bucuresti*
16. Nichita Ileana, 2007. *Bulletin Usamv-Cj*, 64 (1-2). *Researches Regarding The Chalkbrood Disease (Ascosphaera Apis) Of The Honey Bees*, *Bulletin USAMV-CN*, 64/2007 (1-2)
17. Ogradă I.,1986. *Bolile și dăunătorii albineor*, Asociația Crescătorilor de albine din Romania, Redacția publicațiilor apicole, Ediția a III a , Revizuită și actualizată
18. OIE (World Organisation for Animal Health), 2009. *Manual of Diagnostic Tests and Vaccines for Terrestrial Animals (mammals, birds and bees)*, vol.1, 2, ed. 25th Edition 2016
19. Sarah A. Maxfield-Taylor, Alija B. Mujic, Sujaya Rao,2015. *First Detection of the Larval Chalkbrood Disease Pathogen Ascosphaera apis (Ascomycota: Eurotiomycetes: Ascosphaerales) in Adult Bumble Bees*, <https://doi.org/10.1371/journal.pone.0124868>
20. Savu V., Agripina Șapcaliu, 2013. *Patologia albinelor*. Editura Fundației România de Măine.București. ISBN 978-973-163-951-2. 31-38.
21. Wubie AJ, Xu S, Hu Y, Li W, Guo Z, Xue F, et al. 2013. *Current developments in Ascosphaera apis (Maasen ex Claussen) L. S. Olive & Spiltoir the causative agent of chalkbrood disease in honeybees (Hymenoptera: Apidae)*. *J Food Agric Enviro.*; 11: 2190–2200
22. www.apimondia.org (2017)
23. www.oie.org (2017)

THE RELEVANCE OF A DIGITAL SYSTEM BASED ON NANOPARTICLES BIOSENSORS IN ASSESSING THE ANTIOXIDANT POTENTIAL OF SOME FOODS

Sebastian OGNEAN¹, Titus CRIȘAN^{1*}, Constantin BELE², Octavia TAMAS-KRUMPE²,
Andreea BUTA², Helga DEMENY², Laurenț OGNEAN²

¹ Faculty of Electrical Engineering, Technical University of Cluj-Napoca

²Department of Animal Physiology, University of Agricultural Science and Veterinary Medicine

* Corresponding author, e-mail: titus.crisan@ethm.utcluj.ro

Abstract

Image analysis is a highly topical and perspective method in biomedical research and practice that underlies the development of portable tests for the autonomous detection of external energy sources outside the laboratory. The purpose of this paper is to implement a new method of detecting antioxidants in food, based on digital image acquisition and processing, using an experimental device with a paper-based biochemical sensor, marked with silver nanoparticles. The research consisted of evaluating the antioxidant potential of some teas (no = 5) and commercial red wines (no = 5), using the LabVIEW device and the LabVIEW graphical programming environment for data processing in linear 3D regression, referencing the RGB spatial vector. The results obtained in the testing of tea and red wine varieties had the following hierarchy regarding their antioxidant concentration (expressed in $\mu\text{g} / \text{mL}$ gallic equivalents): Twinings traditional afternoon black tea (10.945); Lipton Green Tea (20.450); Lipton forest fruit tea (20.450); Fares forest fruit tea (29.956); Green Tea Earl Gray (34.708) or Recaș wine (15.698); Pinot Noir Folonari wine (15.698); Chateau Malpere wine (20.450); Cabernet Sauvignon wine and Fetească Neagră wine (25.203). In conclusion, we appreciate the great outlook of this fast and cheap method, which can be accessed through software installed on your laptop or smartphone, allowing you to read the result with one click, including by non-experts.

Keywords: antioxidants, paper biosensor, nanoparticles, teas, wines

Introduction

The benefits of digital measurement systems are fully found in the field of biomedical research (Alam et al., 2013, Andrei et al., 2014). They are in the process of being enriched with new biochemical methods of digital measurement of the antioxidant potential of food products. In this respect, it is worth noting the recent advances of experimental analytical devices based on paper-biosensors, which are expedient and inexpensive enough in order to impose themselves as perspective tests (Yetisen et al., 2014).

A basic feature of digital systems is the storage capacity. Similar to animal memory and digital memory, there are three forms depending of its duration, including short-term storage for processing needs, online storage for relatively fast access to images, and archive storage, the access of which is still limited regarding the image (Magalhaes et al., 2008). As a rule, short-term storage is based on the use of computer memory and online storage on the use of different types of media (Munteanu and Todoran, 1997).

Problems in digital image processing communication can provide local communication between processing systems and long distance communication (Holonec et al., 2010). Although the hard drive and the software have great availability for local communications, and the computer network facilities are extremely generous, the image transmission rate is not yet satisfied (Munteanu and Todoran, 1997). It is estimated that it far exceeds other types of data transmissions. Solving long distance communication requires therefore sustained efforts from research and practice (Holonec, 2003).

Antioxidant investigations have intensified over the last 20 years, mainly due to the discovery of beneficial effects on human health. In the body, the excess of reactive oxygen species,

generated by pollution, unhealthy food or smoking, can cause cardiovascular diseases, cancer, diabetes, inflammatory syndromes and other conditions (Pisoschi and Negulescu, 2011; Seifried, 2007). Several studies in this field show that the incidence of these diseases decreases with increased consumption of antioxidant-rich foods (Seifried, 2007). Regarding the use of antioxidant dietary supplements, there are different opinions, including that some excessive antioxidant consumption may cause various disorders, mainly disorders of the immune system (Karadag et al., 2009, Seifried, 2007).

Foods of vegetable origin, mainly fruits, have a rich content of antioxidant principles, their concentration being correlated with the color of the mature fruit. Most of the vitamins and nutrients in the plants also exert an important antioxidant role, vitamin A, beta-carotene and other carotenoids, flavonoids, vitamin C, vitamin E, zinc and selenium having a major impact. Among the hundreds of currently known antioxidants, the following five are more common and can be used at the level of public consumption: vitamins C and E, lipoic acid, glutathione and coenzyme Q10 (Andrei et al., 2014). At the same time, vitamins C and E are not produced in the body and must be fed through food, and lipoic acid, glutathione and coenzyme Q10 are synthesized in the body, but their level decreases with age, requiring supplementation (Andrei et al., 2004; Karadag et al., 2009).

Based on these considerations, in our study we chose to test the antioxidant activity of commercially available teas and bottled red wines using a colorimetric biosensor marked with Ag nanoparticles on paper, integrated into an experimental device. It is envisaged that this stand-alone system, based on acquisition and digital image processing, will allow the determination of the concentrations of certain substances of major interest in the food sector.

Materials and methods

The experimental device consisted of an original color-processing system, taken from a paper-based biosensor, marked with silver nanoparticles to reduce the antioxidant compounds in aqueous samples (Figure 1). The principle of this biosensor is based on the ability of antioxidants to reduce Ag ions present in AgNP species, emerging chromatic transitions with intensity dependent on the structure and concentration of antioxidants.



Figure 1. Overview of the experimental device

Digital image processing has sequentially traced the following hard and soft processing steps: image acquisition, with imaging and digitization sensor of the output signal; image processing and segmentation; recognition and interpretation of data. The hardware components

were the sample, the lighting system, a webcam (Logitech model B910) and a personal computer. The antioxidant capacity of the analyte is detected based on the nanoparticle content of the paper support and the reduction of the Ag to Ag (0) ions, which gives a yellow color to the support, forming a "digital print" (Figure 2). The color intensity is dependent on the sample reduction power, being proportional to the antioxidant concentration. Silver ions have proven to be relevant colorimetric probes because they produce significant staining.

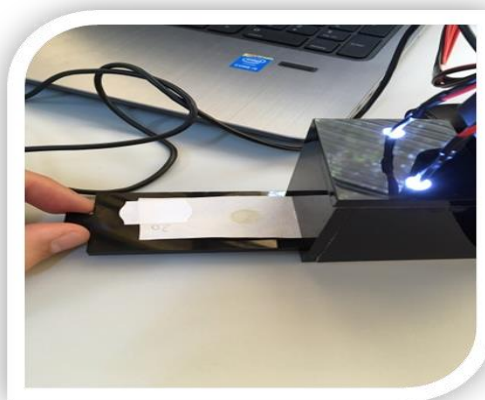


Figure 2. Sliding the loaded stand into the center unit of the device

The processing of the acquired images was performed using the LabVIEW graphics programming environment. In designing the software we used a 3D linear regression program, which was the basis for obtaining a spatial RGB vector as a reference. The operation of this program consists in placing a 3D spatial point corresponding to the lowest Euclidean distance, in relation to the vector values, which corresponds to the equivalent value of gallic acid (μg) (Figure 3).

Sample preparation consisted of preparing the impregnated biosensor on a paper support with gallic acid standard solutions marked with silver nanoparticles, with antioxidants contained in the test product reducing Ag + 1 to Ag0 (metallic).

Antioxidant extraction was done with 5 mL of methanol solution in water (20-80 g) starting from 0.2 g of tea, ultrasonically dried on the ultrasound bath followed by the filtration of the obtained extract by a $0.45\ \mu\text{m}$ filter.

The deposition of the spots on the filter paper consisted in dipping it into the working solution of silver nanoparticles and drying it for an hour. Next, we added $10\ \mu\text{L}$ of the standard solutions (gallic acid) or the solutions to be analyzed and leave to stand for 20 minutes. The Whatman filter paper of 3 mm and VWR 600 was used as comparison.

The calibration was based on the analysis of the correlations between the color intensity and the antioxidant concentration of the tested samples, in the determination of the calibration curve on gallic acid (3OH, 1.0). Thus, the gallic acid equivalent expression of the level of hydroxyl groups in the molecule, as well as its antioxidant resistance, was achieved.

The tested products included several teas (no = 5) and red wines (no = 5), frequently marketed, which we grouped into two samples. In the first sample, we introduced the following teas (prepared as infusions, according to the attached instructions): 1 - Twinings traditional afternoon black tea; 2 - Earl Gray Green Tea; 3 - Fares Berries Tea; 4 - Lipton Berries Tea; 5 - Lipton Green Tea. The second sample was composed of the following bottled wines: 1 - Reçaş red

wine; 2 - Chateau de la Soujeole de Malpere red wine; 3 - Cabernet Sauvignon red wine; 4 - Fetească Neagră red wine; 5 - Pinot Noir Folonari red wine.

Results and discussions

The quality of the paper used significantly influenced the signal strength and implicitly the relevance of the biosensors. In this context, it should be noted that the biosensor paper support must ensure a clear colorimetric signal transduction, a good compatibility with the reagents used, a minimization of nonspecific absorption of the reagents and analytes, and a good degree of homogeneity in order to avoid dispersion of the fluid. Based on these considerations, researchers in the field recommend the use of chromatography paper that meets these requirements, ensures good accessibility of antioxidants to its surface and it is available at a low cost on the market (Varvari et al., 2008; Zhao et al., 2008).

The results obtained in determining the calibration curve at 6 concentrations of gallic acid (5, 10, 20, 30, 40 and 50 $\mu\text{g} / \text{mL}$) revealed positive correlations between color intensity and 5 concentrations. We also noted that after the 50 $\mu\text{g} / \text{mL}$ threshold has been reached, the color intensity was maintained on plateau.

By looking at the increase in antioxidant concentration, expressed in $\mu\text{g} / \text{mL}$ gallic acid equivalent, in the test tea sample we found the following hierarchy (Table 1): Twinings traditional afternoon black tea (10.945), Lipton green tea (20.450), Lipton berries tea (20.450), Fares berries tea (29.956) and Earl Gray Green Tea (34.708) (Figure 3).

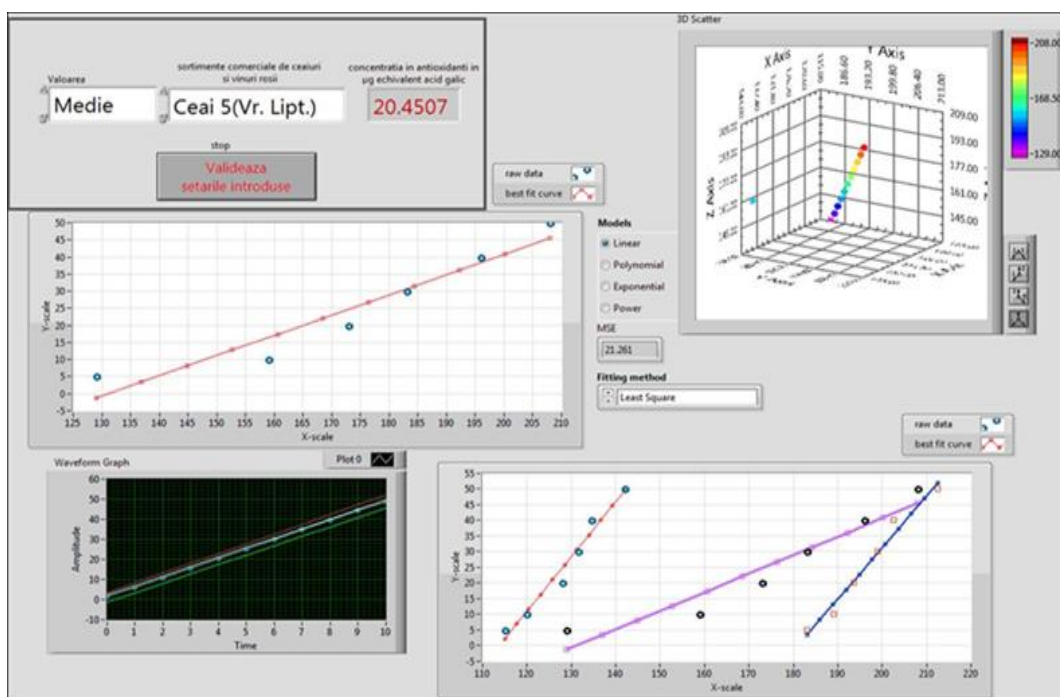


Figure 3. Viewing the content of antioxidants in tea 5

In the case of the sample composed of the 5 red wine varieties, the results obtained indicated the following ranking according to their concentration in antioxidants: Reaș red wine

(15.698), Pinot Noir Folonari red wine (15.698), Chateau Malpere red wine (20.450), Cabernet Sauvignon and Fetească Neagră red wine (25.203) (Table 1).

Table 1.

Concentrations in antioxidants (μg gallic equivalents) of some teas and red wines, determined with biosensors and digital image processing







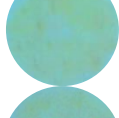
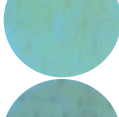
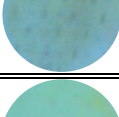

Products (n=10)	Conc. (echiv.A G-μg)	Acquired images	Red (level)			Green (level)			Blue (level)			
			Paper spot	Min.	Max.	Media	Min.	Max.	Media	Min.	Max.	Media
Tea 1 (Black)	10.945		124	144	130	172	188	180	128	162	145	
Tea 2 (Earl Grey)	34.708		107	129	118	174	194	184	168	220	194	
Tea 3 (F.p. Fares)	29.956		144	132	138	182	198	190	168	194	181	
Tea 4 (Lipt. berry)	20.450		106	131	118.5	178	195	186.5	151	190	170.5	
Tea 5 (Lipt. Green)	20.450		126	152	139	174	186	180	143	175	159	
Wine 1 (Recaș)	15.698		119	145	132	165	182	173.5	134	181	157.5	
Wine 2 (Chateau Malpere)	20.450		121	139	130	186	206	196	147	180	163.5	
Wine 3 (Cabernet Sauvignon)	25.203		112	139	125.5	173	197	185	161	191	176	
Wine 4 (Fetească Neagră)	25.203		96	127	111.5	142	177	160	156	212	184	
Wine 5 (Pinot Noir Folonari)	15.698		133	153	143	171	186	178.5	140	168	154	

Image analysis is a highly current and prospective method that underlies the development of portable external energy source detection platforms with autonomous operation outside of laboratory conditions (Jayaprakasha et al., 2002). Such independent platforms are an alternative to laboratory analyzes and have the advantage of providing qualitative and quantitative information, even to non-expert users. Digital image processing goes through a series of hard and soft processing steps that end with the development of image processing solutions. This category also includes analytical devices with paper-based biosensors, which are becoming more and more attractive.

In biomedical testing, it is now preferred to use complex digital devices to allow more complex interpretations based on a single determined parameter (Dechakhamphu et al., 2014). With the increase of the health benefits from the consumption of dietary products rich in antioxidants, the need for the implementation of easily usable and effective tests to identify the antioxidant action of food products has been expanded (Ozyurek et al., 2012). In this context, there is also a growing interest in the use of nanoparticles sensors in the detection of antioxidants in food. Moreover, these tests can explore the ability of antioxidants to reduce noble metals, with the formation of nanoparticles or the use of antioxidants as reducing agents.

Conclusions

The research in this paper was completed with the implementation of an original digital color acquisition and processing device using a nanoparticle biosensor impressed by the antioxidants contained in the food. The relevance of digital image analysis was ensured by the processing of data in the LabVIEW graphics programming environment, through 3D linear regression, as reference to the RGB spatial vector. Our results on the evaluation of the antioxidant activity of some teas and red wines with this device provided a particular insight into such tests, accessible through software installed on a laptop or smartphone, with one-click reading.

References

1. Alam N., Bristi N.J., Rafiquzzaman M. (2013). Review on in vivo and in vitro methods evaluation of antioxidant activity. *Saudi Pharmaceutical Journal*, 21, 143–152.
2. Andrei Sanda, Bunea Andrea, Pinteada Adela (2014). *Stresul oxidativ și antioxidanți naturali*. Ed. Academic Pres Cluj-Napoca.
3. Apak R., Gorinstein S., Böhm V., Schaich K.M., Özyürek M., Güçlü K. (2013). Methods of measurement and evaluation of natural antioxidant capacity/activity (IUPAC Technical Report). *Pure Appl. Chem.*, 85(5): 957–998.
4. Dechakhamphu S., Pinlaor S., Sithithaworn P., Bartsch H., Yongvanit P. Evans E., Moreira-Gabriel E.F., Coltro W.K.T., Garcia C.D. (2014). Rational selection of substrates to improve color intensity and uniformity on microfluidic paperbased analytical devices. *Analyst*, 139: 2127–2132.
5. Holonec Rodica (2003). *Electrical Measurements and Instrumentation*. Ed. Mediamira, Cluj-Napoca.
6. Holonec Rodica, Tebrean B., Tarnovan I.G., Todoran Gh. (2010). *Electronic Measurements: Laboratory Manual*. Ed. U.T. PRESS, Cluj-Napoca.
7. Jayaprakasha G.K., Jena B.S., Negi P.S., Sakariah K.K. (2002). Evaluation of Antioxidant Activities and Antimutagenicity of Turmeric Oil: A Byproduct from Curcumin Production. *Z Naturforsch*, 57c: 828-835.
8. Karadag A., Beraat O., Samim (2009). Review of methods to determine antioxidant capacities, *Food Anal. Methods* 2, 41–60.
9. Magalhaes L., Segundo M., Reis S., Lima J. (2008). Methodological aspects about in vitro evaluation of antioxidant properties. *Anal. Chim. Acta*, 613: 1-19.
10. Munteanu R., Todoran Gh. (1997). *Teoria și practica prelucrării datelor de măsurare*. Ed. Mediamira, Cluj-Napoca.
11. Ozyurek M., N. Gungor, S. Baki, K. Guçlu, R. Apak. Development of a silver nanoparticle-based method for the antioxidant capacity measurement of polyphenols, *Anal. Chem.*, 2012, 84: 8052–8059.

-
12. Pisoschi A.M, Negulescu G.P. (2011). Methods for Total Antioxidant Activity Determination: A Review. *Biochem & Anal Biochem*, 1:106.
 13. Seifried H., Anderson D., Fishera E, J. Milner J. (2007). A review of the interaction among dietary antioxidants and reactive oxygen species. *J. Nutr. Biochem.*, 18: 567-579
 14. Varvari Lidia, Muresan L., Popescu I. C. (2008). New amperometric biosensor for determination of the total antioxidant capacity, *Proceedings of the International Conference on Metrology of Environmental. Food and Nutritional Measurements*, Budapesta (Ungaria), 13-18.
 15. Yetisen, A. K., Martinez-Hurtado J. L., Garcia-Melendrez A., Cruz Vasconcellos F., Lowe C. R. (2014). A smartphone algorithm with inter-phone repeatability for the analysis of colorimetric tests. *Sensors and Actuators B: Chemical*, 196: 156-160.
 16. Zhao W., Ali M.M., Aguirre S.D., Brook M.A., Li Y. (2008). Paper-based bioassays using gold nanoparticle colorimetric probes, *Anal. Chem.*, 80 (22): 8431–8437.

APPLICATION OF HACCP (HAZARD ANALYSIS CRITICAL CONTROL POINT) TO COW TELEMEEA CHEESE PRODUCTION

Alina BORȘ¹, Oana Raluca RUSU¹, Ionuț BORȘ², Viorel FLORIȘTEAN¹

1- USAMV Iași, Faculty of Veterinary Medicine

2- Research and Development Station for Cattle Breeding, Dancu, Iași

e-mail:alinasabie@yahoo.com

Abstract

Nowadays, Hazard Analysis of Critical Control Points (HACCP) has become a prerequisite for transactions involving food products. Application of HACCP system in the cheese making industry proved to be beneficial and profitable, influencing consumer confidence by producing safe cheese with consistent quality. Cow TELEMEEA is a ripened cheese which due to its composition (moisture, salt level) and properties is susceptible to contamination. The aim of this study was to detail the flow diagram, to assess physical, chemical and biological hazards and to identify critical control points for cow TELEMEEA cheese on processing line. The results have revealed that physical, chemical and biological hazards may occur during processing and four critical control points were found: raw milk reception, raw milk storage, milk pasteurization and cold storage of cheese.

Key words: HACCP, cow, TELEMEEA cheese, hazards

Introduction

Dairy products are considered to be amongst the most nutritionally complete foods. Unfortunately, this characteristic also makes them highly susceptible to bacterial contamination that can lead to outbreaks of food borne disease. Cheese is a very popular dairy product and appreciated by consumers.

Since modern dairy plants are capable of processing large volumes of products, outbreaks can potentially affect large sectors of the population, including highly sensitive population – children, pregnant women, elderly (Kišmartin et. al., 2013).

Pathogenic microorganism (biological hazards) such as *Salmonella* spp., *Staphylococcus* spp., *Listeria monocytogenes*, *Escherichia coli* O157:H7, *Campylobacter jejuni*, *Yersinia enterocolitica* can contaminate milk and milk products and cause foodborne diseases. Noroviruses are the leading cause of foodborne outbreaks of acute gastroenteritis and the most common cause of sporadic infectious gastroenteritis amongst persons of all ages. Antibiotics and antimicrobial residues from milk and milk products can also represent potential health risks to consumers. Other chemical hazards include herbicides, pesticides and toxic metals, and physical hazards include hairs and needles. The dairy industry realised the need for proactive procedures hence implementing HACCP (Hazard Analysis and Critical Control Points) for ensuring that safe dairy products would reach the consumers (Papademas et. al., 2010, El-Hofi et. al., 2010). The HACCP concept was originally developed by the Pillsbury Company for the United States space program, to produce foods which were 100% safe. To achieve this end, Pillsbury controlled all aspects of the food production system including the raw materials, the process, and the environment. After Codex Alimentarius published “Guidelines for application of the Hazard Analysis Critical Control Point (HACCP) system”, HACCP principles have started to become legal obligation in many countries, including Romania.

The objective of our study was to detail the flow diagram, to assess physical, chemical and biological hazards and to identify critical control points for cow TELEMEEA cheese on processing line.

Material and methods

Description of dairy product

Cow TELEMEDIA is a ripened cheese, prepared with pasteurized cow milk, rennet and salt. The cheese is cut into small blocks (of 400 g) and vacuum packed in polyethylene bags along with a little brine. The physical and chemical composition is presented in table 1.

Table 1.

Cow TELEMEDIA cheese composition

Physical and chemical composition		Microbiological parameters	
Moisture % max.	max. 62%	<i>E.coli</i>	min.100 cfu/g
Fat in dry matter % min.	min. 38%	Coagulase positive <i>Staphylococcus</i>	min.100 cfu/g
Fat in product % min.	min.14,5%	<i>Salmonella spp.</i>	abs./25g
Protein % min.	min.16%		
Salt % max.	8% in product 16-20% in brine	<i>Listeria monocytogenes</i>	abs./25 g
Acidity °T	150°T		
Texture	Firm and compact		
Taste	Creamy, slightly acid and salty taste		
Color	White /Ivory-white		

Cow TELEMEDIA cheese flow diagram

After collection and transport, cow milk is received in dairy plant. Samples of raw milk are sent to dairy plant laboratory, to test physical, chemical properties (temperature, pH and acidity, density, fat and protein content) and microbiologic (NTG and somatic cells, antibiotic residues) quality. The proper milk is mechanically filtrated and stored in silo tanks, at 4°C, until processing. The milk is standardized at 2,8 % fat, pasteurized at 85°C, 120 sec., and homogenized. The pasteurized milk, cooled at 46-48°C is directed in coagulation tanks and inoculated with, calcium chloride (CaCl₂), lactic acid and rennet.

The coagulation stage lasts 30-50 min. at 20-25°C. The curd obtained is processed by cutting into small cubes leads, shaping and pressing to syneresis (expulsion of whey and contraction of curd). After syneresis, the curd is cut into 400 g cheese small blocks and salted in 18-22% brine, 24 hours, at 14-16°C. After salting, the cheese is packed in polyethylene bags and covered with 16-18% brine and directed to ripening storage. The ripening stage lasts 20 days at 14-16°C. The storage of cheese is made at 2-8°C and the shelf life is 120 days in appropriate conditions.

The codex protocol for the application of HACCP system includes seven principles (table 2).

Table 2.

HACCP principles

No.	Principles
1	Establish the potential hazards and conduct a hazard analysis
2	Determine the Critical Control Points (CCP)
3	Establish critical limits for each CCP
4	Establish a monitoring system to control each CCP
5	Establish the corrective action to be taken when monitoring indicates that a particular CCP is not under control
6	Establish verification procedures to confirm that the HACCP system is working effectively
7	Establish documentation concerning all procedures and records

Results and discussion

The hazard analysis and CCP determination for cow TELEMIA cheese using decision tree have revealed that physical, chemical and biological hazards may occur during processing steps and four critical control points were established: raw milk reception, raw milk storage, milk pasteurization and cold storage of final product. Two CCPs are detailed in tables 3 and 4.

Receiving of raw milk: the milk should be obtained from healthy animals under hygienic conditions. There are many factors that ensure the high quality of raw milk, but biological, chemical and physical hazards are occasionally identified in raw milk. Raw milk is a proper medium for the growth of microorganism and pathogenic bacteria such as *Salmonella spp.*, *E. coli O157:H7*, *Campylobacter spp.*, *Listeria monocytogenes*, *Staphylococcus aureus*, *Streptococcus spp.* can be derived from the udder, the environment, the milking equipment and employees. Also, raw milk may contain antibiotics, mycotoxins, toxic metals or chemicals (Maupououlos et. al., 1999; Wiedmann et. al., 2006; Karns et. al., 2007).

This stage is the first **CCP** because the reception test stands for an acceptance test. Control of raw milk includes the determination of milk acidity (15-19°T), temperature (4-6°C), aerobic mesophilic count (<100.000 cfu/ml), somatic cell count (<400.000/ml), antibiotic residues (negative).

Table 3.

Hazard analysis and CCP1 (raw milk receiving) management

Critical control point CCP		
Stage	Hazards	Critical limits
Receiving of raw milk	<p><i>Biological:</i> spoilage and pathogenic microorganisms (<i>Salmonella spp.</i>, <i>E. coli O157:H7</i>, <i>L. monocytogenes</i>, coagulase positive <i>Staphylococcus</i>, etc.)</p> <p><i>Chemical:</i> antibiotics herbicides, pesticides, cleaning substances</p> <p><i>Physical:</i> dust, hair, dirt</p>	<p>NTG max. 100.000 ufc/ml</p> <p>Somatic cells max. 400.000/ml</p> <p>Antibiotics residues-negative</p> <p>Temperature max. 6°C</p> <p>Acidity max. 19°T</p>

Monitoring procedures					
What	When	How			Who
Milk temperature, acidity NTG, NCS Antibiotics presence	Before accepting each tanker load and immediately prior to use	Control of milk temperature and acidity Microbiological tests Test for the presence of antibiotics			Employee at reception stage: line manager, veterinarian
Corrective measures		Verification			Records
Who	How	What	Who	When	
Line manager, veterinarian Hold. Do not process until milk parameters have been tested. Reject any loads containing antibiotics		Thermometer record control. Line manager, daily. Lab control, microbiologist, every production date. CCP record control, line manager, daily. Internal audit, auditors, according to audit plan. Maintenance plan – maintenance division, according to plan. Measuring equipment calibration, externally, by legal requirements. The manager verifies corrective measures after deadline for conduction.			Data (temperature) record. Microbial analysis. CCP control record. Internal audit plan. Maintenance plan. Records of authorized institution about calibration or internal calibration record. Corrective/preventive measure claim.

Milk filtration: after reception, milk is filtrated to remove any extraneous material which represents a physical hazard (hair, soil, dust, dirt, etc.).

Storage of raw milk: if the milk is not used in day of production, it should be cooled at refrigerated temperature, below 6°C. The rapidity of milk cooling have a significant impact on its microbial flora. The cooling of milk greatly retards the growth of these mesophilic microorganisms (*Lactococcus spp.*, *Enterococcus spp.*), but psychrotrophic bacteria, such as *Pseudomonas*, *Enterobacteriaceae*, *Flavobacterium* and *Acinetobacter* will continue to grow slowly and dominate the flora. Among Gram- negative, some Gram-positive psychrotrophic bacteria are also found, usually of the genus *Bacillus*. At temperatures below 6°C, *Bacillus cereus* grows and forms spores, which are unaffected by pasteurization. *Bacillus cereus* is of great importance because it is capable of producing a food poisoning toxin. Many yeasts and mould species are also characterized as being psychrotrophic and may contaminate the milk (Ali et. al., 2005; McSweeney, 2007). This stage is the second **CCP** and for controlling this point, storage temperature must be checked.

Milk standardization is made in automatic line - standardization systems by adding skimmilk or cream in whole milk. The fat content in standardized milk is 2,8 %.

Milk pasteurization is identified as a **CCP** stage in dairy plant, of all dairy products. Pasteurization at 85°C, 120 sec. destroy the vegetative forms of bacteria and also extend the shelf life of the product by reducing the number of spoilage microorganism (psychrotrophic bacteria, yeasts and moulds) from raw milk. However, the procedure of pasteurization, can not destroy or

eliminate the toxins, bacterial agglomerations and residues of chemical substances, such as antibiotics and metals. Therefore, the existence of at least one critical control point before pasteurization is essential (reception of raw milk).

Pasteurized milk can have a bacterial flora consisting of thermophilic organisms that have survived pasteurization, such as corynebacteria, micrococci, enterococci, spores of *Bacillus* and *Clostridium* (Fernandes R., 2009). The storage of the product under appropriate conditions (temperature, relative humidity, etc), inhibits the growth of these bacteria.

The insufficient heat treatment may favour the survival of pathogenic bacteria. The pasteurization efficiency should be tested (alkaline phosphatase test) and controlled by establishing management procedures such as maintenance of correct temperature and holding time and efficiency of Cleaning-In -Place (CIP) system. The plate heat exchanger should be cleaned at least once a day (0.5% NaOH, 65±70°C). Cross-contamination of milk after pasteurization stands probably for the greatest risk of a hygiene breakdown and the main sources of contamination are the air, water, equipment, employees, starter cultures, rennet and packaging. Control laboratory does frequently the sampling from the sources which are regarded suspect and exposed to contamination (Mauropoulos et. al., 1999).

Table 4.

Hazard analysis and CCP2 (pasteurization) management

Critical control point CCP			
Stage		Hazards	Critical limits
Milk pasteurization 85°C, 120 sec		Biological: survival of pathogenic microorganisms (aerobic mesophilic bacteria, <i>Salmonella</i> , <i>Escherichia coli</i> , <i>Listeria monocytogenes</i> , coagulase positive <i>Staphylococcus</i>) due to improper pasteurization temperature and/or time.	< 85°C < 120 sec.
Monitoring procedures			
What	When	How	Who
Pasteurization temperature	Continuously during pasteurization	Control of starting and final temperature for every batch in buffer tank.	Employee at pasteurization stage: line manager, veterinarian
Pasteurization time	Before start-up of pasteurization	Control of thermograph records to assure that thermograph and probe detect same temperature. Control of vital equipment for temperature regulation (probes, valves, thermograph).	

Corrective measures		Verification			Records
Who	How	What	Who	When	
Line manager, veterinarian If the temperature is not correct (equipment or power failure), line employee discharges the milk, to balance tank and circulate it to pasteurizer. The manager of line is informed and he decides on further actions and informs manager of maintenance if necessary.		Thermograph record control. Line manager, daily. Lab control, microbiologist, every production date. CCP record control, line manager, daily. Internal audit, auditors, according to audit plan. Maintenance plan – maintenance division, according to plan. Measuring equipment calibration, externally, by legal requirements. The manager verifies corrective measures after deadline for conduction.			Pasteurizer thermograph record. Microbial analysis. CCP control record. Internal audit plan. Maintenance plan. Records of authorized institution about calibration or internal calibration record. Corrective/preventive measure claim.

The coagulation stage is made after addition of CaCl_2 , lactic acid and rennet solution in pasteurized and cooled milk. Rennet, in combination with lactic acid, causes coagulation of the milk by precipitating casein as an aqueous gel. When the acidity and curd firmness reach the correct level, the whey is separated from the curd (syneresis). The curd (coagulum) is processed by cutting, shaping and pressing to eliminate the whey and adjust the moisture content in cheese. After cutting, the cheese pieces are salted in brine.

Brine salting of cheese is made with 18-22 brine, for 24 hours. Salt influence the ripening stage trough its effects on water activity, contributes to the flavor and texture, extend the shelf life due to control of microbial growth and activity, and various enzyme activities in cheese (Fernandes R., 2009).

Packing and ripening of cheese: the salted cheese is packed in polyethylene bags and covered with 16-18% brine and directed to ripening storage. The packages must be kept in appropriate hygienic conditions and microbiologically tested. Ripened cheese require some degree of ripening for the full development of flavor and texture. During ripening, further moisture loss occurs, and a complex combination of microbial and enzymatic reactions take place, involving milk enzymes, the coagulant, and proteases and peptidases from the starter culture and non-starter microorganisms, which remain viable although their growth is inhibited. The ripening stage lasts 20 days at 14-16°C.

Cheese cold storage is made at 2-8°C and low relative humidity in storage rooms. To prevent the growth of undesirable microorganisms (spoilage and pathogens) as cross contamination, the temperature and relative humidity should be constantly monitored. This stage is identified as last **CCP** in cheese processing line, in dairy plant.

There are pathogens such as *Mycobacterium spp.* which endures extreme pH conditions and high values of salt concentration (Maupoulos et. al., 1999). *Listeria monocytogenes* is a psychrotrophic bacteria which grows rapidly at 8-12°C, high moisture and 5.0 up to 6.0-7.0 pH conditions. *Staphylococcus aureus* is able to tolerate salt and moderate acidity, and can multiply during cheese manufacture and ripening. For that reason, pasteurization must destroy this pathogen.

Also, it is essential that adequate hygiene procedures to be practiced during cheese processing and ripening to prevent environmental contamination with *L. monocytogenes* (Fernandes R., 2009).

Conclusions

1. Implementation of the HACCP system in cheese processing line proves to be a necessary tool for improving the safety and quality characteristics of these dairy products.
2. Following hazard analysis, four CCP (critical control points) were established for cow TELEMIA cheese: raw milk reception, raw milk storage, milk pasteurization and cold storage of cheese.
3. The application of the HACCP system is not a stand-alone system, but it should be seen as an element of food safety management. It complements basic good hygienic practices in food safety assurance by targeting product-specific hazards and devising control measures necessary for managing risks relevant to the product and conditions of operations.

References

1. Ali A.A., Fischer R.M., 2005 - *Implementation of HACCP to Bulk Cream and Butter Production Line*, Food Reviews International, 21:189–210.
2. El-Hofi M., El-Tanboly E.S., Ismail A., 2010 - *Implementation of the Hazard Analysis Critical Control Point (HACCP) system to white cheese production line*, Acta Sci. Pol., Technol. Aliment. 9(3):331-342.
3. Fernandez R., 2009- *Microbiology handbook -dairy products*, Leatherhead Publishing, Leatherhead Food International Ltd, 66-76.
4. Karns J. S., Van Kessel J. S., McClusky B. J., Perdue M. L., 2007 - *Incidence of Escherichia coli O157:H7 and E. coli Virulence Factors in US Bulk Tank Milk as Determined by Polymerase Chain Reaction*, Journal of Dairy Science 90: 3212–3219
5. Kišmartin I., Babić J., Ačkar D., Slaćanac V., Šubarić D., Jozinović A., 2013 - *Control of HACCP system efficiency in cream cheese production*, Journal of Hygienic Engineering and Design, 2:30-35.
6. Maupououlos A.A., Arvanitoyannis I.S., 1999 - *Implementation of hazard analysis critical control point to Feta and Manouri cheese production lines*, Food Control 10: 213-219.
7. McSweeney P.L.H., 2007- *Cheese problems solved*, CRC Press,
8. Papademas P., Bintsis T., 2010 - *Food safety management systems (FSMS) in the dairy industry: A review*, International Journal of Dairy Technology, 63:1-15.
9. Wiedmann M., 2006 – *An Integrated Science Based Approach to Dairy Food Safety: Listeria monocytogenes as a Model System*, Journal of Dairy Science 86: 1865–1875.

LEFT SIDED CONGESTIVE HEART FAILURE DUE TO SEVERE AORTIC DEGENERATION AND INSUFFICIENCY IN A DOG – A CASE REPORT

R.A. BAIAN, E. CONDURACHI, V. VULPE, S.A. PAȘCA

Faculty of Veterinary Medicine, University of Agricultural Sciences and Veterinary Medicine
„Ion Ionescu de la Brad” Iași
Email: vasile_vulpe@yahoo.com

Abstract

Aortic degeneration is an uncommon finding in dogs with uncertain etiology, being associated with endocrine disorders which may induce hypercalcemia, hyperkalemia, or with toxicosis, renal disorders and endocarditis. This entity may develop a diastolic volume overload leading to left sided congestive heart failure. The aim of this study is to report and discuss a case of a dog with left sided congestive heart failure due to severe aortic regurgitation associated with myxomatous mitral valve disease and systemic hypertension.

Case presentation

A 16 years old mix breed male dog, weighting 25 kg was referred to the Cardiology Service of the Veterinary Teaching Hospital of Iași with a history of breathlessness, tachypnea, weight and appetite loss for 3 days. Physical examination revealed decreased body condition score, pale mucous membranes, increased respiratory rate and effort and orthopneic position. Lung auscultation revealed wet crackles on both lungs and cardiac auscultation revealed a left apical systolic plateau murmur of 5th grade and a basal left sided diastolic murmur. The rectal temperature was within normal limits.

A five minutes six-lead electrocardiography was performed with the dedicated PolySpectrum 8V ECG device with the dog in sternal recumbence. The ECG trace revealed a sinus rhythm with a HR of 125 bpm, presence of respiratory arrhythmia and 7 left ventricular premature complexes, organized in 2 single VPCs, one couplet and one triplet (fig. 1 A and C). Also, a run of accelerated idioventricular rhythm of four right ventricular complexes with a mean HR of 120 bpm was observed. A left lateral thoracic radiography revealed left sided cardiomegaly with dorsal displacement of the trachea and a perihilar interstitial and alveolar pattern extending into the diaphragmatic lung lobes was observed (fig. 1 B). The diagnosis of a cardiac disease with pulmonary edema was suspected.

Due to the severe condition of the dog, the complete cardiological examination was postponed and oxygen therapy and furosemide were administered as emergency. Diuretic therapy with furosemide 2mg/kg P.O. BID was recommended and recheck was scheduled after 7 days.

At recheck, one week later, the dog was alert, pink mucous membranes, the respiratory effort decreased and cardiac auscultation revealed a left apical systolic plateau murmur of 5th grade and a basal left sided diastolic murmur. Due to the improved general condition, the patient was subjected to a complete cardiological examination consisting of five minutes six leads electrocardiography, thoracic radiography, blood pressure measurement with a veterinary oscillometric device (Vet HDO) and echocardiography (General Electric, Logiq V5) as previously described (Thomas, Gaber et al. 1993; Egner, Carr et al. 2003; Thrall 2013; Tilley and Smith Jr 2016).

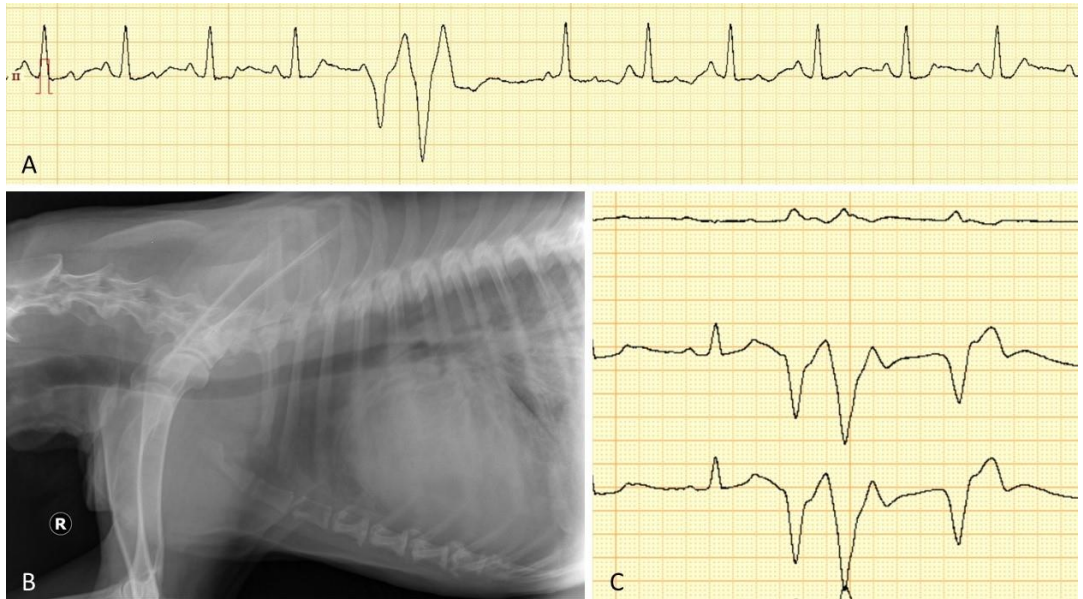


Figure 1 A. Lead II electrocardiography (10 mm/mV, 50 mm/sec) of a dog with severe respiratory distress: sinus rhythm with a couplet of left ventricular premature complexes visible after the 4th complex; B. right lateral thoracic radiography of the same dog: cardiac enlargement with dorsal displacement of the trachea and a patchy alveolar pulmonary pattern is visible around the perihilar area extended into the caudal lung lobes; C – electrocardiographic trace of the same dog – a triplet composed of 3 successive ventricular complexes is seen;

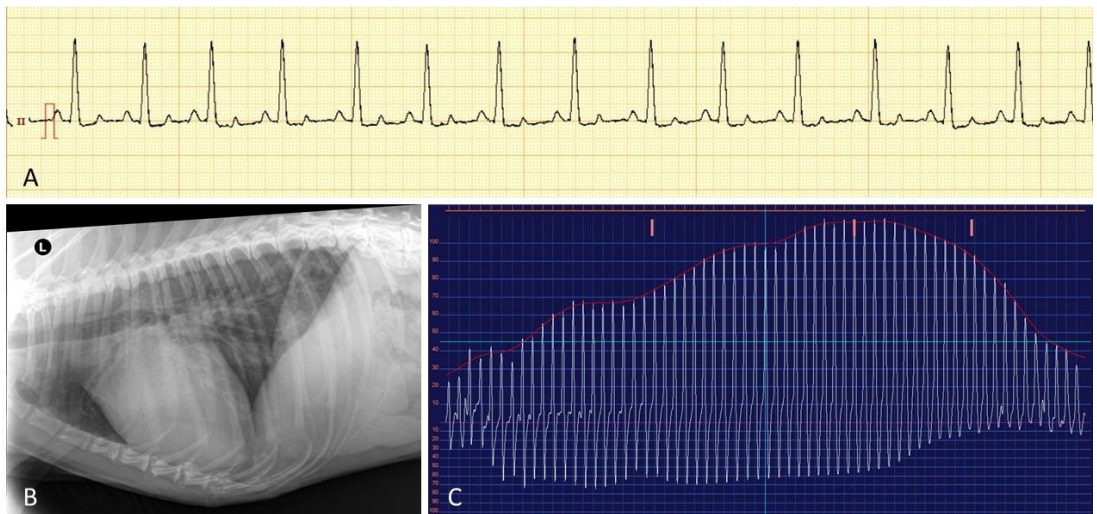


Figure 2. A. Lead 2 electrocardiography (10 mm/mV, 50 mm/sec) of the same dog, one week after oral furosemide monotherapy – HR – 145 bpm, sinus rhythm, absent respiratory arrhythmia and no ventricular premature complexes were present on 5 minutes recording; B. left lateral thoracic radiography of the dog after one week of oral furosemide monotherapy – an improvement on the pulmonary pattern is visible, with resolution of the pulmonary edema. The cardiac enlargement is still present; C. Pulsatile wave graphic of the arterial blood pressure measurement – note the increase in presystolic waves – consistent with presystolic arterial hypertension.

Electrocardiography revealed a sinus rhythm with a heart rate of 145 bpm, with the presence of respiratory arrhythmia, normal mean electrical axis and no ventricular premature complexes on 5 minutes recording (fig.2 A). The blood pressure was measure at the tail with a D2 cuff and the mean value of five measurements was 143/56 (systolic/diastolic pressure) (fig. 2 C). Echocardiography revealed left ventricular eccentric hypertrophy in systole (LVIDs = 26.9 mm; LVIDsn = 1.28) and diastole (LVIDd = 54.6 mm; LVIDdn = 2.11) and atrial dilatation (La/Ao = 1.97). The mitral valve was hyperechoic and thickened, with a mitral regurgitating jet of 4.96 m/s and a pressure gradient of 98.57 mmHg (fig. 3 C). The aortic valve was thickened with hyperechoic aspect and abnormal movement of the leaflets and a diastolic regurgitating jet was present with a velocity of 4.67 m/s and a pressure gradient of 87.13 mmHg (fig. 3 A, B and D). The systolic function of the left ventricle was increased with a shortening fraction of 50.7% and an ejection fraction of 81.5%. The trans-mitral flow interrogation revealed an impaired relaxation pattern with E-wave velocity of 0.7 m/s and deceleration time of 63 milliseconds and a A-wave velocity of 1.11 m/s. The E/A ratio was 0.64. The pulmonary flow was laminar within normal ranges. Subjective evaluation of the right atria and ventricle did not reveal any changes. There were no signs of pulmonary hypertension.

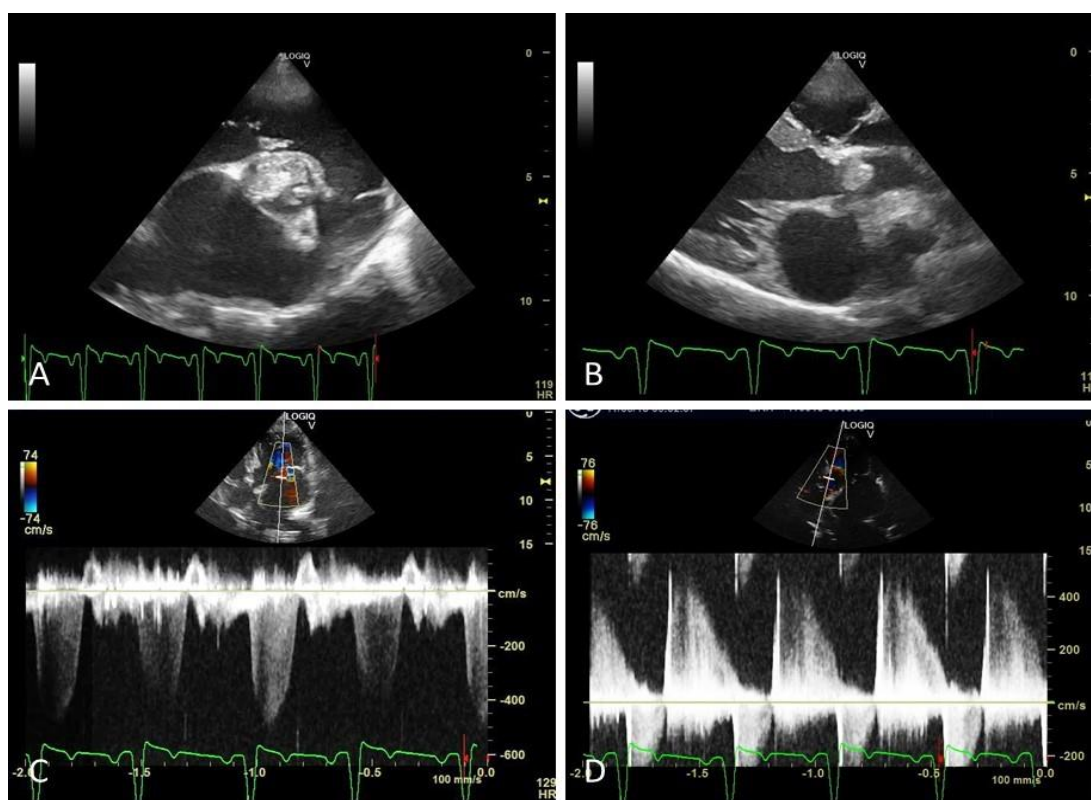


Figure 3 Echocardiography of a dog after one week of therapy with furosemide monotherapy for pulmonary edema: A. Right parasternal short axis view at the heart base – not the increase in the left atrium and the pulmonary veins and the hyperechoic aspect of the closed aortic valves; B. Right parasternal long axis five chamber view – the aortic valve is thickened and hyperechoic with an abnormal position; C. Continuous Doppler interrogation of the mitral regurgitating jet, measuring a maximum velocity of 4.96 m/s with a pressure gradient of 98.57 mmHg; D. Continuous Doppler interrogation of the aortic valve over the regurgitating jet, measuring a maximum velocity of 4.67 m/s with a maximum pressure gradient of mmHg.

Thoracic radiography revealed increased cardiac size with a VHS of 11.9v, dorsal displacement of the trachea and a diffuse interstitial pattern extended into the caudal lung lobes. No alveolar pattern was visible as compared to the thoracic radiography performed one week previously (fig. 2 B). Moreover, severe spondylosis was observed between T12-L3 and L3-S1. Cardiological diagnosis was aortic degeneration associated with myxomatous mitral valve disease and left sided congestive heart failure. Also, the dog was diagnosed with severe spondylosis and arterial hypertension. Therapy was assigned and the dog was released home. One month later the owner requested euthanasia because of the severe pain and ataxia due to spondylosis and necropsy was performed.

Gross pathology of the heart revealed left ventricle and atrial dilation, myxomatous degeneration of the mitral valve and severe degenerative lesions of the aortic leaflets (fig. 4 A and B).

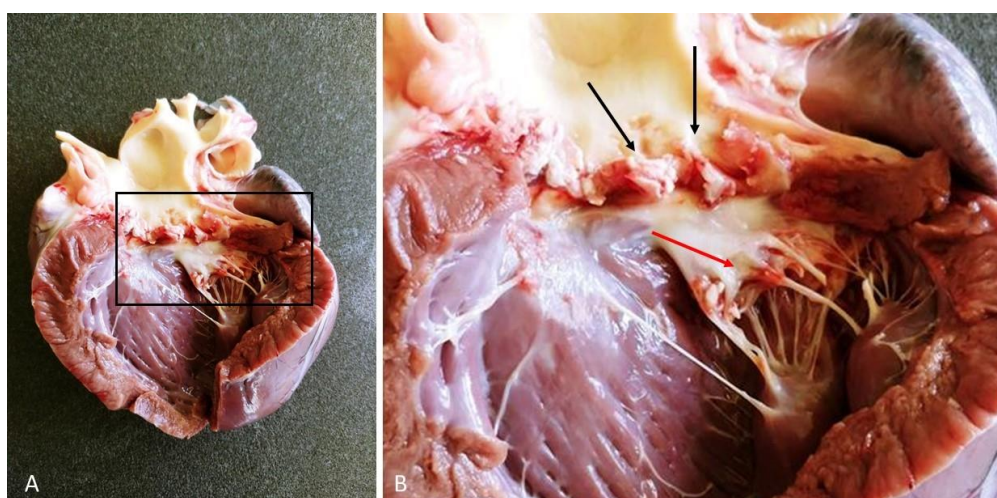


Figure 4 A. Gross pathology of the heart showing left ventricular eccentric hypertrophy; B. Magnification of the same image focusing on the aortic (black arrow) and mitral valve (red arrow) which appear thickened and degenerated.

Histopathological examination revealed mucoid degeneration of the aortic leaflets expressed by the thickening of the leaflets showing a polypoid aspect, defragmentation of the fibrillar structures (elastin and collagen fibers) and increased accumulation of fundamental substance. Aortic wall examination revealed a significant thickening of the intimal layer, lipid accumulation and acid mucopolysaccharides deposits into the media layer, between the leiocytes, with a fibrillar aspect, showing mild basophil coloration. The accumulation of mucopolysaccharides induced a dissociation of the media layer and fragmentation of the myocytes. Aortic calcification was observed, with intimal localization, expressed through the basal layer and endothelial cell mineralization (fig. 5).

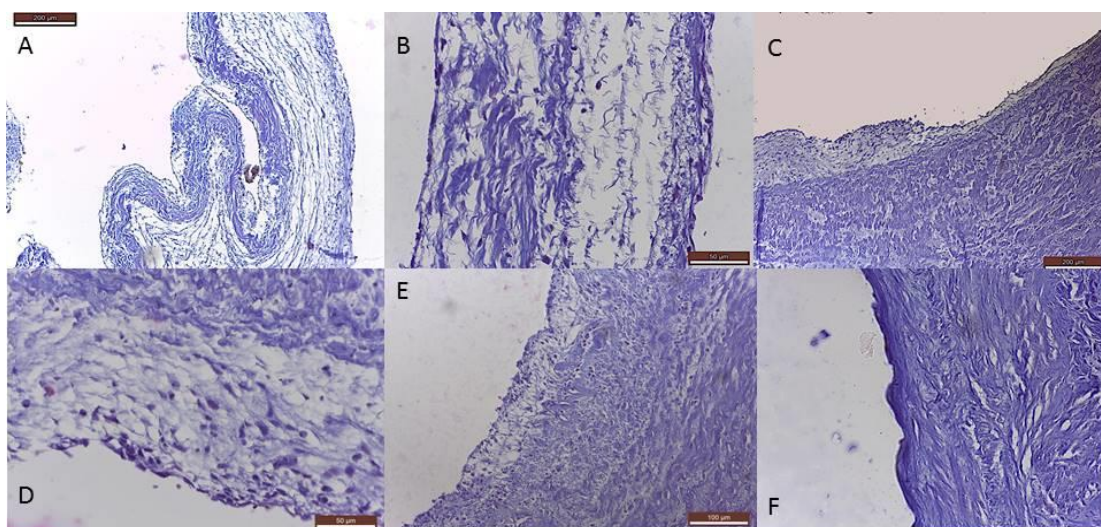


Figure 5 Histopathological images of the lesions: A. Histologic image of the aortic valve – section through proliferation, with mucoid degeneration and fibrosis B. Section through the aortic valve – the fragmentation of the elastic and collagenous fibers within the valvular structure is visible; C. Section through the aortic wall – intimal lipidosis inducing an irregular aspect of the aortic lumen, also note the mucous degeneration of the media layer, hyperproduction of proteoglycans, inducing disorganization of the muscular layer; D. Section through the aortic wall – intimal lipidosis; E. Section through the aortic wall – subendothelial lipid accumulation is visible and degeneration of the media and intimal layers though the synthesis of mucopolysaccharides by the myofibroblasts; F. Section through the aortic wall – Intimal calcification expressed through the mineralization of the basal membrane and the endothelial cells; Trichrome Masson;

Discussions

This paper describes a case of a dog with myxomatous mitral valve disease and severe degeneration of the aortic valve which induced hemodynamic changes and left sided congestive heart failure. The etiology of the aortic degeneration and mineralization is uncertain, however multiple factor are incriminated such as endocrine disorders that may imbalance the calcium concentration in the body, toxics, chronic kidney failure or chronic endocarditis. Endocarditis had been reported, in dogs, with prevalence of 0.9-6.6% (Macdonald 2010), multiple pathogens being involved such as *Staphylococcus spp.*, *Streptococcus spp.*, *Escherichia coli*, *Pseudomonas spp.*, or *Bartonella* (Calvert 1982; Sisson and Thomas 1984; Kelly, Rolain et al. 2006; Sykes, Kittleson et al. 2006; Sykes, Kittleson et al. 2006). Like any inflammatory process, the chronic phase induces fibrosis of the affected tissue and changes in the organ architecture. These structural changes will develop a coaptation deficit of the aortic valve leaflets allowing the blood to return into the left ventricle during the diastole. The early filling of the left ventricle will lead to volume overload and eccentric hypertrophy. These hemodynamic changes will worsen the myxomatous valve disease progression by increasing the amount of blood regurgitating into the left atrium and by filling the left ventricle in early diastole and increasing the pressure during late diastole, leaving the left atrial cavity with a residual volume. These mechanisms together, worsen the left atrial volume and pressure overload leading to dilatation and pulmonary capillary wedge pressure and finally left sided congestive heart failure. Cardiogenic pulmonary edema develops once the left ventricular end-diastolic pressure exceeds 20-25 mmHg (Guyton and Lindsey 1959).

The development of endocarditis and degenerative valvular lesions must have underlying

factors such as bacteriemia and disruption of the endothelial tissue. The most common predisposing factors in dogs are subaortic stenosis which create a turbulent flow. However, the patient presented in this paper did not show any echocardiographic signs of subaortic stenosis, but a mild obstruction of the aortic annulus cannot be ruled out. Other common factors that predispose to bacteriemia is discospondylitis. Our patient had severe spondylosis, which may be possibly developed secondary to intervertebral disc infection.

The presence of the ventricular premature complexes was found only in the first visit, when the dog was dyspneic and had pulmonary edema, however, these complexes disappeared after the pulmonary edema was treated. It is known that both myocardial fibrosis and hypoxia may induce ventricular premature complexes. The mechanism behind the generation of ectopic beats is unidirectional block inside a region with diffuse fibrosis and hypoxia, where micro-reentries are formed (Sachetto, Alonso et al. 2018) and also hypoxemia and respiratory acidosis during prolonged pulmonary edema may trigger abnormal automaticity (Hansel, Solleder et al. 2009).

From the anatomopathological point of view, the intimal lipidosis is the promoter for the aortic atheromatosis, the lipid infiltration inducing lately transformation of the myocytes into fibroblasts, synthesis of the collagen fibers and incorporation of the lipids into the arterial wall. The two dystrophic processes coexist inside the aortic wall. On the other side, these changes lead to arteriosclerosis of the arterial wall. Lipid deposit and proteoglycans synthesis by the myofibroblasts lead to compression of the myocytes and diffuse parietal sclerosis.

Mineralization of the aortic wall was observed at the anatomopathological examination. Causes of the arterial medial mineralization are reported to be associated with carcinogenic plant toxicosis, hypothyroidism, hypercholesterolemia, hypercalcemia, vitamin D toxicosis, primary hyperparathyroidism, and chronic kidney failure with secondary hyperparathyroidism. One study reported the radiographic features of the aortic mineralization in 20 dogs without any clinical signs linked to the radiographic findings. However, these changes have been associated with older dogs, and 13 of 20 had signs related to neoplasia (Douglass, Berry et al. 2003). Another study reported a prevalence of aortic and cardiac mineralization seen on radiography of 0.61%. Similarly, this entity was overrepresented in geriatric dogs and also in Rottweilers. The authors suggested that this pathology may be either age-related degenerative process or chronic disease-related process (Schwarz, Sullivan et al. 2002).

Finally, the cause of the aortic valve degeneration is unclear, however, the hemodynamic changes can be well documented by echocardiography and therapy can be assigned to ensure a better quality of life.

Conclusions

Aortic degeneration may be clinically suspected by the diastolic basal murmur and confirmed through echocardiographic examination. Due to the chronic changes of the valvular structure, the therapy aims to restore the hemodynamic changes and prevent the onset of left sided congestive heart failure.

References

1. Calvert, C. A. (1982). "Valvular bacterial endocarditis in the dog." *J Am Vet Med Assoc* 180(9): 1080-1084.
2. Douglass, J. P., C. R. Berry, et al. (2003). "Radiographic features of aortic bulb/valve mineralization in 20 dogs." *Vet Radiol Ultrasound* 44(1): 20-27.
3. Egner, B., A. Carr, et al. (2003). *Essential facts of Blood pressure in dogs and cats*. Belin, Germany, Blackwell Verlag GmbH.
4. Guyton, A. C. and A. W. Lindsey (1959). "Effect of elevated left atrial pressure and decreased plasma protein concentration on the development of pulmonary edema." *Circ Res* 7(4): 649-657.

-
5. Hansel, J., I. Solleder, et al. (2009). "Hypoxia and cardiac arrhythmias in breath-hold divers during voluntary immersed breath-holds." *Eur J Appl Physiol* 105(5): 673-678.
 6. Kelly, P., J. M. Rolain, et al. (2006). "Bartonella quintana endocarditis in dogs." *Emerg Infect Dis* 12(12): 1869-1872.
 7. Macdonald, K. (2010). "Infective endocarditis in dogs: diagnosis and therapy." *Vet Clin North Am Small Anim Pract* 40(4): 665-684.
 8. Sachetto, R., S. Alonso, et al. (2018). "Killing Many Birds With Two Stones: Hypoxia and Fibrosis Can Generate Ectopic Beats in a Human Ventricular Model." *Front Physiol* 9: 764.
 9. Schwarz, T., M. Sullivan, et al. (2002). "Aortic and cardiac mineralization in the dog." *Vet Radiol Ultrasound* 43(5): 419-427.
 10. Sisson, D. and W. P. Thomas (1984). "Endocarditis of the aortic valve in the dog." *J Am Vet Med Assoc* 184(5): 570-577.
 11. Sykes, J. E., M. D. Kittleson, et al. (2006). "Clinicopathologic findings and outcome in dogs with infective endocarditis: 71 cases (1992-2005)." *J Am Vet Med Assoc* 228(11): 1735-1747.
 12. Sykes, J. E., M. D. Kittleson, et al. (2006). "Evaluation of the relationship between causative organisms and clinical characteristics of infective endocarditis in dogs: 71 cases (1992-2005)." *J Am Vet Med Assoc* 228(11): 1723-1734.
 13. Thomas, W. P., C. E. Gaber, et al. (1993). "Recommendations for standards in transthoracic two-dimensional echocardiography in the dog and cat. Echocardiography Committee of the Specialty of Cardiology, American College of Veterinary Internal Medicine." *J Vet Intern Med* 7(4): 247-252.
 14. Thrall, D. E. (2013). *Textbook of veterinary diagnostic radiology*, Elsevier.
 15. Tilley, L. P. and W. W. K. Smith Jr (2016). *Electrocardiography. Manual of Canine and Feline Cardiology*. W. W. K. Smith Jr, L. Tilley, M. Oyama and M. Sleeper. St Louis, Missouri, Elsevier: 49-76.

CANINE PYOMETRA: MICROBIOLOGICAL DIAGNOSIS AND THERAPY

¹George Cosmin NADĂȘ, ²Cosmin Dan Filipoi, ¹Flore Chirilă, ¹Cosmina Maria BOUARI, ¹Ioana Buzura-Matei and ¹Nicodim Iosif FIȚ

1- University of Agricultural Sciences and Veterinary Medicine, Faculty of Veterinary Medicine, 3-5 Calea Mănăștur street., 400372, Cluj-Napoca, Romania

2 – Tierklinik Hochmoor, Germany
filipoi_cosmin_dan@yahoo.com

Abstract

Pyometra is a common illness in adult intact female dogs and cats and a less frequent diagnosis in other small animal species. The aim of this study was to evaluate the microbial flora isolated from uterine exudates of bitches suffering from pyometra and test their susceptibility to antibiotics in dogs presented to a clinic in North Rhine-Westphalia region, Germany. Between February and September 2018, a total of 40 dogs suffering from pyometra were included in this study. Cotton swabs were used to collect pus from the uterus. The identification of bacteria was possible using MALDI-TOF MS device, in a private clinic from Germany. The susceptibility to antibiotics was evaluated using Kirby-Bauer disk diffusion test. The results demonstrated that Escherichia coli was the most frequently isolated bacteria, present in 28 from 40 samples (70%), followed by Streptococcus sp. in 5 samples (12.5%), Staphylococcus pseudintermedius in 3 samples (7.5%), Enterococcus sp. and Pasteurella multocida, each in 2 samples (5%) and Staphylococcus haemolyticus, Pseudomonas aeruginosa, Pseudomonas putida, Klebsiella pneumoniae, Haemophilus hemoglobinophilus, Acinetobacter pittii, Pseudomonas koreensis and Enterobacter cloacae, each in 1 sample (2.5%). Regarding antibiotic susceptibility, the most efficient antibiotics were represented by Marbofloxacin, Enrofloxacin Doxycycline and Amoxicillin and clavulanic acid, while the least efficient were Penicillin G and Clindamycin.

Keywords: pyometra, bitches, isolation, susceptibility testing.

Introduction

Pyometra is a common illness in adult intact female dogs and cats and a less frequent diagnosis in other small animal species. (Hagman, 2018). The pathogenesis of pyometra is only partly understood, but it's generally acknowledged that primary hormonal imbalance or abnormal response to normal concentrations of estrogens, and progesterone affects the epithelial cells of the uterus and facilitates bacterial adherence, colonization and growth (Fieni, 2014).

The disease is defined by accumulation of purulent material within the uterus, which manifests in both local and systemic symptoms, and demands costly surgical or medical intervention in order to resolve (Gibson A., 2013). Progesterone induces changes in the uterus which prepare a suitable environment for early embryo development, including endometrial proliferation, increased uterine glandular secretions and decreased myometrial contractions, as well as a relaxation in normal uterine cellular immune defenses (Noakes D., 2009).

The clinical signs are usually expressed in the diestrus phase, 4-8 weeks after the estrus, bitches usually present anorexia, lethargy, polydipsia and polyuria. Fever is not common, but when the cervix is open, a purulent hemorrhagic discharge is observed. The most common bacterium isolated is *Escherichia coli*, normal approach is to grow the pathogens from the uterine exudates and test their susceptibility to antimicrobial agents.

Recent papers published in the field demonstrated that Matrix-assisted laser desorption/ionization time-of-flight (MALDI-TOF) mass spectrometry (MS) offers the possibility of accurate, rapid, inexpensive identification of bacteria, fungi, and mycobacteria isolated in clinical microbiology laboratories (Murray P.R., 2012).

The aim of this study was to evaluate the microbial flora isolated from uterine exudates of bitches suffering from pyometra and test their susceptibility to antibiotics in dogs presented to a clinic in North Rhine-Westphalia region, Germany.

Materials and methods

Between February and September 2018, a total of 40 dogs suffering from pyometra were included in this study. The clinical cases presented for consultation had in most situations closed cervix (n=29; 72.5%), the rest were open cervix. Clinical findings included polyuria, polydipsia, lethargy, anemia, leukocytosis and, in chronic cases increased renal parameters. The diagnosis was established after anamnesis, physical examination and abdominal radiography. Ovariohysterectomy was the treatment of choice for all cases, associated with antimicrobial therapy according to the in vitro susceptibility test.

Cotton swabs were used to collect pus from the uterus. The swabs were initially used to prepare slides and examine them after Gram staining technique was performed. The examination aimed to evaluate the shape, size and arrangement of bacteria, in most cases Gram negative cocobacilli, typical for genus *Escherichia*. The inoculation of blood agar plated was then performed for the characterization of isolates.

The identification of bacteria was possible using MALDI-TOF MS device, in a private laboratory from Germany. Isolated 24 h colonies were selected and suspended in 70% ethanol with the purpose of inactivating bacteria, then centrifuged. The supernatant was removed and the cells resuspended in 70% formic acid for disruption of the cell wall. Acetonitrile is added for protein extraction and the sample is again centrifuged for concentration. The target plate is covered with 1 µl of supernatant, allowed to dry and then covered with the matrix consisting of a saturated solution of α -cyano-4-hydroxy-cinnamic acid in 50% acetonitrile and 2.5% trifluoroacetic acid.

The susceptibility to antibiotics was evaluated using Kirby-Bauer disk diffusion test. The isolated colonies grown on blood agar were used to prepare a suspension in broth of 0.5 density on McFarland scale. This suspension was then used to flood Mueller-Hinton agar plates. The excess fluid was removed and the surface allowed drying for 20 minutes. The following antibiotics as filter paper disks were used: Amoxicillin and clavulanic acid, Cefovecin, Clindamycin, Doxycycline, Enrofloxacin, Marbofloxacin, and Penicillin G.

Results and discussions

The results demonstrated that *Escherichia coli* was the most frequently isolated bacteria, present in 28 from 40 samples (70%), followed by *Streptococcus* sp. in 5 samples (12.5%), *Staphylococcus pseudintermedius* in 3 samples (7.5%), *Enterococcus* sp. and *Pasteurella multocida*, each in 2 samples (5%) and *Staphylococcus haemolyticus*, *Pseudomonas aeruginosa*, *Pseudomonas putida*, *Klebsiella pneumoniae*, *Haemophilus hemoglobinophilus*, *Acinetobacter pittii*, *Pseudomonas koreensis* and *Enterobacter cloacae*, each in 1 sample (2.5%). Bacterial associations were identified in 9 (22.5%) cases, most common between *Escherichia coli* and other species, while 3 samples were negative for microbial growth.

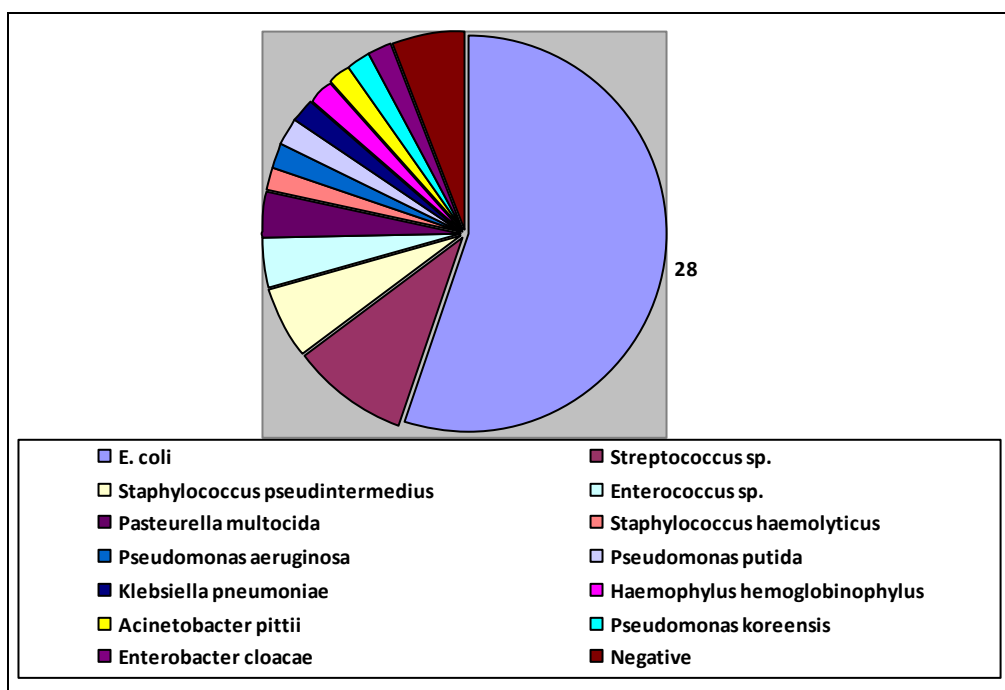


Figure 1. The type and number of bacterial species isolated from pyometra samples in dogs

Regarding antibiotic susceptibility, the most efficient antibiotics were represented by Marbofloxacin, with the average of inhibition area diameter of 23.17 mm, Enrofloxacin with 22.46 mm, Doxycycline with 22.09 mm, Amoxicillin and clavulanic acid with 20.94 mm and Cefovecin with 20.02 mm, while the least efficient were Penicillin G with 14.41 and Clindamycin with 16.19 mm.

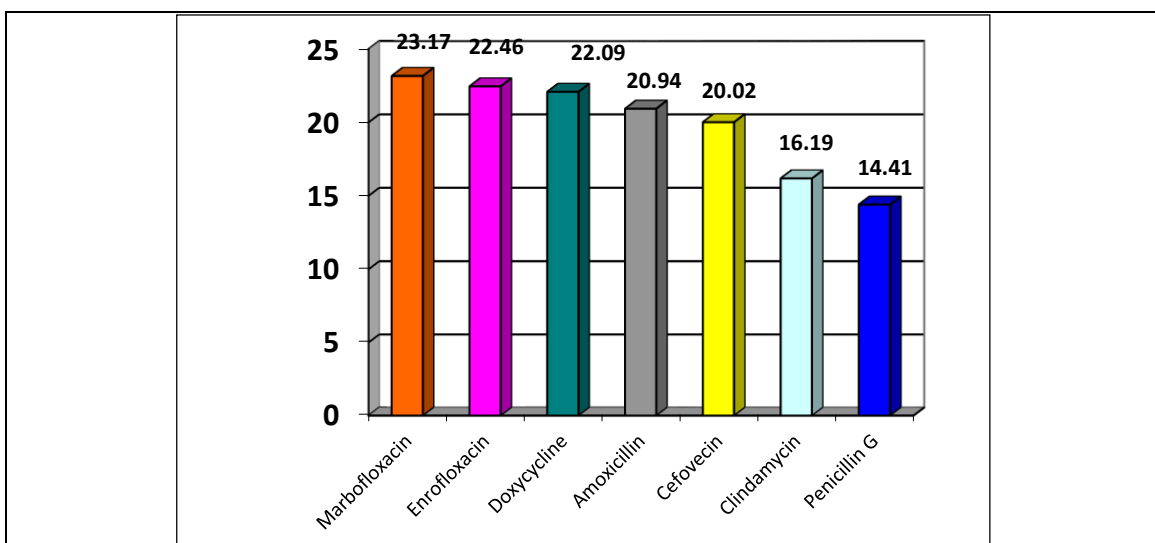


Figure 2. Average inhibition area diameter of the susceptibility testing

Conclusions

The study of canine pyometra concerning etiologic agents and susceptibility profiles concluded that:

- MALDI-TOF MS offers the possibility of accurate and rapid identification of bacteria isolated in clinical microbiology laboratories;
- *E. coli* was the most frequently isolated bacterium;
- Regarding the antimicrobial susceptibility, the most recommended antibiotics were represented by quinolones (Marbofloxacin and Enrofloxacin), Doxycycline and Amoxicillin and clavulanic acid;
- The least efficient antibiotics were Penicillin G and Clindamycin.

References

1. Contri, A., Gloria, A., Carluccio, A. et al., 2015, Effectiveness of a modified administration protocol for the medical treatment of canine pyometra, *Vet Res Commun* 39:1.
2. Fieni, F., Topie, E. and Gogny, A., 2014, Medical Treatment for Pyometra in Dogs. *Reprod Dom Anim*, 49: 28-32.
3. Gibson, A., Dean, R., Yates, D., & Stavisky, J., 2013. A retrospective study of pyometra at five RSPCA hospitals in the UK: 1728 cases from 2006 to 2011. *The Veterinary record*, 173(16), 396.
4. Hagman R. Pyometra in Small Animals. 2018, *Vet Clin North Am Small Anim Pract.*, Jul;48(4):639-661.
5. Hagman R, Greko C., 2005. Antimicrobial resistance in *Escherichia coli* isolated from bitches with pyometra and from urine samples from other dogs. *Vet Rec.*;157(7):193-6.
6. Inoue I, Shibata S, Fukata T., 2013. Efficacy of fosfomycin on *Escherichia coli* isolated from bitches with pyometra. *J Vet Med Sci.*;75(5):657-8.
7. Murray, P. R., 2012. What is new in clinical microbiology-microbial identification by MALDI-TOF mass spectrometry: a paper from the 2011 William Beaumont Hospital Symposium on molecular pathology. *The Journal of molecular diagnostics : JMD*, 14(5), 419-23.
8. Noakes D. E., Parkinson T. J., England G. C. W., 2009. *Veterinary Reproduction and Obstetrics*, Saunders.